

UNIVERSITY OF SOUTHAMPTON

Non-Equilibrium Nuclear Spin States

by

Christian Bengs

A thesis submitted in partial fulfillment for the
degree of Doctor of Philosophy

in the
Faculty of Engineering and Physical Sciences
School of Chemistry

January 2021

UNIVERSITY OF SOUTHAMPTON

ABSTRACT

FACULTY OF ENGINEERING AND PHYSICAL SCIENCE
SCHOOL OF CHEMISTRY

Doctor of Philosophy

by Christian Bengs

Any physical quantum system is in thermal contact with its environment and if left undisturbed, will always come to thermal equilibrium with its surroundings. Nuclear magnetic resonance techniques however displace the system from its thermal equilibrium position. The amount of time a system may be displaced from its thermal equilibrium position is inherently time limited due to constant information exchange between the system and the environment. This fundamental process is known as quantum relaxation or quantum decoherence.

In this thesis we focus our attention on the relaxation dynamics of nuclear spin ensembles. Particular spin configurations may display surprisingly long relaxation time constants and surprising dynamical behaviour as the system deviates further from its thermal equilibrium position. A simple framework for the description of nuclear spin systems far from thermal equilibrium is described and its necessity is experimentally demonstrated by consideration of simple model systems. The presented framework aims to advance recent developments in the storage of hyperpolarised materials, which ideally possess exceptionally long relaxation times and highly ordered spin configurations.

Contents

Acknowledgements	ix
1 Introduction	1
1.1 Nuclear magnetism	2
1.1.1 The NMR setup	2
1.1.2 Precession and relaxation	3
1.1.3 The NMR signal	6
1.1.4 Microscopic nuclear magnetism	7
1.1.5 Nuclear Zeeman effect	10
1.2 Mathematical framework	12
1.2.1 State vectors	12
1.2.2 Operators	13
1.2.3 State and operator representations	15
1.2.4 Time evolution of states	17
1.2.5 Unitary transformations	18
1.3 Nuclear spin interactions	20
1.3.1 External spin Hamiltonian	23
1.3.1.1 Static magnetic field	23
1.3.1.2 Radio-frequency field	23
1.3.2 Internal spin Hamiltonian	24
1.3.2.1 Chemical shift	24
1.3.2.2 J-coupling	25
1.3.2.3 Dipolar coupling	25
1.3.2.4 Spin-rotation coupling	25
1.3.2.5 Quadrupole coupling	26
1.4 Interaction-frame Hamiltonian	26
1.5 Quantum measurements	29
1.5.1 Single spin systems	29
1.5.2 Spin ensemble	31
1.6 Time evolution of the ensemble	33
1.7 Thermal equilibrium	35
2 Far from thermal equilibrium	37
2.1 Theoretical Background	39
2.1.1 Liouville space	39
2.1.1.1 Superoperators	39
2.1.2 Spin Hamiltonian	40

2.1.2.1	Coherent Hamiltonian	40
2.1.2.2	Fluctuating Hamiltonian	47
2.1.3	Equation of Motion	48
2.2	Semi-classical relaxation theory	49
2.2.1	Semi-classical relaxation superoperator	49
2.2.2	Transition probabilities	52
2.2.3	Coherence decay rate constants	53
2.2.4	Semi-classical equation of motion	53
2.3	Thermalisation	54
2.3.1	Thermal Corrections	55
2.3.1.1	Jeener's Method	57
2.3.1.2	Levitt-di Bari and Levante-Ernst method	58
2.4	Lindblad thermalisation	60
2.4.1	Quantum-Mechanical Spectral Densities	61
2.5	Defect of Double Commutators	64
2.6	Case Studies	66
2.6.1	Homonuclear spin-1/2 pairs	66
2.6.2	Heteronuclear spin-1/2 pairs	69
2.6.3	Singlet-Triplet conversion	70
2.7	Fullerene-encapsulated water ($\text{H}_2\text{O}@C_{60}$)	75
2.7.1	Proton line shape factors	77
2.7.2	$\text{H}_2\text{O}@C_{60}$ spin isomer conversion	83
3	Close to thermal equilibrium	93
3.1	Coupled spin-1/2 pairs	93
3.1.1	The coherent Hamiltonian	94
3.1.2	Single Transition operators	94
3.1.3	A convenient basis	95
3.2	Generalised magnetisation-to-singlet transfer	95
3.2.1	Transfer scheme	97
3.2.2	A simple example	105
3.2.3	Experimental demonstration	106
3.3	Singlet mediated double quantum excitation	110
3.3.1	Double quantum excitation in equivalent spin systems	111
3.3.2	Experimental demonstration	114
4	Conclusions	117
A	Appendix	119
A.1	Lindblad form	119
A.2	Eigenoperators	120
A.3	Longitudinal recovery for singlet-triplet-conversion	121
	Bibliography	125

Abbreviations

Acronym	Definition	Acronym	Definition
ad	Adiabatic	na	Non-Adiabatic
coh	Coherent	NOE	Nuclear Overhauser Effect
CS	Chemical-Shift	NMR	Nuclear Magnetic Resonance
CSS	Chemical Shift Scaling	ODCB	Ortho-Dichlorobenzene
DD	Dipole-Dipole	PAS	Principal Axis System
DNP	Dynamic Nuclear Polarisation	ppm	Parts Per Million
DQ	Double Quantum	Q	Quadrupole
FID	Free Induction Decay	QM	Quantum Mechanical
fluc	Fluctuating	ran	Random
FML	Fast Motion Limit	ref	Reference
ev	Evolution	res	Resonant
eq	Equilibrium	RF	Radio Frequency
gM2S	generalised Magnetisation to Singlet	rms	Root-Mean-Square
gS2M	generalised Singlet to Magnetisation	rot	Rotating
IME	Inhomogeneous Master Equation	SC	Semi-Classical
ind	Induced	SE	Spin Echo
iso	Isotropic	sec	Secularised
J	Jeener	sLdB	Simplified Levitt-Di Bari
JSE	J Synchronised Echo	sm	Singlet Mediated
lab	Laboratory	SO	Singlet Order
LB	Lindblad	SR	Spin-Rotation
LdB	Levitt-Di Bari	S2M	Singlet to Magnetisation
M2S	Magnetisation to Singlet	QRIP	Quantum Rotor Induced Polarisation

Declaration of Authorship

This thesis is the result of work done wholly while I was in registered candidature for a PhD degree at the University of Southampton. The material presented here is based on work mostly done by myself. Where the work was carried out jointly with others, a substantial part is my own original work and co-workers and their roles have been clearly indicated. The material contained herein has not been submitted by the author for a degree at any other institution.

Signed:

January 2021

Acknowledgements

I think it goes without saying that I am greatly indebted to my supervisors Malcolm Levitt and Giuseppe Pileio.

I would like to thank Malcolm for his continuous support and advice throughout the last three years. The lessons I received about scientific thinking and scientific communication are invaluable. Malcolm is a truly excellent supervisor that deeply cares for his students. His endless efforts in keeping the group operational so that we can freely follow our interests is exceptional. That being said I would like to thank Malcolm for helping me to dodge much of the universities bureaucracy and for putting up with my reluctance to comply.

I would also like to thank Peppe (Giuseppe) for his ongoing advice throughout my whole PhD. When I was still a small bambino PhD you were never too busy to sit down with me and go through many of the subtle concepts of spin dynamical theory. And while I always appreciated your scientific insight, I am truly grateful for your education on Italian customs. Mille grazie!

With such caring supervisors it is not too surprising that the MagRes section in Southampton is made up of incredible people. With that being said, I would like to thank (in memological order. Yes, I just made up a new english word, you are welcome): James Eills, William Hale, Stuart Elliott, Aliko Moysiadi, Gabriele Stevanato, David Goodwin, Javier Alonso-Valdesueiro, Benno Meier, Karel Kouřil, Hana Kouřilová, Shamim Alom, George Bacanu, Jai Balachandra, Steven Worswick, Sylwia Ostrowska, Barbara Ripka, Mohamed Sabba, Jyrki Rantaharju, Johannes Colell, James Whipham, Marek Plata, Giulia Melchiorre, Andrew Hall, Marcel Utz, Maria Concistre and James Emsley.

In particular I would like to thank Benno Meier, Karel Kouřil and Hana Kouřilová for their design of bullet DNP setup, which initiated the work on a master equation for spin systems far from equilibrium. I would also like to thank Stuart Elliott for his experimental efforts on the fullerene encapsulated water molecules and observation of the peculiar peak intensities. I owe many thanks to James Eills and Gabriele Stevanato for our many fruitful collaborations on the manipulation of non-equilibrium spin order throughout the duration of my PhD.

On a more personal note I am incredible fortunate, you not so much, to have enjoyed the company of Aliko Moysiadi, James Eills, Stuart Elliott, William Hale and Andy Price.

An dieser Stelle möchte ich mich ebenfalls bei meiner Familie bedanken. Auch wenn ich in den letzten Jahren zu wenig Zeit mit euch verbracht habe, so konnte ich mich doch immer auf eure Unterstützung und euren Rat verlassen. Ich möchte mich besonders bei meinen Eltern bedanken, die es in dieser Zeit nie gescheut haben, persönlich zurückzutreten, um mir meine Wünsche zu ermöglichen.

To my family

Chapter 1

Introduction

The humble beginnings of Nuclear Magnetic Resonance (NMR) can be tracked back all the way to the 1940s. Following Rabi's description of the magnetic resonance effect Purcell, Torrey, Pound and Bloch, Hansen, Packard almost simultaneously (24th of December, 1945 and 29th of January, 1946) reported the observation of nuclear induction for the first time [1–3].

Since then, it is probably fair to say that NMR has grown into something much bigger than the founding fathers could have hoped for. The applicability of NMR is seemingly endless and ranges from elementary physics to quantum computation, material science, organic chemistry, medical science, biology and many other fields of active research. Major landmarks in the field of NMR include the development of magnetic resonance imaging, two-dimensional NMR and its extension to protein structure elucidation [4–7]. For obvious reasons these developments continue to influence our every day life by guiding biomedical and pharmaceutical research.

Nowadays NMR is considered a standard tool in many areas of active research. Nonetheless, it seems that whenever the community is convinced to have reached the stories end, a new idea magically appears and opens up a new chapter. In recent years this has certainly been the development of hyperpolarisation techniques [8–19].

Despite a great number of benefits, NMR suffers from a weak magnetic response of the sample. Hyperpolarisation techniques try to address this problem by displacing the system from its equilibrium position to a highly non-equilibrium state. The non-equilibrium state often displays a much stronger magnetic response than the thermal state under identical conditions. In practical applications this leads to a tremendous reduction in experimental time.

It will be the aim of this thesis to explore some properties of equilibrium and non-equilibrium systems with focus on their theoretical description. Surprisingly, the standard description of NMR experiments can lead to non-physical predictions in the case of strongly perturbed spin systems. A new approach for the treatment of highly non-equilibrium systems will be discussed in order to clarify and remedy the situation.

1.1 Nuclear magnetism

1.1.1 The NMR setup

For conventional high-field NMR experiments the sample is initially placed inside the center of a magnet. As illustrated in figure 1.1a it is NMR convention to assume that the main magnetic field \mathbf{B}^0 is aligned with the z -axis of the laboratory frame

$$\mathbf{B}^0 = B_z^0 \mathbf{e}_z = \begin{bmatrix} 0 \\ 0 \\ B_z^0 \end{bmatrix}. \quad (1.1)$$

The magnetic field strength along the z -axis B_z^0 is specified in units of Tesla [T].

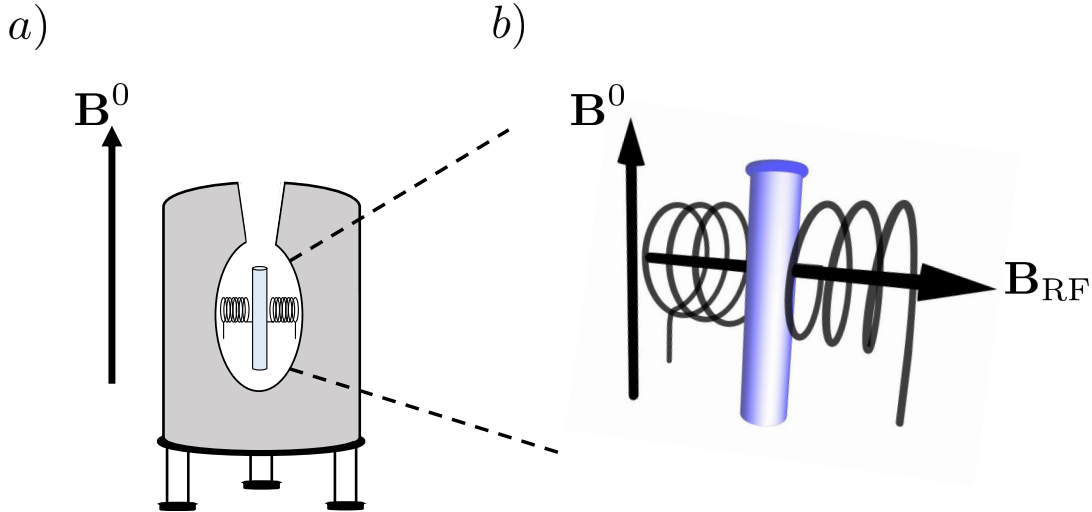


FIGURE 1.1: **a)** Schematic representation of a modern high-field NMR magnet. The main magnetic field \mathbf{B}^0 is by convention along the z -axis. The sample is located in the center of the magnet and surrounded by RF coils. **b)** A closer look at the sample region of the magnet. The solenoid RF coil generates a field \mathbf{B}_{RF} that is perpendicular to the main magnetic field. **Note:** In modern NMR spectrometers the RF coil is usually given by a saddle coil.

The potential energy E_{mag} arising from the interaction of a magnetic material and a magnetic field is given by the following expression

$$E_{\text{mag}}(\theta) = -\boldsymbol{\mu} \cdot \mathbf{B}^0 = -\|\boldsymbol{\mu}\| \|\mathbf{B}^0\| \cos(\theta), \quad (1.2)$$

where θ represents the angle between the magnetic field and the magnetic moment $\boldsymbol{\mu}$, and the norm of a vector $\|\mathbf{v}\|$ is defined by

$$\|\mathbf{v}\| = \sqrt{\mathbf{v} \cdot \mathbf{v}}. \quad (1.3)$$

Equation 1.2 implies that the (bulk) magnetic moment of the sample tends to align itself with the main magnetic field. This leads to a net polarisation of the sample along the z -axis and the sample becomes magnetised. The build up of the magnetisation follows an exponential law (a more thorough discussion follows later)

$$\boldsymbol{\mu}(t) = \begin{bmatrix} 0 \\ 0 \\ M_{\text{eq}}^0(1 - \exp(-t/T_1)) \end{bmatrix} \quad \text{and} \quad \boldsymbol{\mu}(\infty) = \begin{bmatrix} 0 \\ 0 \\ M_{\text{eq}}^0 \end{bmatrix}. \quad (1.4)$$

The equilibrium magnetisation or net polarisation of the sample is denoted by M_{eq}^0 (see figure 1.2). The characteristic time constant T_1 with which the magnetisation builds up is called *longitudinal relaxation time constant*.

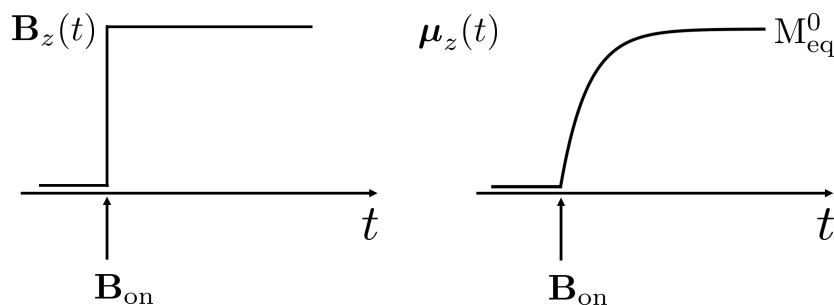


FIGURE 1.2: After the sample is exposed to a magnetic field along the z -axis (left) the magnetisation μ_z slowly starts to build up (right). The build up follows an exponential law and eventually reaches its equilibrium value M_{eq}^0 .

1.1.2 Precession and relaxation

The magnetic moment may be perturbed from its equilibrium position by the application of an oscillating radio frequency (RF) field. As indicated in figure 1.1b the radio frequency field is generated by a coil perpendicular to the main magnetic field. If the perturbation is sufficiently strong and quick (a so-called RF *pulse*) the magnetic moment may be completely rotated into the xy -plane of the laboratory system. Being in the xy -plane the main field exerts a torque onto the magnetic moment

$$\boldsymbol{\tau} = \boldsymbol{\mu} \times \mathbf{B}^0. \quad (1.5)$$

Following the original description by Bloch, both the magnetic moment and the torque may be related to the angular momentum of an object [3]

$$\frac{d}{dt}\mathbf{L} = \boldsymbol{\tau}, \quad \boldsymbol{\mu} = \gamma\mathbf{L} \quad \text{and} \quad \gamma = 2\pi \times \frac{q}{2m}g_{\text{cl}}, \quad (1.6)$$

where q denotes the charge of the object in Coulomb [C] and m its mass in kilogram [kg]. The dimensionless constant g_{cl} is the classical g -factor. The overall proportionality constant γ relating a magnetic moment to its angular momentum is the *gyromagnetic ratio* and usually specified in [rad T⁻¹ s⁻¹].

Substitution of the relations above into equation 1.5 leads to the so-called *Bloch equation*

$$\frac{d}{dt}\boldsymbol{\mu} = -\gamma \mathbf{B}^0 \times \boldsymbol{\mu},$$

$$\frac{d}{dt} \begin{bmatrix} \mu_x(t) \\ \mu_y(t) \\ \mu_z(t) \end{bmatrix} = -\gamma B_z^0 \begin{bmatrix} -\mu_y(t) \\ \mu_x(t) \\ 0 \end{bmatrix}, \quad (1.7)$$

where the minus sign follows from the anti-commutativity of the cross product. For a conventional NMR setup the Bloch equations are readily solved and yield the following expressions

$$\begin{bmatrix} \mu_x(t) \\ \mu_y(t) \\ \mu_z(t) \end{bmatrix} = \begin{bmatrix} \cos(\omega^0 t) \\ -\sin(\omega^0 t) \\ 0 \end{bmatrix} \quad \text{for} \quad \boldsymbol{\mu}(0) = \begin{bmatrix} 1 \\ 0 \\ 0 \end{bmatrix}. \quad (1.8)$$

The equations above indicate a rotation of the magnetic moment in the xy -plane with angular frequency $\omega^0 = -\gamma B_z^0$. The angular frequency ω^0 is called *Larmor frequency* and the motion of the magnetic moment *Larmor precession*.

The velocity of the Larmor precession is determined by the magnitude of the Larmor frequency, but the sense of rotation depends upon the sign of the gyromagnetic ratio. Figure 1.3 illustrates that the magnetic moment precesses clockwise for positive gyromagnetic ratios ($\gamma > 0$) and counter-clockwise for negative gyromagnetic ratios ($\gamma < 0$).

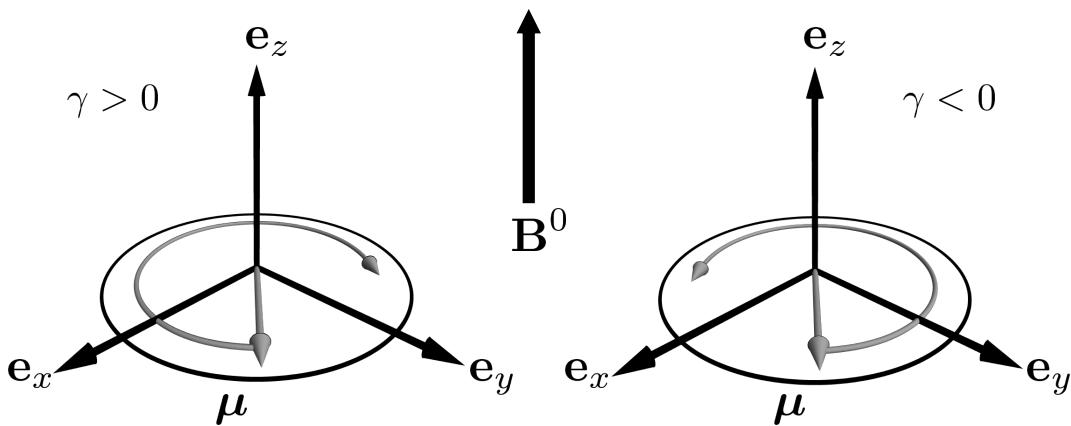


FIGURE 1.3: Sense of rotation for a magnetic moment $\boldsymbol{\mu}$ depending on the sign of the gyromagnetic ratio γ . For positive γ the sense of rotation is clockwise, whereas for negative γ the sense of rotation is anti-clockwise.

The Bloch equations in their current form are slightly flawed. Not only do they indicate that the magnetic moment rotates in xy -plane, but it does so for all time. This cannot be the case, as experiments indicate a decay of the transverse magnetisation and a recovery of the longitudinal magnetisation with increasing time. A more realistic description of the NMR experiments is therefore given by the modified expressions below [20]:

$$\begin{bmatrix} \boldsymbol{\mu}_x(t) \\ \boldsymbol{\mu}_y(t) \\ \boldsymbol{\mu}_z(t) \end{bmatrix} = \begin{bmatrix} \cos(\omega^0 t) \exp(-t/T_2) \\ -\sin(\omega^0 t) \exp(-t/T_2) \\ M_{\text{eq}}^0 (1 - \exp(-t/T_1)) \end{bmatrix} \quad \text{for } \boldsymbol{\mu}(0) = \begin{bmatrix} 1 \\ 0 \\ 0 \end{bmatrix}. \quad (1.9)$$

where T_2 represents the *transverse relaxation time constant*. A graphical representation of the *modified Bloch equation* is shown in figure 1.4 (left panel). The magnetic moment slowly spirals its way up again until it is fully aligned with the z -axis.

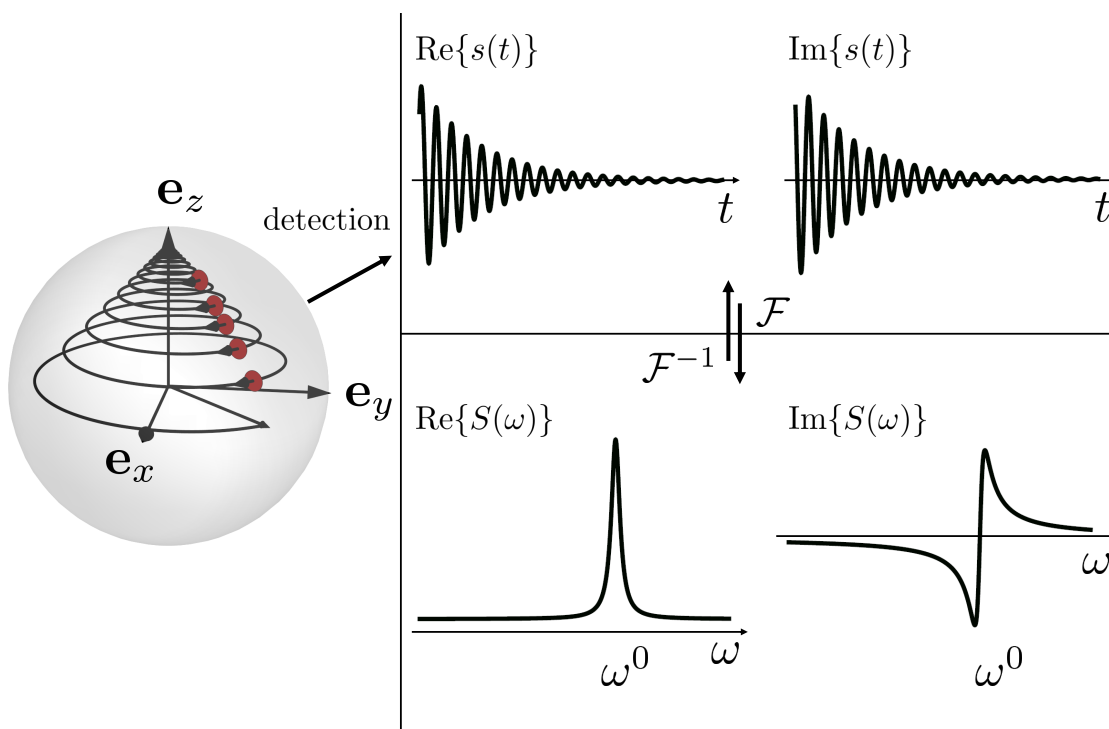


FIGURE 1.4: **left panel**) Representation of the modified Bloch equations on a unit sphere. If the initial position of the magnetic moment $\boldsymbol{\mu}$ lies in the xy -plane the magnetic moment starts precessing around the z -axis of the laboratory frame. Due to relaxation the magnetic moment slowly spirals its way upwards. The transverse components can be seen to die out whereas the longitudinal magnetisation recovers. **right panel**) The oscillation of the transverse magnetisation is picked up by a detector. The resulting complex FID is illustrated at the top. The Fourier transform \mathcal{F} converts the FID into a complex spectrum. The real part of the spectrum (left) is the absorption Lorentzian and the imaginary part (right) is the dispersive Lorentzian. Oscillating components of the time-domain signal appear at a frequency ω^0 . The whole process may be reversed by applying the inverse Fourier transform \mathcal{F}^{-1} to $S(\omega)$.

1.1.3 The NMR signal

It is exactly this precession motion that an NMR experiment aims to observe. According to Maxwell's equations (Faradays induction law) a time-varying magnetic field is capable of inducing an electric current [21]

$$\nabla \times \mathbf{E} = -\frac{\partial}{\partial t} \mathbf{B}. \quad (1.10)$$

As a consequence, the transverse component of the rotating magnetic moment generates an oscillating electric current in the RF coil. This current may be picked up by a suitable detector [22]. The resulting NMR signal is called a *free induction decay* (FID). For technical reasons it is conventional to combine the x - and y -component of the oscillation into a single signal object known as *complex* FID

$$\begin{aligned} s(t) &= M_{\text{eq}}^0 (\boldsymbol{\mu}_x(t) + i \boldsymbol{\mu}_y(t)) \\ &= M_{\text{eq}}^0 (\cos(\omega^0 t) - i \sin(\omega^0 t)) \exp(-t/T_2) \\ &= M_{\text{eq}}^0 \exp(-i\omega^0 t) \exp(-t/T_2). \end{aligned} \quad (1.11)$$

While the complex FID contains all the necessary information, its interpretation by eye is difficult. For this reason, NMR data is usually presented in form of a *spectrum*. The NMR spectrum is generated by applying a *Fourier transform* to the signal $s(t)$. The Fourier transform is a mathematical tool that helps to identify the frequency components of a given signal. This is achieved by converting a function of time into a function of frequency. The formal definition of the (one-sided) Fourier transform is given below:

$$S(\omega) = \mathcal{F}\{s(t)\} = \int_0^{\infty} s(t) \exp(-i\omega t) dt, \quad (1.12)$$

with $S(\omega)$ denoting the resulting spectrum. Application of the Fourier transform to the prototype signal of equation 1.11 results in a so-called *complex Lorentzian*

$$S(\omega) = \mathcal{F}\{M_{\text{eq}}^0 \exp(-i\omega^0 t) \exp(-t/T_2)\} = \frac{M_{\text{eq}}^0 T_2}{1 + (T_2 (\omega^0 - \omega))^2} - i \frac{M_{\text{eq}}^0 (T_2)^2 (\omega^0 - \omega)}{1 + (T_2 (\omega^0 - \omega))^2}. \quad (1.13)$$

The Lorentzian decomposes into a real and an imaginary part. The real part represents an *absorption* and the imaginary part a *dispersion* Lorentzian.

The complex FID of equation 1.9 with its corresponding complex Lorentzian are shown in figure 1.4 (right panel). The interpretation of the signal is now considerably easier. Whenever the signal contains a frequency component ω the resulting spectrum shows a *spectral peak* at that particular position, otherwise it is zero.

1.1.4 Microscopic nuclear magnetism

The description above constitutes the *classical* description of NMR. The magnetic moment is treated as a bulk property of the sample and the dynamics are governed by classical equations. From a microscopic point of view however, the question "what generates nuclear magnetism?" still remains.

A partial resolution to this problem was given by the famous *double slit* experiment by Otto Stern and Walther Gerlach [23]. Consider the following thought experiment: "What happens to a particle with *no* angular momentum moving through an inhomogeneous magnetic field?"

According to equation 1.2 the magnetic energy of the particle depends on its magnetic moment. The exerted magnetic force on the particle may be deduced by differentiating the potential energy

$$\mathbf{F}_{\text{mag}} = \nabla(\boldsymbol{\mu} \cdot \mathbf{B}) = \mu_z \frac{d\mathbf{B}_z(z)}{dz} \mathbf{e}_z, \quad (1.14)$$

where it is assumed (for simplicity) that the magnetic field varies along the z -axis only. This is an obvious oversimplification as this would contradict Gauss's flux theorem [21]. The force above indicates a deflection of the particles path along the z -axis. The magnitude of the deflection depends upon its magnetic moment.

Since equation 1.6 relates the magnetic moment of a particle to its angular momentum, an angular momentum-less particle would not experience a deflection force ($\mathbf{F}_{\text{mag}} = 0$) and continue its linear motion.

It is exactly this experiment that Stern and Gerlach realised. The angular momentum-less particles were provided by a silver atom beam. The electronic configuration of a silver atom is given by: $[\text{Kr}]4d^{10}5s^1$. The unpaired $5s^1$ electron occupies the necessary orbital angular momentum ground state ($J = 0$).

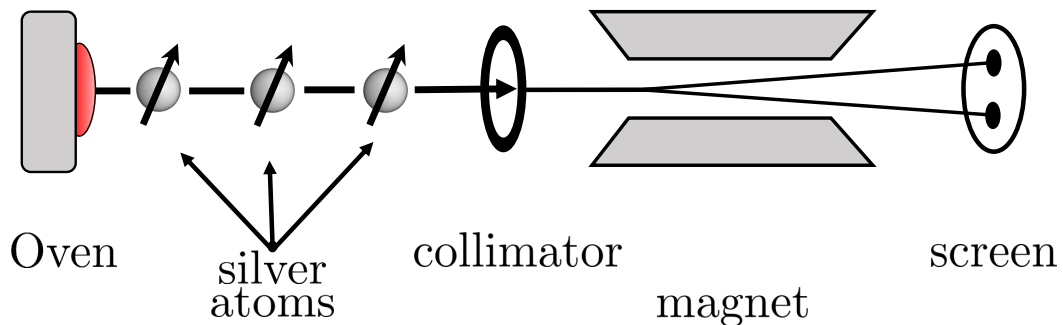


FIGURE 1.5: Brief sketch of the double slit experiment. The whole setup is under a strong vacuum. A small electric oven provides a beam of silver atoms which is focused by a collimator. On their way to the screen the silver atoms experience an in-homogeneous magnetic field provided by an electromagnet.

An outline of the double slit experiment can be seen in figure 1.5. Surprisingly, the

results indicated a clear deflection pattern with the beam being split into two distinct rays. This observation was not in agreement with physical laws at the time.

A full resolution to this problem was later given by Goudsmit and Uhlenbeck [24]. Within the framework of the newly developed quantum physics, they proposed the existence of *intrinsic* angular momentum carried by the electron. Similar to the classical case, it had to be proportional to the magnetic moment of the electron

$$\boldsymbol{\mu} = \gamma_e \vec{I}, \quad \gamma_e = \frac{q}{2m_e} g_e \quad \text{and} \quad \vec{I} = \begin{bmatrix} \hat{I}_x \\ \hat{I}_y \\ \hat{I}_z \end{bmatrix}. \quad (1.15)$$

Here γ_e denotes the gyromagnetic ratio of the electron, m_e its mass and g_e its g-factor. The object \vec{I} indicates a quantum mechanical (vector) operator and measures spin angular momentum along the $\{x, y, z\}$ -axis. An arrow is used to distinguish classical vectors and vector operators. It is however common to loosely write \mathbf{I} instead of \vec{I} whenever there is no cause for confusion.

This new type of angular momentum later came to be known as *spin angular momentum*, so that \hat{I} represents a spin angular momentum operator.

Being a quantum mechanical object means that spin angular momentum is *quantised*. Quantisation implies that a particular degree of freedom stores energy in discrete packages proportional to $\hbar \approx 1.054 \times 10^{-34} \text{ J s}$. The discrete states a system may occupy are then labelled by *quantum numbers*. In the case of spin angular momentum one may classify the state by its (ground state) spin I and a projection quantum number m_I . The projection number refers to the spin angular component along the z -axis (by convention). A spin angular momentum state is then identified with a collection of quantum numbers as indicated below:

$$\text{physical state} \mapsto |I, m_I\rangle. \quad (1.16)$$

The collection of quantum numbers $|I, m_I\rangle$ is called a *state vector* or *ket vector* (more on ket vectors follows later).

For the double slit experiment two discrete states are identified: "up" for the top beam of atoms and "down" for the lower beam of atoms. The electron may then occupy two different *spin states*. From the quantum theory of angular momentum it follows that the spin quantum number has to equal $I = 1/2$ [25]. The projection number m_I may then either be $m_I = +1/2$ for "up" or $m_I = -1/2$ for "down". This may be visualised as shown in figure 1.6.

The double slit experiment indisputably identified spin angular momentum for electrons. Similar considerations later showed that nuclei (in fact all elementary particles) possess spin angular momentum as well. In this case one speaks of *nuclear spin angular momentum*. The existence of nuclear spin is what enables NMR experiments. If nuclear

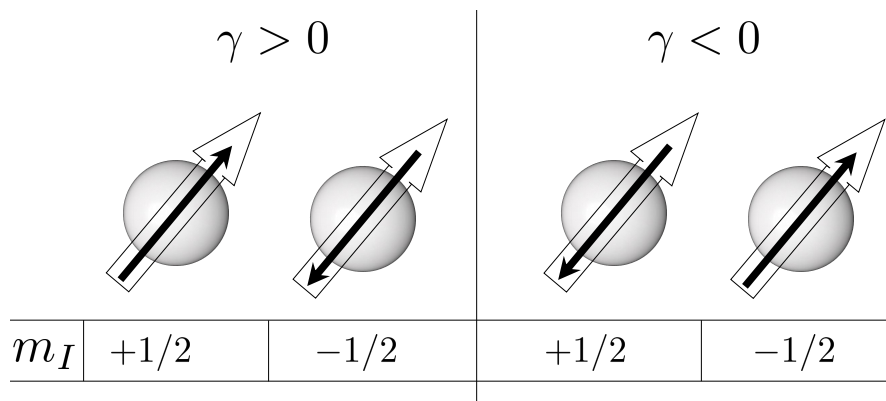


FIGURE 1.6: Relative orientation of the magnetic moment and spin angular momentum depending on the sign of the gyromagnetic ratio and its projection number m_I . The spin angular momentum is indicated by solid arrows and the magnetic moment by hollow arrows. According to equation 1.15 the spin angular momentum and magnetic moment are parallel for positive γ and anti-parallel for negative γ . Strictly speaking this applies to systems that occupy a spin $+1/2$ state. The relative orientation of the spin angular momentum is inverted if the system occupies a spin $-1/2$ state.

spins are visualised as vectors being "attached" to the nuclei of a sample, macroscopic magnetism may be understood as a summation of contributions from all the individual spin angular momenta (see figure 1.7).

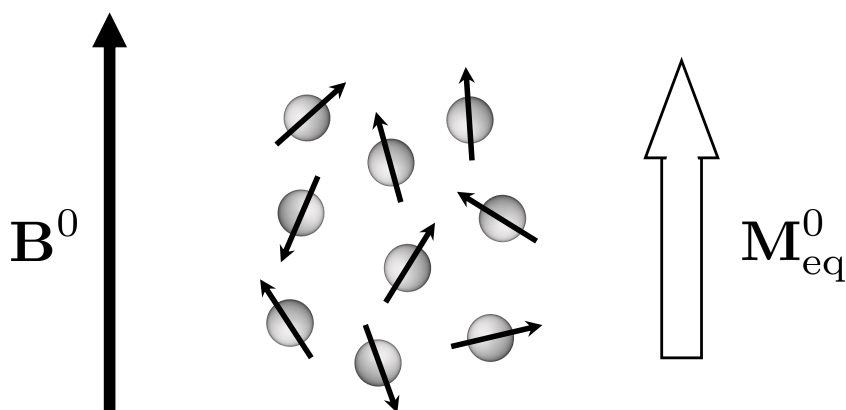


FIGURE 1.7: In zero magnetic field the spin angular momentum vector of a particle may point into any spatial direction. There is no preferential axis since space is isotropic. The isotropy of space is broken through the application of a static magnetic field. The magnetic potential energy depends upon the relative orientation of the magnetic field and the spin angular momentum through equation 1.2. The thermodynamic principle of minimum energy then implies that the particles preferably occupy the lower energy spin state. For $\gamma > 0$ this is the $m_I = +1/2$ spin state. As a result there is a slight net polarisation along the positive z -axis at thermal equilibrium.

It is worthwhile to stress that the term "spin" might be misleading. It suggests a physical rotation of the particle, but this is not true. The necessary velocities to generate

such large magnetic moments for small charge distributions (like the electron) would greatly exceed the speed of light. This was already recognised by Uhlenbeck [24]. Spin angular momentum therefore has nothing to do with the particle undergoing a rotation. Spin is simply an intrinsic property of particles very much like mass, charge, etc.

1.1.5 Nuclear Zeeman effect

In the absence of a magnetic field the net magnetic moment vanishes. This does not mean that spin angular momentum vanishes (similar to how a person does not suddenly disappear as one enters zero gravity). It simply means that the interaction between the spins and the magnetic field got weaker. At zero magnetic field the spin states $|1/2, +1/2\rangle$ and $|1/2, -1/2\rangle$ have identical energy and are said to be *degenerate*. In general the projection number m_I for a particle with spin I may take one of the values from the set $\{-I, -I + 1, \dots, I - 1, I\}$. It follows that a spin state is $(2I + 1)$ -fold degenerate at zero magnetic field [22].

If the sample is subjected to a magnetic field (by convention along the z -axis), the energies start to split. The energy level splitting due to the interaction with a static magnetic field is called *Zeeman effect*. In the case of nuclei one discusses the *nuclear Zeeman effect*. Figure 1.8 illustrates the nuclear Zeeman effect for protons ($I = 1/2$) and deuterons ($I = 1$).

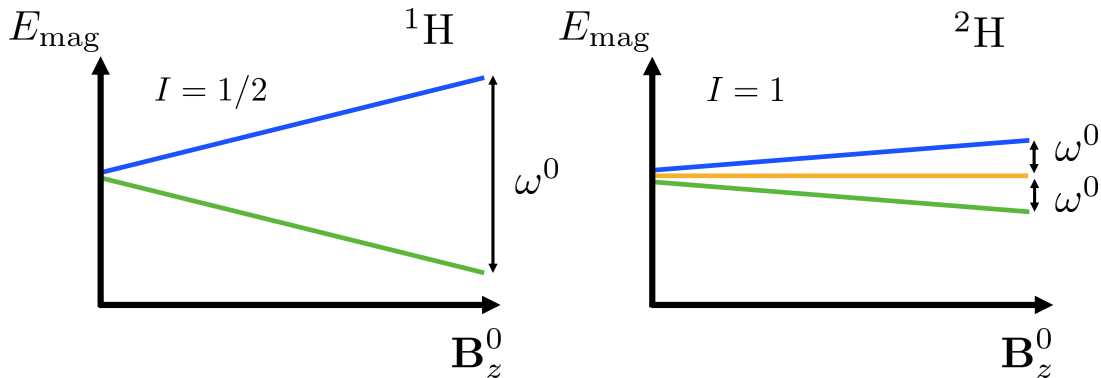


FIGURE 1.8: Nuclear Zeeman effect for protons with $I = 1/2$ and deuterons with $I = 1$. At zero magnetic field the spin states are $(2I + 1)$ -degenerate. This leads to two degenerate states for protons and three degenerate states for deuterons. Application of a static magnetic field leads to a splitting of the energy levels and the degeneracy is completely lifted. The difference in energy between two adjacent energy levels equals the Larmor frequency of the nuclei for that particular field.

According to equation 1.15 the magnetic moment of the sample $\boldsymbol{\mu}$ may be expressed in terms of a spin angular momentum vector \vec{I} . The quantum mechanical version for the magnetic energy of the sample (see equation 1.2) may then be expressed shown below:

$$E_{\text{mag}} = -\boldsymbol{\mu} \cdot \mathbf{B}^0 = -\gamma_i \vec{I} \cdot \mathbf{B}^0, \quad (1.17)$$

where γ_i is the gyromagnetic ratio of nuclei i . Since the only non-vanishing magnetic field component is along the z -axis, equation 1.17 reduces to the following:

$$E_{\text{mag}} = -\gamma_i B_z^0 I_z = \omega^0 I_z. \quad (1.18)$$

The presence of the z -angular momentum operator I_z indicates that the magnetic energy of a state $|I, m_I\rangle$ is given by

$$E_{\text{mag}}(m_I) = m_I \omega^0. \quad (1.19)$$

The energy difference between any two adjacent energy levels (see figure 1.8) then reduces to the Larmor frequency ω^0

$$E_{\text{mag}}(m_I) - E_{\text{mag}}(m_I - 1) = m_I \omega^0 - (m_I - 1) \omega^0 = \omega^0. \quad (1.20)$$

As described earlier, typical NMR experiments measure the frequency of the oscillating transverse component of the magnetisation vector. But this frequency is identical to the Larmor frequency of the sample. It therefore follows, that NMR experiments are sensitive to transitions between adjacent energy levels.

1.2 Mathematical framework

The discussion in the previous section illustrated the quantum mechanical origins of nuclear magnetism. The next several chapters introduce these concepts in a more formal way to facilitate the quantum description of NMR. For NMR purposes the system may only occupy a finite number of spin states. This has some implications for the underlying structure of the *state space*. Much of the following discussion will be written from this point of view.

1.2.1 State vectors

In quantum mechanics the physical state of the system is described by a so-called *ket* $|\psi\rangle$. A ket is an element of some Hilbert space \mathcal{H} . For finite systems \mathcal{H} possesses dimensionality $\dim(\mathcal{H}) = N_{\mathcal{H}}$ and $|\psi\rangle$ may be considered a vector in \mathcal{H} . It is therefore custom to call $|\psi\rangle$ a *ket vector*.

In analogy to the Hilbert space \mathcal{H} , one may define its *dual space* \mathcal{H}^* through the *adjoint* map (\dagger)

$$(c|\psi\rangle)^\dagger = c^* \langle\psi| \in \mathcal{H}^*, \quad (1.21)$$

here $c \in \mathbb{C}$ is some complex number and $(*)$ denotes complex conjugation. The adjoint of a ket $|\psi\rangle$ is called a *bra* or *bra vector*. The dual space \mathcal{H}^* therefore has the same dimensionality as \mathcal{H} .

The scalar product of any two vectors ($|\psi\rangle, |\phi\rangle$) is defined by the *bra-ket* operation $\langle\phi|\psi\rangle$. The norm of a vector $|\psi\rangle$ is then given by the following expression

$$\| |\psi\rangle \| = \sqrt{\langle\psi|\psi\rangle}. \quad (1.22)$$

For a finite dimensional Hilbert space one may always choose an orthonormal basis $\{|b_n\rangle\}$ of ket vectors

$$\langle b_m | b_n \rangle = \delta_{mn}, \quad \langle b_m | b_m \rangle = 1, \quad (1.23)$$

where δ_{mn} denotes the *Kronecker delta* with the property $\delta_{nn} = 1$ and $\delta_{mn} = 0$ for $m \neq n$. A representation for a state $|\psi\rangle$ is constructed by making use of a basis vector expansion

$$|\psi\rangle = \sum_n^{N_{\mathcal{H}}} |b_n\rangle \langle b_n | \psi \rangle = \sum_n^{N_{\mathcal{H}}} |b_n\rangle c_n, \quad \sum_n^{N_{\mathcal{H}}} |b_n\rangle \langle b_n| = \mathbb{1}. \quad (1.24)$$

The scalars $c_n \in \mathbb{C}$ are the expansion coefficients and $\mathbb{1}$ denotes the identity on \mathcal{H} . An explicit form of the inner product may then be given as follows

$$\langle\phi|\psi\rangle = \sum_{n,m}^{N_{\mathcal{H}}} \langle\phi|b_m\rangle \langle b_m|b_n\rangle \langle b_n|\psi\rangle = \sum_{n,m}^{N_{\mathcal{H}}} \delta_{mn} d_m^* c_n = \sum_n^{N_{\mathcal{H}}} d_n^* c_n. \quad (1.25)$$

1.2.2 Operators

In quantum mechanics transformations of states are represented by *linear operators*. In general, the application of an operator \hat{Q} onto a state $|\psi\rangle$ leads to a new state $|\psi'\rangle$

$$|\psi'\rangle = \hat{Q} |\psi\rangle. \quad (1.26)$$

To simplify notation for the rest of the discussion the "hat" of an operator is omitted $\hat{Q} = Q$. Once a basis has been fixed (linear) operators may be represented by $N_{\mathcal{H}} \times N_{\mathcal{H}}$ -dimensional matrices. The matrix elements are determined by their action on the basis elements

$$[Q]_{mn} = \langle b_m | Q | b_n \rangle. \quad (1.27)$$

The action of any operator Q onto some state $|\psi\rangle$ may then be calculated according to standard matrix-vector multiplication

$$\begin{aligned} |\psi'\rangle &= Q |\psi\rangle \\ &= \sum_{m,n}^{N_{\mathcal{H}}} |b_m\rangle \langle b_m | Q | b_n \rangle \langle b_n | \psi \rangle \\ &= \sum_{m,n}^{N_{\mathcal{H}}} |b_m\rangle \langle b_m | Q | b_n \rangle c_n = \sum_{m,n}^{N_{\mathcal{H}}} |b_m\rangle [Q]_{mn} c_n. \end{aligned} \quad (1.28)$$

The transformation of bra vectors follow in similar fashion

$$\begin{aligned} \langle \psi' | &= \langle \psi | Q = \sum_n^{N_{\mathcal{H}}} c_n \langle b_n | Q \\ &= \left(\sum_n^{N_{\mathcal{H}}} Q^\dagger | b_n \rangle c_n^* \right)^\dagger \\ &= \left(\sum_{m,n}^{N_{\mathcal{H}}} |b_m\rangle \langle b_m | Q^\dagger | b_n \rangle c_n^* \right)^\dagger = \left(\sum_{m,n}^{N_{\mathcal{H}}} |b_m\rangle [Q^\dagger]_{mn} c_n^* \right)^\dagger \\ &= \left(\sum_{m,n}^{N_{\mathcal{H}}} |b_m\rangle [Q]_{nm}^* c_n^* \right)^\dagger = \sum_{m,n}^{N_{\mathcal{H}}} c_n [Q_{nm}] \langle b_m |. \end{aligned} \quad (1.29)$$

The relations above indicate that ket vectors may be represented by *column vectors* and bra vectors by *row vectors*.

Associated to each operator Q there exists a special set of ket vectors $\{|q_n\rangle\}$. The members of the set $\{|q_n\rangle\}$ are called *eigenstates* or *eigenvectors* of the operator Q . When Q acts on one of its eigenstates, Q returns the same ket vector up to some constant

$$Q |q_n\rangle = q_n |q_n\rangle. \quad (1.30)$$

The constant q_n is an *eigenvalue* of Q corresponding to the eigenstate $|q_n\rangle$. The set of all eigenvalues $\{q_n\}$ is also called the *spectrum* of the operator Q .

The eigenvalues of an operator are in general complex. But for *self-adjoint* or *hermitian* operators A all eigenvalues are real

$$A|a_n\rangle = a_n|a_n\rangle, \quad a_n \in \mathbb{R}. \quad (1.31)$$

As the name suggests self-adjoint operators equal their adjoint

$$A^\dagger = A. \quad (1.32)$$

Self-adjoint operators additionally possess a *complete set* of orthogonal eigenstates

$$\langle a_m|a_n\rangle = \delta_{mn}. \quad (1.33)$$

The eigenstates of an operator O may therefore be chosen as an orthogonal basis for the Hilbert space \mathcal{H} .

Hermitian operators are central to quantum mechanics. The *postulates of quantum mechanics* assume that every *physical observable* of the system may be represented by a linear self-adjoint operator [25]. The eigenvalues $\{a_n\}$ of a hermitian operator A may then be understood as the possible measurement outcomes of the observable A . If a measurement results in a_n the system is certainly occupying one of the possible eigenstates $|a_n\rangle$ associated with a_n [26]. This process is often referred to as the *wavefunction collapse* [25].

Once the system has collapsed into a particular state of A it is natural consider if there exist any additional observables B that may be measured without further disturbing the system. The operators A and B are then said to be compatible and may be measured "simultaneously".

Such observables may be found by considering the order in which A and B are measured. In general, the measurement of an observable A followed by the measurement of an observable B is different than the reversed measurement. To "quantify" the discrepancy between the two measurement sequences one introduces the *commutator* $[A, B]$ of A and B

$$[A, B] = AB - BA. \quad (1.34)$$

It follows that two observables A and B may only be measured simultaneously if they *commute*

$$[A, B] = 0. \quad (1.35)$$

From a mathematical point of view commuting operators share a common set of eigenstates $\{|a_n, b_m\rangle\}$, so that each eigenstate may be characterised by the eigenvalues of A and B

$$A|a_n, b_m\rangle = a_n|a_n, b_m\rangle \quad \text{and} \quad B|a_n, b_m\rangle = b_m|a_n, b_m\rangle. \quad (1.36)$$

1.2.3 State and operator representations

As discussed earlier, for a spin with spin quantum number I the projection quantum number m_I may take one of the values within the set $\{m_I\}$

$$\{m_I\} = \{-I, -I + 1, \dots, I - 1, I\}. \quad (1.37)$$

The projection quantum number represents the number of independent spin states. In general there are $(2I + 1)$ independent spin states for a spin I

$$\{|I, m_I\rangle\} = \{|I, -I\rangle, |I, -I + 1\rangle, \dots, |I, I - 1\rangle, |I, I\rangle\}. \quad (1.38)$$

The set of spin states $\{|I, m_I\rangle\}$ spans the Hilbert space \mathcal{H} of the spin. The dimension of \mathcal{H} for a single spin I is therefore given by the following:

$$N_{\mathcal{H}} = \dim(\mathcal{H}) = 2I + 1. \quad (1.39)$$

A representation may be constructed by mapping each of the independent spin states onto one of the standard basis vectors of $\mathbb{C}^{N_{\mathcal{H}}}$. For a spin $I = 1/2$ particle for example there are two independent spins states. A vector representation may be constructed as shown below:

$$|1/2, -1/2\rangle \mapsto \begin{bmatrix} 1 \\ 0 \end{bmatrix} \quad \text{and} \quad |1/2, +1/2\rangle \mapsto \begin{bmatrix} 0 \\ 1 \end{bmatrix}. \quad (1.40)$$

The same reasoning applies to spin systems with several spins. For a system of N spins with spin quantum numbers $\{I_1, I_2 \dots I_N\}$ the first spin may occupy one of its possible $(2I_1 + 1)$ states, the second spin one of its $(2I_2 + 1)$ possible states, etc. The number of independent spin states is therefore by the following:

$$N_{\mathcal{H}} = \prod_{i=1}^N (2I_i + 1). \quad (1.41)$$

Mathematically the composite space is constructed by forming *tensor products* (\otimes) with the individual spin spaces \mathcal{H}_i

$$\mathcal{H} = \mathcal{H}_1 \otimes \mathcal{H}_2 \otimes \dots \otimes \mathcal{H}_N. \quad (1.42)$$

Having chosen a representation for the individual members, the tensor product for two matrices A and B may be carried out as follows:

$$A \otimes B = \begin{bmatrix} [A]_{11}B & [A]_{12}B & \dots & [A]_{1N_{\mathcal{H}}}B \\ [A]_{21}B & [A]_{22}B & \dots & [A]_{2N_{\mathcal{H}}}B \\ \vdots & \vdots & \vdots & \vdots \\ [A]_{N_{\mathcal{H}}1}B & [A]_{N_{\mathcal{H}}2}B & \dots & [A]_{N_{\mathcal{H}}N_{\mathcal{H}}}B \end{bmatrix}. \quad (1.43)$$

For two spins with $I = 1/2$ for example the formula above leads to the following:

$$\begin{aligned} \begin{aligned} | -1/2, -1/2 \rangle = \\ | 1/2, -1/2 \rangle \otimes | 1/2, -1/2 \rangle \end{aligned} &\mapsto \begin{bmatrix} 1 \\ 0 \\ 0 \\ 0 \end{bmatrix}, & \begin{aligned} | -1/2, +1/2 \rangle = \\ | 1/2, -1/2 \rangle \otimes | 1/2, +1/2 \rangle \end{aligned} &\mapsto \begin{bmatrix} 0 \\ 1 \\ 0 \\ 0 \end{bmatrix}, \\ \\ \begin{aligned} | +1/2, -1/2 \rangle = \\ | 1/2, +1/2 \rangle \otimes | 1/2, -1/2 \rangle \end{aligned} &\mapsto \begin{bmatrix} 0 \\ 0 \\ 1 \\ 0 \end{bmatrix}, & \begin{aligned} | +1/2, +1/2 \rangle = \\ | 1/2, +1/2 \rangle \otimes | 1/2, +1/2 \rangle \end{aligned} &\mapsto \begin{bmatrix} 0 \\ 0 \\ 0 \\ 1 \end{bmatrix}. \end{aligned} \quad (1.44)$$

Note that whenever all spins share the same spin number I it is common to only use the projection quantum numbers m_I to label a specific spin state.

The operators for the composite space are constructed in similar fashion. An operator Q solely acting on the i 'th spin is constructed by a sequence of N unity operators with the i 'th unity operator being replaced by Q

$$Q_i = \mathbb{1}_1 \otimes \dots \otimes \mathbb{1}_{i-1} \otimes Q \otimes \mathbb{1}_{i+1} \otimes \dots \otimes \mathbb{1}_N, \quad (1.45)$$

where $\mathbb{1}_j$ represents the unity operator for the j 'th spin. Many-body interactions are constructed by simple composition of single-body operators. Some matrix examples for two spins with $I = 1/2$ are given below:

$$\begin{aligned} I_{1z} = I_z \otimes \mathbb{1}_2 \mapsto \begin{bmatrix} \frac{1}{2} & 0 & 0 & 0 \\ 0 & \frac{1}{2} & 0 & 0 \\ 0 & 0 & -\frac{1}{2} & 0 \\ 0 & 0 & 0 & -\frac{1}{2} \end{bmatrix}, & I_{2z} = \mathbb{1}_1 \otimes I_z \mapsto \begin{bmatrix} \frac{1}{2} & 0 & 0 & 0 \\ 0 & -\frac{1}{2} & 0 & 0 \\ 0 & 0 & \frac{1}{2} & 0 \\ 0 & 0 & 0 & -\frac{1}{2} \end{bmatrix}, \\ \\ I_{1z}I_{2z} = I_z \otimes I_z \mapsto \begin{bmatrix} \frac{1}{4} & 0 & 0 & 0 \\ 0 & -\frac{1}{4} & 0 & 0 \\ 0 & 0 & -\frac{1}{4} & 0 \\ 0 & 0 & 0 & \frac{1}{4} \end{bmatrix}, \end{aligned} \quad (1.46)$$

where I_{iz} measures the spin angular momentum along the z -axis of the i 'th spin and $I_{iz}I_{jz}$ measures the correlation between the z -angular momentum of spins i and j .

1.2.4 Time evolution of states

The time evolution of a generic state vector $|\psi\rangle$ is governed by the (time-dependent) *Schrödinger equation*

$$\frac{d}{dt} |\psi(t)\rangle = -i\mathcal{H}(t) |\psi(t)\rangle, \quad (1.47)$$

where the operator \mathcal{H} is the *Hamiltonian* of the system. Explicit expressions for the Hamiltonian of a spin system will be given in section 1.3. The Hamiltonian is always hermitian

$$\mathcal{H}(t) = \mathcal{H}^\dagger(t). \quad (1.48)$$

Physically the Hamiltonian describes the *total energy* of the system. The eigenstates of the Hamiltonian are called *energy eigenstates* and the eigenvalues are the *energy levels* of the system

$$\mathcal{H}(t) |n\rangle = E_n |n\rangle. \quad (1.49)$$

The energies E_n are specified in Joule [J]. It is however NMR convention to work in *natural units*. For this purpose the Hamiltonian is redefined as follows:

$$H(t) = \hbar^{-1} \mathcal{H}(t). \quad (1.50)$$

The eigenstates remain unchanged but the eigenenergies are now specified in angular frequencies [rad s^{-1}]. The term *eigenfrequencies* of the Hamiltonian is then more appropriate

$$H(t) |n\rangle = \omega_n |n\rangle. \quad (1.51)$$

For a time-dependent Hamiltonian the eigenstates and eigenvalues are in general functions of time. Their explicit time-dependence has been suppressed for simplicity.

The solution to the Schrödinger equation may be specified in terms of a *time ordered* exponential

$$|\psi(t)\rangle = \mathcal{T} \exp \left\{ -i \int_0^t H(s) ds \right\} |\psi(0)\rangle = U(t, 0) |\psi(0)\rangle. \quad (1.52)$$

Time ordering is indicated by the *Dyson time ordering* operator \mathcal{T} [25]. Formally the Dyson time ordering operator acts on the series expansion of the exponential. A time ordered exponential resulting from the solution of the Schrödinger equation is often abbreviated by $U(t, 0)$. The operator $U(t, 0)$ is called the *system propagator* as it translates the system forwards in time. It is common practice to suppress the initial time point $U(t, 0) = U(t)$ if the evolution starts at time $t = 0$.

1.2.5 Unitary transformations

Another special class of linear operators are *unitary operators*. Unitary operators are defined by the requirement that the corresponding inverse operation is given by their adjoint

$$VV^\dagger = V^\dagger V = \mathbb{1}. \quad (1.53)$$

A physical motivation may be given as follows. For *closed* quantum systems (systems that are not in contact with a thermal environment) dynamics are in principle reversible because the energy of the system is a constant. Any unitary transformation V should therefore leave the inner product of a state vector invariant

$$\langle \psi | \psi \rangle = \langle V\psi | V\psi \rangle, \quad \langle V\psi | V\psi \rangle = \langle \psi | V^\dagger V | \psi \rangle, \quad \implies V^\dagger V = \mathbb{1}. \quad (1.54)$$

A particular simple example of a unitary transformation is the propagator of the system

$$U^\dagger(t)U(t) = \mathbb{1}. \quad (1.55)$$

In general the (time-ordered) exponential of an operator $iQ(t)$, where Q is hermitian, always leads to a unitary transformation.

A small subtlety arises when working with transformations of this kind. The transformation V and the state $|\psi\rangle$ are *geometric objects* and *coordinate independent*. In other words the choice of coordinates should not matter.

When working with coordinates however the transformation of a state $|\psi\rangle$ may be understood in two distinct ways. To see this the state $|\psi\rangle$ is first expanded in terms of a given basis

$$|\psi\rangle = \left(\sum_{n=1}^{N_{\mathcal{H}}} c_n |b_n\rangle \right). \quad (1.56)$$

The transformation V may now act either on the vector coordinates c_n or the basis vectors $|b_n\rangle$. In the first case one speaks of *active* transformations whereas in the latter case one speaks of *passive* transformations.

Geometrically an active transformation "physically" moves the state vector leaving the basis vectors invariant. A passive transformation leaves the state vector invariant but moves the basis vectors. This is simply a matter of convention.

If the passive point of view is chosen the *new basis vectors* may be expressed in terms of the *old basis vectors* as follows:

$$|\tilde{b}_n\rangle = \sum_{m=1}^{N_{\mathcal{H}}} |b_m\rangle [V]_{mn}. \quad (1.57)$$

The transformed state $|\tilde{\psi}\rangle$ in terms of the new basis is then given by the expression below:

$$|\tilde{\psi}\rangle = \sum_{n=1}^{N_{\mathcal{H}}} c_n |\tilde{b}_n\rangle. \quad (1.58)$$

The coordinates c_n of the state $|\tilde{\psi}\rangle$ are unchanged and only the basis elements have been moved.

If the active point of view is chosen the *new vector components* may be expressed in terms of the *old vector components* as shown below:

$$\tilde{c}_n = [V]_{nm} c_m. \quad (1.59)$$

For the active point of view the new state $|\tilde{\psi}\rangle$ then reads as follows:

$$|\tilde{\psi}\rangle = \sum_{n=1}^{N_{\mathcal{H}}} \tilde{c}_n |b_n\rangle. \quad (1.60)$$

Here the basis vectors remain the same but the vector coordinates have changed.

In agreement with most physics literature the active point of view is chosen. So whenever an expression like $V|\psi\rangle$ is encountered it should be interpreted as the corresponding matrix-vector multiplication

$$V|\psi\rangle = \begin{bmatrix} V_{11} & V_{12} & \cdots & V_{1N_{\mathcal{H}}} \\ V_{21} & V_{22} & \cdots & V_{2N_{\mathcal{H}}} \\ \vdots & \vdots & \vdots & \vdots \\ V_{N_{\mathcal{H}}1} & V_{N_{\mathcal{H}}2} & \cdots & V_{N_{\mathcal{H}}N_{\mathcal{H}}} \end{bmatrix} \begin{bmatrix} c_1 \\ c_2 \\ \vdots \\ c_{N_{\mathcal{H}}} \end{bmatrix}. \quad (1.61)$$

With this convention it is straightforward to show that the vector coordinates \tilde{c}_n with respect to the transformed basis $|\tilde{b}_n\rangle$ are calculated by the adjoint operation $V^\dagger|\psi\rangle$.

As a consequence of the observation above the physical evolution of the system may equally well be described by an unitarily equivalent state vector $|\tilde{\psi}\rangle$

$$|\tilde{\psi}(t)\rangle = V^\dagger(t)|\psi(t)\rangle, \quad (1.62)$$

where $V^\dagger(t)$ takes the state $|\psi\rangle$ to a new (time-dependent) *reference frame* or *non-inertial frame*.

The Schrödinger equation satisfied by the transformed state vector $|\tilde{\psi}(t)\rangle$ may be derived by considering its time derivative

$$\begin{aligned}
\frac{d}{dt}|\tilde{\psi}(t)\rangle &= \frac{d}{dt} \left(V^\dagger(t) |\psi(t)\rangle \right) = \left(\frac{d}{dt} V^\dagger(t) \right) |\psi(t)\rangle + V^\dagger(t) \left(\frac{d}{dt} |\psi(t)\rangle \right) \\
&= \left(\frac{d}{dt} V^\dagger(t) - i V^\dagger(t) H(t) \right) |\psi(t)\rangle \\
&= \left(\frac{d}{dt} V^\dagger(t) - i V^\dagger(t) H(t) \right) V(t) V^\dagger(t) |\psi(t)\rangle \\
&= -i \left(V^\dagger(t) H(t) V(t) + i \left(\frac{d}{dt} V^\dagger(t) \right) V(t) \right) |\tilde{\psi}(t)\rangle \\
&= -i \tilde{H}(t) |\tilde{\psi}(t)\rangle.
\end{aligned} \tag{1.63}$$

The dynamics of the system are now governed by the *transformed Hamiltonian* \tilde{H} . The first contribution to \tilde{H} corresponds to the Hamiltonian as experienced by an observer within the new reference frame. The second contribution to \tilde{H} is an *inertial term* and describes the relative movement of the two frames.

1.3 Nuclear spin interactions

The dynamics of any quantum system are determined by the Schrödinger equation and require careful construction of the appropriate Hamiltonian. The interaction of nuclear spins with their environment and other spins is described by the *nuclear spin Hamiltonian*.

In general nuclear spins may interact with magnetic and electric fields. These may originate from external or internal perturbations. External perturbations refer to electric or magnetic fields that are applied by an apparatus, whereas internal perturbations arise from the sample itself. As illustrated in figure 1.9 spin interactions may therefore be divided into *external spin interactions* and *internal spin interactions*.

While the zoo of spin interactions is certainly large, it is useful to note that every spin interaction reduces to the same recipe

$$H_\Lambda = C_\Lambda \mathbf{I}_i \cdot W_\Lambda \cdot \mathbf{I}_j \quad \text{or} \quad H_\Lambda = C_\Lambda \mathbf{I}_i \cdot W_\Lambda \cdot \mathbf{K}, \tag{1.64}$$

where W_Λ represents a 3×3 *Cartesian tensor* or simply an *interaction tensor* and C_Λ an interaction specific constant. The interaction tensor is contracted with the Cartesian vector operators ($\mathbf{I}_i, \mathbf{I}_j$) or a Cartesian (classical) vector \mathbf{K} .

Tensors are generalisations of vectors. As such they may be represented by *tensor components* with respect to a particular coordinate system. Cartesian tensors are in

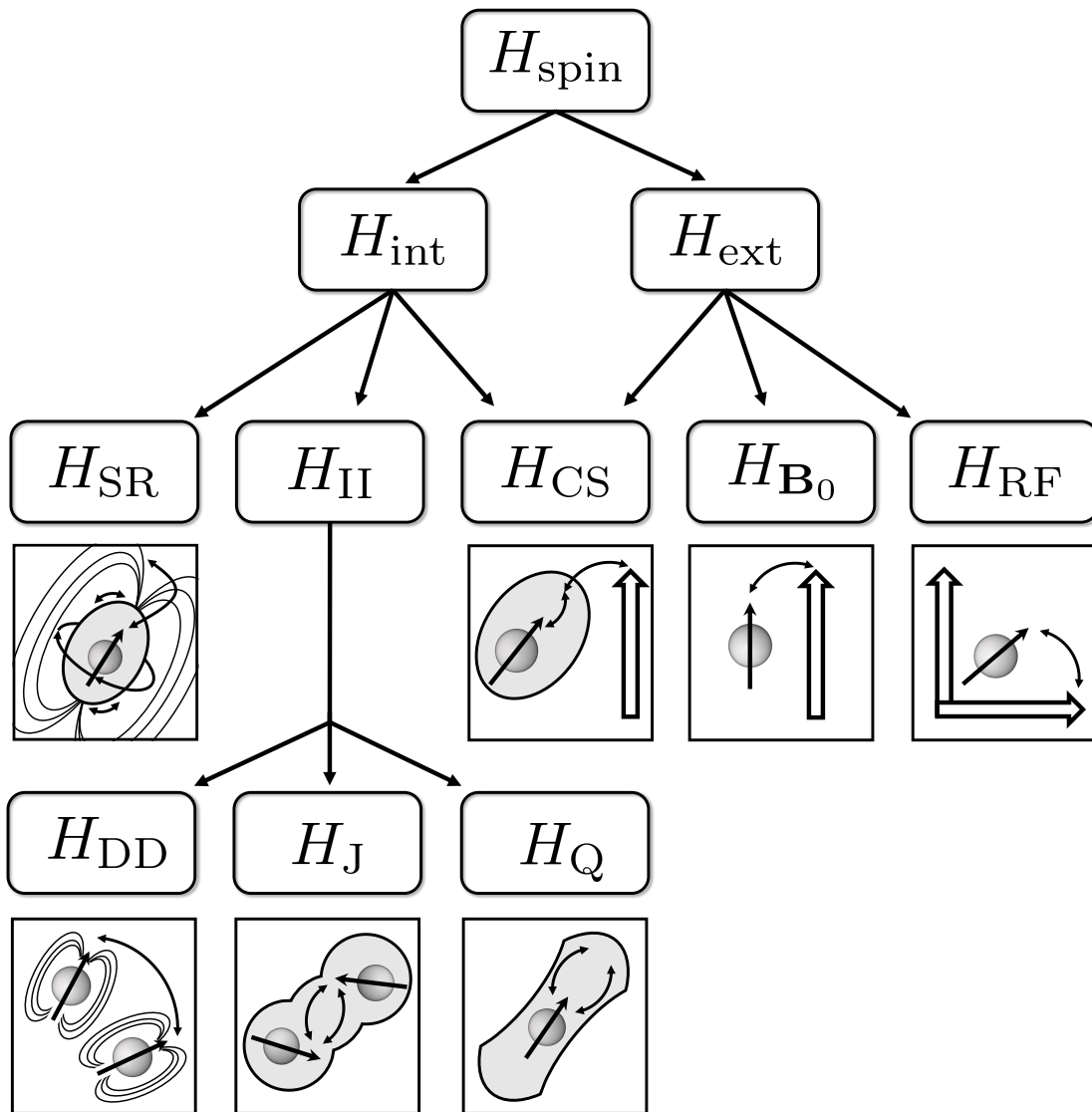


FIGURE 1.9: Overview of the most common nuclear spin interactions. The spin Hamiltonian is roughly separated into internal and external interactions. External interactions refer to the coupling of the spin angular momenta to external magnetic fields. Internal interactions refer to the coupling of spin angular momenta to their molecular environment. The spin angular momenta are represented by small spheres with an arrow. An interaction tensor is represented by shaded areas around the spin. External magnetic fields are represented by hollow arrows and dipolar magnetic fields are represented by their field lines. A detailed discussion of these interactions is given in the main text.

general specified by 9 coefficients that are conveniently collected in terms of a matrix

$$W_{\Lambda} = \begin{bmatrix} W_{xx} & W_{xy} & W_{xz} \\ W_{yx} & W_{yy} & W_{yz} \\ W_{zx} & W_{zy} & W_{zz} \end{bmatrix}. \quad (1.65)$$

The notation $W_{\mu\nu}$ for the tensor components indicates the tensor's extension into that particular Cartesian direction.

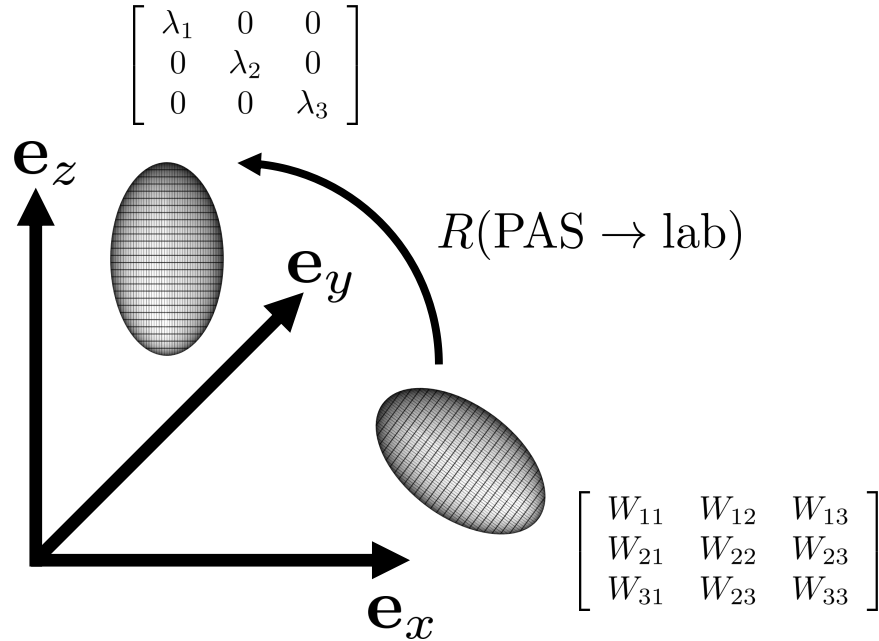


FIGURE 1.10: Graphical representation of a Cartesian interaction tensor with its corresponding matrix elements. The laboratory coordinate frame axes are indicated by $\{\mathbf{e}_x, \mathbf{e}_y, \mathbf{e}_z\}$. A Cartesian tensor may in general be specified by the extension of an ellipsoid and its orientation with respect to the laboratory coordinate frame. A suitable rotation $R(\text{PAS} \rightarrow \text{lab})$ may align the tensor and the laboratory frame axes. In this case the matrix representation of the tensor appears to be diagonal to an observer within the laboratory frame.

For (most) spin interaction tensors there exists a special coordinate system that diagonalises the interaction matrix. This coordinate system is called the *principal axes system* (PAS) and the corresponding eigenvalues are the *principal values* of the tensor.

As figure 1.10 indicates a tensor may then be visualised as an *ellipsoid* in space by making use of its principal values.

If the axes of the laboratory frame and the PAS are aligned the interaction tensor appears to be diagonal with respect to the laboratory frame. The rotation $R(\text{PAS} \rightarrow \text{lab})$ relating the two frames is only unique up to permutation of the diagonal elements. To ensure uniqueness of the rotation the diagonal elements are sorted according to the following convention

$$|\lambda_3 - W_{\text{iso}}| \geq |\lambda_1 - W_{\text{iso}}| \geq |\lambda_2 - W_{\text{iso}}| \quad \text{with} \quad W_{\text{iso}} = \frac{1}{3}\text{Tr}(W). \quad (1.66)$$

1.3.1 External spin Hamiltonian

1.3.1.1 Static magnetic field

The application of a static magnetic field leads to the Zeeman effect. The Zeeman effect describes the coupling between the spin angular momentum vector \hat{I} and the main magnetic field \mathbf{B}^0

$$H_Z = C_Z^i \mathbf{I}_i \cdot \mathbb{1} \cdot \mathbf{B}^0 = C_Z^i B_z^0 I_{iz} = \omega_i^0 I_{iz}, \quad C_Z^i = -\gamma^i. \quad (1.67)$$

Here $-\gamma_i B_z^0 = \omega_i^0$ is the Larmor frequency of the i 'th spin. It can be seen that the principal axes of the Zeeman interaction tensor coincide with the laboratory frame axes and the principal values are all 1.

1.3.1.2 Radio-frequency field

In order to manipulate the spin angular momentum a transverse radio-frequency field is applied to the sample. The transverse field is usually only applied for a short amount of time and one speaks of an RF pulse. During the RF pulse the magnetic field may be expressed as shown below:

$$\mathbf{B}_{\text{RF}}(t) = B_{\text{RF}} \cos(\omega_{\text{ref}} t + \phi_{\text{p}}) \mathbf{e}_x. \quad (1.68)$$

The transverse magnetic field oscillates at a *reference frequency* ω_{ref} along the x -axis of the laboratory frame with maximum amplitude B_{RF} . Some additional flexibility is provided by the *reference phase* ϕ_{p} . The interaction tensor and orientation is the same as for the static Hamiltonian so that the resulting Hamiltonian H_{RF} has the form

$$\begin{aligned} H_{\text{RF}}(t) &= C_{\text{RF}}^i \mathbf{I}_i \cdot \mathbb{1} \cdot \mathbf{B}_{\text{RF}}(t) \quad \text{with} \quad C_{\text{RF}}^i = -\gamma^i \\ &= C_{\text{RF}}^i B_{\text{RF}} \cos(\omega_{\text{ref}} t + \phi_{\text{p}}) I_{ix} \\ &= \omega_{\text{RF}} \cos(\omega_{\text{ref}} t + \phi_{\text{p}}) I_{ix}. \end{aligned} \quad (1.69)$$

The Hamiltonian above is complicated, but if $\omega_{\text{ref}} \approx \omega_i^0$ the transverse field may be decomposed into a *resonant*

$$H_{\text{RF}}^{\text{res}}(t) = \frac{1}{2} \omega_{\text{RF}} (\cos(\omega_{\text{ref}} t + \phi_{\text{p}}) I_{ix} + \sin(\omega_{\text{ref}} t + \phi_{\text{p}}) I_{iy}) \quad (1.70)$$

and *off-resonant* part

$$H_{\text{RF}}^{\text{off res}}(t) = \frac{1}{2} \omega_{\text{RF}} (\cos(\omega_{\text{ref}} t + \phi_{\text{p}}) I_{ix} - \sin(\omega_{\text{ref}} t + \phi_{\text{p}}) I_{iy}). \quad (1.71)$$

For conventional high-field NMR experiments the off-resonant term of the RF Hamiltonian may be neglected so that the effective RF Hamiltonian simply reduces to the

resonant part

$$H_{\text{RF}}(t) \approx H_{\text{RF}}^{\text{res}}(t) = \omega_{\text{nut}}(\cos(\omega_{\text{ref}}t + \phi_{\text{p}})I_{ix} + \sin(\omega_{\text{ref}}t + \phi_{\text{p}})I_{iy}), \quad (1.72)$$

where $\omega_{\text{nut}} = \frac{1}{2}\omega_{\text{RF}}$ refers to the nutation frequency of the RF pulse. The reasoning to introduce the term "nutation frequency" may be understood by looking at the dynamics from within a second frame rotating with frequency ω_{ref} with respect to the laboratory frame. This issue will be discussed in section 1.4.

1.3.2 Internal spin Hamiltonian

1.3.2.1 Chemical shift

The chemical shift Hamiltonian lies at the intersection of internal and external interactions. A nucleus is in general surrounded by electrons which may be understood as a local charge distribution. The static magnetic field exerts a torque onto the electron charge distribution causing the distribution to reorient in space. The resulting current induces a local magnetic field. The *induced magnetic* field \mathbf{B}_{ind} at spin site i is to a good approximation given by

$$\mathbf{B}_{\text{ind}}^i = W_{\text{CS}}^i \cdot \mathbf{B}^0, \quad (1.73)$$

where W_{CS}^i is the chemical shift tensor. The induced magnetic field is capable of interacting with the nuclear spins in a similar fashion to the static magnetic field. The chemical shift Hamiltonian therefore takes the form

$$H_{\text{CS}} = C_{\text{CS}}^i \mathbf{I}_i \cdot W_{\text{CS}}^i \cdot \mathbf{B}^0 \quad \text{with} \quad C_{\text{CS}}^i = -\gamma_i. \quad (1.74)$$

The chemical shift tensor is in general orientation dependent. It is convenient to decompose the interaction tensor into an *isotropic* part (orientation independent) and an *anisotropic* part (orientation dependent)

$$\begin{aligned} H_{\text{CS}} &= C_{\text{CS}}^i \mathbf{I}_i \cdot (W_{\text{CSI}}^i + W_{\text{CSA}}^i) \cdot \mathbf{B}^0, \\ W_{\text{CSI}}^i &= \frac{1}{3}\text{Tr}(W_{\text{CS}}^i)\mathbb{1}, \quad W_{\text{CSA}}^i = W_{\text{CS}}^i - W_{\text{CSI}}^i. \end{aligned} \quad (1.75)$$

In isotropic solutions the anisotropic part vanishes due to molecular averaging effects

$$H_{\text{CS}} \approx H_{\text{CSI}} = \delta_{\text{iso}}^i I_{iz}, \quad (1.76)$$

where the *isotropic* chemical shift is usually denoted by $\delta^{\text{iso}} = \frac{1}{3}\text{Tr}(W_{\text{CS}}^i)$. It can be seen that the isotropic chemical shift interaction influences the apparent Larmor frequency of the spins. This determines the relative peak positions in the spectrum. It is therefore common to absorb the isotropic chemical shift into the Zeeman Hamiltonian: $H_Z = H_Z + H_{\text{CSI}}$.

1.3.2.2 J-coupling

J-coupling interactions refer to *indirect* dipole-dipole interactions of nuclear spins mediated by surrounding bonding electrons. This type of interaction reflects the local electronic environment of the spins and may only be observed if the spins are separated by a small number of chemical bonds. The corresponding Hamiltonian may again be separated into an isotropic and anisotropic part

$$\begin{aligned} H_J &= C_J^{ij} \mathbf{I}_i \cdot W_J^{ij} \cdot \mathbf{I}_j = C_J^{ij} \mathbf{I}_i \cdot (W_{JI}^{ij} + W_{JA}^{ij}) \cdot \mathbf{I}_j, \\ C_J^{ij} &= 2\pi, \quad W_{JI}^{ij} = \frac{1}{3} \text{Tr}(W_J^{ij}) \mathbb{1}, \quad W_{JA}^{ij} = W_J^{ij} - W_{JI}^{ij}. \end{aligned} \quad (1.77)$$

Only the isotropic part survives for conventional liquids

$$H_J \approx H_{JI} = 2\pi \mathbf{I}_i \cdot W_{JI}^{ij} \cdot \mathbf{I}_j = 2\pi J_{ij} \mathbf{I}_i \cdot \mathbf{I}_j, \quad J_{ij} = \frac{1}{3} \text{Tr}(W_J^{ij}), \quad (1.78)$$

where J_{ij} is the *isotropic J-coupling* between spins i and j .

1.3.2.3 Dipolar coupling

Dipolar interactions or *dipole-dipole* interactions represent the direct coupling of a pair of spins through space. As illustrated in figure 1.9 each spin can be visualised as a magnetic dipole creating a local magnetic field. If two spins are sufficiently close they will experience the local dipolar fields produced of each other. The dipolar interaction Hamiltonian is constructed in analogy to the classical case

$$\begin{aligned} H_{DD} &= C_{DD}^{ij} (3(\mathbf{I}_i \cdot \mathbf{e}_{ij})(\mathbf{I}_j \cdot \mathbf{e}_{ij}) - \mathbf{I}_i \mathbf{I}_j) = C_{DD}^{ij} \mathbf{I}_i \cdot W_{DD}^{ij} \cdot \mathbf{I}_j, \\ C_{DD}^{ij} &= -\frac{\mu_0}{4\pi} \frac{\gamma_i \gamma_j \hbar}{r_{ij}^3}, \quad W_{DD}^{ij} = 3\mathbf{e}_{ij}^\dagger \otimes \mathbf{e}_{ij} - \mathbb{1}, \end{aligned} \quad (1.79)$$

where r_{ij} denotes the distance and \mathbf{e}_{ij} a unit vector between the spins i and j . The prefactor $\mu_0 = 4\pi \times 10^{-7} [\text{Hm}^{-1}]$ is the *magnetic constant*.

From the definition of the dipolar interaction tensor W_{DD}^{ij} it is straightforward to show that this tensor is traceless. This has the important consequence that dipolar interactions do not contribute to the liquid-state NMR spectrum.

1.3.2.4 Spin-rotation coupling

The *spin-rotation* interaction is somewhat similar to the chemical shift interaction. In case of the chemical shift interaction the static magnetic field sets the electron density into motion leading to an induced local magnetic field. For the spin-rotation case the movement of the molecule itself sets the charge distribution into motion (electrons and nuclei). As a consequence the molecular motion induces a local magnetic field. The

local magnetic field may be expressed in terms of a spin-rotation tensor W_{SR}^i and the angular momentum vector \mathbf{J} of the molecule

$$\mathbf{B}_{\text{ind}}^i = W_{\text{SR}}^i \cdot \mathbf{J}. \quad (1.80)$$

The interaction Hamiltonian may be defined as shown below:

$$H_{\text{SR}} = C_{\text{SR}}^i \mathbf{I}_i \cdot W_{\text{SR}}^i \cdot \mathbf{J} \quad \text{with} \quad C_{\text{CS}}^i = -\gamma_i. \quad (1.81)$$

The spin-rotation tensor is in general not traceless and does not vanish in isotropic liquids. But since the distribution of molecular angular momenta \mathbf{J} is isotropic in solution spin-rotation interactions do not lead to an observable resonance shift of the nuclear Larmor frequency.

1.3.2.5 Quadrupole coupling

For spins with $I > 1/2$ the positive charge distribution of the nucleus is not spherical (the nucleus cannot be visualised as a spherical object). This means that the nucleus displays a *nuclear quadrupole moment*. The nucleus itself is constrained by the electric potential generated by the electrons. The potential may be characterised by its spatial derivatives, the first being the *electric field* and the second being the *electric field gradient*. The nuclear quadrupole moment is capable of interacting with the electric field gradient of the electron cloud. This interaction is called *quadrupole coupling*

$$H_{\text{Q}} = C_{\text{Q}}^i \mathbf{I}_i \cdot W_{\text{Q}}^i \cdot \mathbf{I}_i \quad \text{with} \quad C_{\text{Q}}^i = \frac{eQ_i}{2I_i(2I_i - 1)\hbar}, \quad (1.82)$$

where Q_i is the nuclear quadrupole moment of the i 'th spin. The quadrupole tensor W_{Q}^i is by definition traceless and unlike other nuclear spin interactions the quadrupole coupling is *bilinear* in the spin operators. The quadrupole interactions is therefore somewhat similar to a dipole-dipole interaction "with itself."

1.4 Interaction-frame Hamiltonian

In most practical situations it is difficult to solve the Schrödinger equation with a generic Hamiltonian $H(t)$ and approximate schemes are necessary. A commonly employed technique is the *interaction frame formalism*. Here the Hamiltonian of the system is first separated into a "dominant" contribution $H_0(t)$ and a "secondary" contribution $H_1(t)$

$$H(t) = H_0(t) + H_1(t). \quad (1.83)$$

In a second step the total propagator of the system $U(t)$ is expressed as a product of the dominant term $U_0(t)$ and the secondary term $\tilde{U}_1(t)$

$$U(t) = U_0(t)\tilde{U}_1(t). \quad (1.84)$$

The necessity for the tilde in the expressions above will be explained shortly. The idea is that both $U_0(t)$ and $\tilde{U}_1(t)$ may be calculated by considering two Schrödinger equations separately. The calculation of the overall propagator has therefore been split into two subproblems. The Schrödinger equation for the $H_0(t)$ problem takes the form

$$\frac{d}{dt}U_0(t) = -iH_0(t)U_0(t) \quad (1.85)$$

and the solution is given by a time-ordered exponential

$$U_0(t) = \mathcal{T} \exp \left\{ -i \int_0^t H_0(s) ds \right\}. \quad (1.86)$$

The general strategy is to choose $H_0(t)$ as simple as possible so that an exact solution to the time-ordered exponential is available.

Naively one might expect that the $\tilde{U}_1(t)$ term may be calculated by solving the $H_1(t)$ problem, but this is false. The $\tilde{U}_1(t)$ term obeys a Schrödinger equation with a transformed Hamiltonian $\tilde{H}_1(t)$. The transformed Hamiltonian may be calculated by considering the time evolution of the transformed state vector $|\tilde{\psi}(t)\rangle = U_0^\dagger(t)|\psi(t)\rangle$. According to section 1.2.5 this transformation amounts to a time-dependent change of basis. Substitution of $H_1(t)$ and $U_0(t)$ into equation 1.63 leads to the following:

$$\begin{aligned} \frac{d}{dt}|\tilde{\psi}(t)\rangle &= -i\tilde{H}_1(t)|\tilde{\psi}(t)\rangle, \quad \tilde{H}_1(t) = \left(U_0^\dagger(t)H_1(t)U_0(t) + i \left(\frac{d}{dt}U_0^\dagger(t) \right) U_0(t) \right), \\ \implies \frac{d}{dt}\tilde{U}_1(t) &= -i\tilde{H}_1(t)\tilde{U}_1(t). \end{aligned} \quad (1.87)$$

The term "interaction frame" is justified because the Hamiltonian $\tilde{H}_1(t)$ represents the secondary contribution as viewed from within a coordinate system whose movement is determined by $H_0(t)$.

So far the complexity of the problem has not been reduced, but shifted to the $\tilde{H}_1(t)$ problem. Since $H_0(t)$ represents the dominant part of the motion, the contribution of the $\tilde{H}_1(t)$ part is often greatly suppressed inside the interaction frame of $H_0(t)$. This provides a reasonable starting point for further approximations.

In NMR a commonly encountered interaction frame is the *rotating-frame* generated by the Zeeman Hamiltonian H_Z . The idea of the rotating-frame is illustrated in figure 1.11.

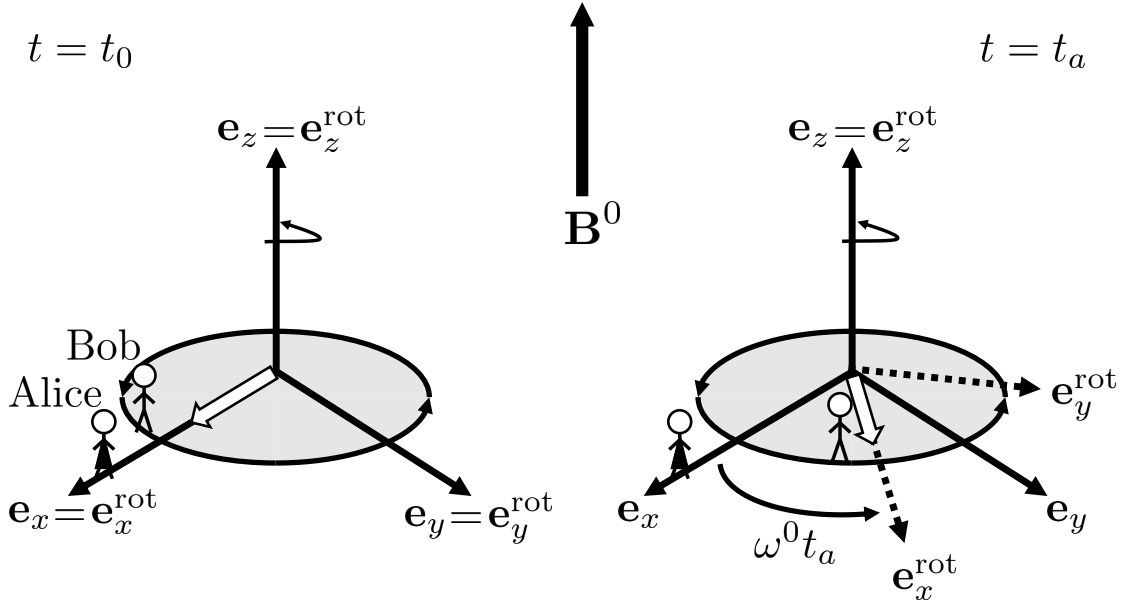


FIGURE 1.11: Geometrical interpretation of a rotating frame transformation with Larmor frequency $\omega^0 > 0$. Laboratory frame axes are labelled by $\{\mathbf{e}_x, \mathbf{e}_y, \mathbf{e}_z\}$ and rotating frame axes by $\{\mathbf{e}_x^{\text{rot}}, \mathbf{e}_y^{\text{rot}}, \mathbf{e}_z^{\text{rot}}\}$. For an observer like Bob that lives inside the rotating frame the magnetic moment appears to be static and there is no indication for the presence of a magnetic field. But an observer like Alice that lives in the laboratory frame knows that Bob is in reality rotating in synchrony with the magnetic moment restoring faith in the laws of physics.

An observer in the laboratory frame will conclude that the spin magnetic moment is rotating rapidly in the xy -plane. A second observer however, in a non-inertial frame that is rotating at the same angular frequency as the Larmor frequency ω^0 , will conclude that the spin magnetic moment is not rotating at all. From the second observer's point of view the Zeeman interaction has been "removed". This is the geometric idea of an interaction frame transformation.

The Zeeman interaction frame is commonly used to justify the absence of the off-resonant part $H_{\text{RF}}^{\text{res}}(t)$ of the radio-frequency Hamiltonian. For this setup one may identify

$$H_0(t) = \omega^0 I_z, \quad H_1(t) = 2\omega_{\text{nut}} \cos(\omega_{\text{ref}}t + \phi_p) I_x \quad \text{and} \quad V(t) = \exp\{-i\omega_{\text{ref}}t I_z\}, \quad (1.88)$$

so that the interaction frame Hamiltonian $\tilde{H}_1(t)$ takes the form

$$\begin{aligned} \tilde{H}(t) &= V^\dagger(t)H(t)V(t) - \omega_{\text{ref}}I_z \\ &= (\omega^0 - \omega_{\text{ref}})I_z + 2\omega_{\text{nut}} \cos(\omega_{\text{ref}}t + \phi_p)(\cos(\omega_{\text{ref}}t)I_x - \sin(\omega_{\text{ref}}t)I_y). \end{aligned} \quad (1.89)$$

If the reference frequency ω_{ref} is sufficiently close to the Larmor frequency $\omega^0 \sim \text{MHz}$ of the spins, the interaction frame Hamiltonian oscillates rapidly in time. A sufficient approximation of the interaction frame Hamiltonian is then provided by its time-average

over one evolution period $T = 2\pi/\omega_{\text{ref}}$

$$\tilde{H}_{\text{RF}} = \frac{\omega_{\text{ref}}}{2\pi} \int_0^{2\pi/\omega_{\text{ref}}} \tilde{H}_1(s) ds = (\omega^0 - \omega_{\text{ref}})I_z + \omega_{\text{nut}}(\cos(\phi_p)I_x + \sin(\phi_p)I_y). \quad (1.90)$$

The interaction Hamiltonian \tilde{H}_{RF} is a contribution of two terms. The first term represents the residual Larmor precession and is called frequency *off-set*. The second term can be identified as the resonant part Hamiltonian of the RF Hamiltonian (see equation 1.72) viewed from within a rotating-frame.

In the case of additional interactions the same approximations are imposed on the individual contributions leading to the so-called *rotating-frame Hamiltonian* \tilde{H}_{rot} instead of just the RF Hamiltonian.

Since most spin dynamical calculations are performed within the rotating frame it is common to simply drop the tilde $H_{\text{rot}} = \tilde{H}_{\text{rot}}$ and refer to H_{rot} as the Hamiltonian of the system.

1.5 Quantum measurements

A *quantum measurement* describes the process of extracting information from a quantum system. Quantum systems are funny in the sense that the evolution of the system is deterministic and governed by the Schrödinger equation, but the measurement process is inherently indeterministic. It is impossible to predict the exact outcome of a measurement. It is only possible to predict the probability of a certain outcome. This constitutes the *probabilistic interpretation of quantum mechanics*.

1.5.1 Single spin systems

In NMR a single spin system usually refers to the spin system of a single molecule. In this case the system may be described by a state vector $|\psi\rangle$. The evolution of $|\psi\rangle$ is described by equation 1.47.

The measurement of a physical observable A of the system $|\psi\rangle$ may result in one of the eigenvalues a_i . Assuming that the measurement returned the eigenvalue a_i the wave function collapses into the corresponding eigenstate $|a_i\rangle$. Any subsequent measurement of the observable A will then always lead to the same result a_i . No more information regarding A may be obtained. If on the other hand the system is restored to its original state $|\psi\rangle$, a second measurement of A may in general lead to observation of a different eigenvalue a_j . Continuing in this fashion allows sampling of the spectrum of the observable A .

If the measurement on the restored state $|\psi\rangle$ is performed N times and the eigenvalue

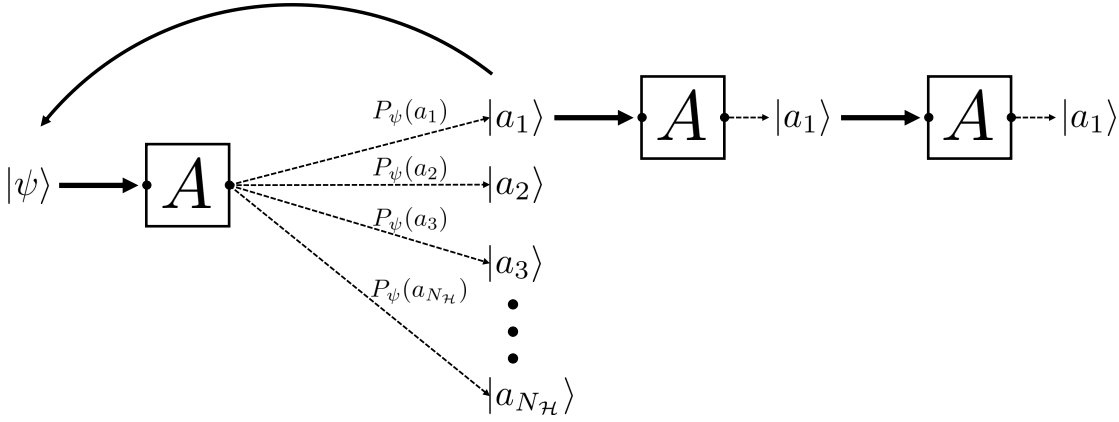


FIGURE 1.12: Quantum measurement on a single quantum system. The system is initially prepared in some state $|\psi\rangle$. The measurement of an observable A returns one of its eigenvalues a_i determined by the probability distribution $P_\psi(a_i)$. If another measurement of the observable A follows immediately no further information can be extracted as the wave function has collapsed. To extract new information from the system it has to be restored to its original state before performing the measurement.

a_i has been measured n_i times, it is possible to define the *relative frequency* of a measurement event

$$f(a_i) = \frac{n(a_i)}{N}. \quad (1.91)$$

For large N the frequency may be equated with the corresponding probability

$$\lim_{N \rightarrow \infty} f(a_i) = p(a_i), \quad (1.92)$$

where $p(a_i)$ is the probability of measuring the eigenvalue a_i .

This simple example illustrates the idea that the measurement of an observable A is characterised by a *probability distribution*. The measurement process for a single quantum system is illustrated in figure 1.12. The probability distribution is denoted by $P_\psi(a_i)$ emphasizing that it depends on the current state of the system. An explicit representation for $P_\psi(a_i)$ may be constructed by making use of the eigenvectors of A

$$P_\psi(a_i) = \langle \psi | a_i \rangle \langle a_i | \psi \rangle = |\langle a_i | \psi \rangle|^2, \quad \sum_{i=1}^{N_{\mathcal{H}}} P_\psi(a_i) = \sum_{i=1}^{N_{\mathcal{H}}} \langle \psi | a_i \rangle \langle a_i | \psi \rangle = \langle \psi | \psi \rangle = 1. \quad (1.93)$$

The state of the system and its probability distribution after measurement of an eigenvalue a_j may be expressed as follows:

$$\begin{aligned} |\psi\rangle &\mapsto |\psi'\rangle = \frac{\langle a_j | \psi \rangle}{|\langle a_j | \psi \rangle|} |a_j\rangle \quad \text{and} \quad \langle \psi' | \psi' \rangle = 1, \\ P_{\psi'}(a_i) &= \langle \psi' | a_i \rangle \langle a_i | \psi' \rangle = \langle a_j | a_i \rangle \langle a_i | a_j \rangle = \delta_{ij}, \end{aligned} \quad (1.94)$$

where the updated probability distribution $P_{\psi'}(a_i)$ indicates that subsequent measurements of A return the value a_j with a probability $p(a_j) = 1$.

A useful quantity is the *expectation value* $\langle A \rangle$ of an observable A . The expectation value of an operator is given by the statistical average of its eigenvalues.

$$\langle A \rangle = \sum_{i=1}^{N_{\mathcal{H}}} a_i P_{\psi}(a_i) = \sum_{i=1}^{N_{\mathcal{H}}} a_i \langle \psi | a_i \rangle \langle a_i | \psi \rangle = \langle \psi | A | \psi \rangle. \quad (1.95)$$

1.5.2 Spin ensemble

Conventional NMR experiments are not performed on single spin systems, but on a collection of identical (but distinguishable) spin systems. Such a collection is called a *spin ensemble* \mathcal{E} . In contrast to the previous section the NMR signal represents a *global measurement*. This means all spins are observed simultaneously.

Measurements on ensembles display some subtle differences compared to measurements on single quantum systems. In order to deal with ensembles one has to make a big assumption. Individual members of the ensemble are *non-interacting* and can be treated separately (this assumption is not true and interactions within the ensemble are the origin of spin relaxation).

The top panel of figure 1.13 illustrates a global measurement of an ensemble where every member is in the *same* quantum state $|\psi\rangle$. Such an ensemble is called a *pure state* since it can be described by a single state vector. Upon measurement of the observable A each member of the ensemble returns one of the possible eigenvalues a_i according to the probability distribution $P_{\psi}(a_i)$. In general there are n_1 systems returning the eigenvalue a_1 , n_2 systems returning the eigenvalue a_2 , etc. The global measurement $\langle A \rangle_{\text{G}}$ is the result of all individual contributions

$$\begin{aligned} \langle A \rangle_{\text{G}} &= \sum_{i=1}^{N_{\mathcal{H}}} n_i a_i \approx \sum_{k=1}^N \sum_{i=1}^{N_{\mathcal{H}}} P_{\psi_k}(a_i) a_i \\ &= \sum_{k=1}^N \langle \psi_k | A | \psi_k \rangle = \sum_{k=1}^N \langle \psi | A | \psi \rangle = N \langle A \rangle, \end{aligned} \quad (1.96)$$

where $|\psi_k\rangle$ represents the state vector of the k 'th member of the ensemble. The last equality follows from the assumption that all members occupy the same quantum state. A more convenient way to evaluate expectation values when working with ensembles is the *density operator formalism*. The *density operator* ρ of an ensemble is defined as follows:

$$\rho = N^{-1} \sum_{k=1}^N |\psi_k\rangle \langle \psi_k| = N^{-1} \sum_{k=1}^N \sigma_k, \quad (1.97)$$

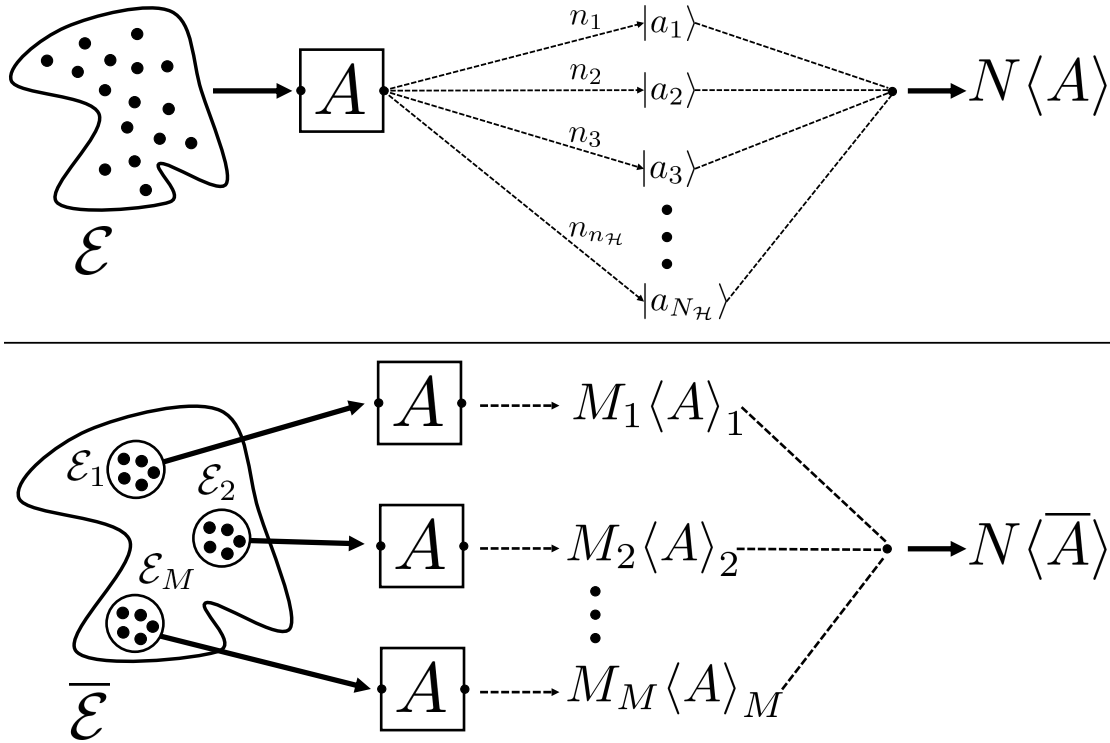


FIGURE 1.13: Global quantum measurements on a pure state (top) and a mixed state (bottom) with N particles. In a pure state \mathcal{E} all members of the ensemble \mathcal{E} are prepared in the same quantum state $|\psi\rangle$. The measurement on each individual member is performed simultaneously but may be treated according to a single quantum system. The measurement result then returns n_i times the eigenvalue a_i . The individual contributions combine to give the overall measurement result $N\langle A \rangle$. A mixed state $\bar{\mathcal{E}}$ consists of a statistical mixture of M pure states \mathcal{E}_i . When a measurement is performed on a mixed state each subensemble is treated according to the pure state case. The pure state measurement results $M_i\langle A \rangle_i$ are then combined according to their statistical weights to give the overall measurement result $N\langle \bar{A} \rangle$. The measurement process on a mixed state therefore involves two different averaging procedures.

where σ_k is the density operator for a single member of the ensemble. The calculation of a global expectation value may then be calculated as shown below:

$$\langle A \rangle_G = N \text{Tr}(A^\dagger \rho) \quad \text{with} \quad \text{Tr}(Q) = \sum_{i=1}^{N_{\mathcal{H}}} \langle i|Q|i \rangle, \quad (1.98)$$

where the trace of an operator $\text{Tr}(Q)$ is defined as the sum of its diagonal elements. In physical experiments it is rare to find a pure state. The system is usually in a *statistical mixture* or *mixed state*. A statistical mixture is constructed by mixing several pure states together. The resulting ensemble $\bar{\mathcal{E}} = \{\mathcal{E}_1, \mathcal{E}_2, \dots, \mathcal{E}_M\}$ is characterised by M subensembles \mathcal{E}_j with M_j members. A measurement of the observable A for a mixed state is illustrated at the bottom of figure 1.13. For a mixed state the measurement result is made up of contributions from all subensembles. The subensembles may again

be evaluated according to the pure state case

$$\begin{aligned}
 \langle \bar{A} \rangle_G &= \sum_{j=1}^M M_j \langle A \rangle_G^j = \sum_{j=1}^M M_j \text{Tr}(A^\dagger \sigma_j) \\
 &= N \sum_{j=1}^M w_j \text{Tr}(A^\dagger \sigma_j) = N \text{Tr}(A^\dagger \sum_{j=1}^M w_j \sigma_j) \\
 &= N \text{Tr}(A^\dagger \bar{\rho}),
 \end{aligned} \tag{1.99}$$

where the mixed state density operator $\bar{\rho}$ is a weighted combination of pure state density operators with *statistical weights* w_j

$$\bar{\rho} = \sum_{j=1}^M w_j \sigma_j, \quad w_j \geq 0 \quad \forall j \quad \text{and} \quad \sum_{j=1}^M w_j = 1. \tag{1.100}$$

Although the final results of equation 1.98 and 1.99 look similar, they represent very different things. Equation 1.99 involves two different averages. The first average is performed on each subensemble and represents a quantum mechanical average. The second average is a classical *ensemble average*. It represents the probability of finding a randomly selected ensemble member in state $|\psi_k\rangle$. To distinguish these two cases the term "weight" is chosen rather than "probability" and an "overbar" rather than "angular brackets".

Having said all of that, it is NMR convention to forget about these things and simply work with the quantities defined below:

$$\rho = N^{-1} \bar{\rho} \quad \text{and} \quad \langle A \rangle = N^{-1} \langle \bar{A} \rangle_G. \tag{1.101}$$

1.6 Time evolution of the ensemble

The equation of motion for the ensemble may be derived by considering the time derivative of the density operator

$$\begin{aligned}
 \frac{d}{dt} \rho(t) &= N^{-1} \sum_{k=1}^N \frac{d}{dt} |\psi_k(t)\rangle \langle \psi_k(t)| \\
 &= N^{-1} \sum_{k=1}^N \left(\frac{d}{dt} |\psi_k(t)\rangle \right) \langle \psi_k(t)| + |\psi_k(t)\rangle \left(\frac{d}{dt} \langle \psi_k(t)| \right).
 \end{aligned} \tag{1.102}$$

The individual members obey the Schrödinger equation (and its adjoint version for bra vectors)

$$\begin{aligned}\frac{d}{dt}\rho(t) &= -iN^{-1} \sum_{k=1}^N H_k |\psi_k(t)\rangle \langle \psi_k(t)| - |\psi_k(t)\rangle \langle \psi_k(t)| H_k \\ &= -iN^{-1} \sum_{k=1}^N [H_k, |\psi_k(t)\rangle \langle \psi_k(t)|].\end{aligned}\quad (1.103)$$

The assumption that all members of the ensemble are identical implies that they experience the same Hamiltonian $H_k = H$

$$\begin{aligned}\frac{d}{dt}\rho(t) &= -iN^{-1} \sum_{k=1}^N [H, |\psi_k(t)\rangle \langle \psi_k(t)|] \\ &= -i[H, \rho(t)].\end{aligned}\quad (1.104)$$

The resulting equation of motion is the so-called *Liouville-von-Neumann equation* (LvN equation). The solution to the Liouville-von-Neumann equation may be constructed by sandwiching the initial density operator $\rho(0)$ between the forward and backward propagator of the system

$$\rho(t) = U(t)\rho(0)U^\dagger(t) = N^{-1} \sum_{k=1}^N U(t) |\psi_k(0)\rangle \langle \psi_k(0)| U^\dagger(t). \quad (1.105)$$

The matrix elements $[\rho]_{rs}$ of a density operator ρ have a simple interpretation in the eigenbasis of the Hamiltonian H . The diagonal elements $[\rho]_{rr}$ are given by

$$\begin{aligned}\langle r|\rho(t)|r\rangle &= \langle r|U(t)\rho(0)U^\dagger(t)|r\rangle \\ &= \exp(-i\omega_r t) \langle r|\rho(0)|r\rangle \exp(i\omega_r t) \\ &= \langle r|\rho(0)|r\rangle = N^{-1} \sum_{k=1}^N \langle r|\psi_k(0)\rangle \langle \psi_k(0)|r\rangle \\ &= N^{-1} \sum_{k=1}^N p_r^k(0) = \overline{p_r(0)}.\end{aligned}\quad (1.106)$$

They represent the initial fraction of ensemble members in the eigenstate $|r\rangle$ and are therefore also called *spin populations*.

The diagonal elements $[\rho]_{r,s}$ are given by

$$\begin{aligned}
\langle r|\rho(t)|s\rangle &= \langle r|U(t)\rho(0)U^\dagger(t)|s\rangle \\
&= \exp(-i\omega_r t)\langle r|\rho(0)|s\rangle \exp(i\omega_s t) \\
&= \langle r|\rho(0)|s\rangle \exp(-i(\omega_r - \omega_s)t) \\
&= N^{-1} \sum_{k=1}^N \langle r|\psi_k(0)\rangle \langle \psi_k(0)|s\rangle \exp(-i(\omega_r - \omega_s)t) \\
&= N^{-1} \sum_{k=1}^N c_r^{k,*}(0)c_s^k(0) \exp(-i(\omega_r - \omega_s)t) \\
&= \overline{c_r^*(0)c_s(0)} \exp(-i(\omega_r - \omega_s)t).
\end{aligned} \tag{1.107}$$

They represent the presence of *superpositions* between states ($|r\rangle, |s\rangle$) across the ensemble. Superpositions indicate that two states ($|r\rangle, |s\rangle$) may *interfere* with or talk to each other. In particular they evolve in unison with time as indicated by the exponential factor. The off-diagonal elements are therefore often called *spin coherences*.

All of this would not be very useful if there was no way to determine the initial values for spin populations and coherences. The next section addresses this issue.

1.7 Thermal equilibrium

In typical NMR experiments the system is in a mixed state. Equation 1.100 however does not indicate how to choose the weights or states of the mixture. From a physical point of view it is reasonable to assume that the sample will reach a *thermal equilibrium* with its environment if it is left unperturbed for a sufficient amount of time. The term environment is vague and refers to anything that is not the sample.

Thermodynamical arguments then assure that the system obeys the *Boltzmann distribution*. The corresponding thermal equilibrium density operator ρ_{eq} for a generic spin system may then be specified as follows:

$$[\rho_{\text{eq}}]_{rr} = \frac{\exp(-\beta_\theta \omega_i)}{\sum_{i=1}^{N_{\mathcal{H}}} \exp(-\beta_\theta \omega_i)} \quad \text{and} \quad [\rho_{\text{eq}}]_{rs} = 0, \tag{1.108}$$

where the energies ω_i refer to the energy levels of the system and the temperature parameter is given by $\beta_\theta = \frac{\hbar}{k_B T}$. A more compact form for the thermal equilibrium density operator may be stated by making use of the Hamiltonian H of the system

$$\rho_{\text{eq}} = \frac{\exp\{-\beta_\theta H\}}{\text{Tr}(\exp\{-\beta_\theta H\})} \quad \text{with} \quad \text{Tr}(\rho_{\text{eq}}) = 1. \tag{1.109}$$

The Boltzmann distribution indicates that energy levels with higher energies are less likely to be occupied. This follows from the principle of *entropy maximisation*. By first occupying the lower energy states the ensemble will simply be found in more distinct

configurations.

The absence of coherences may be rationalised by a uniform distribution of phase angles at thermal equilibrium so that the ensemble average vanishes.

Chapter 2

Far from thermal equilibrium

The following material is based on reference 27.

NMR experiments are usually performed on samples which are allowed to reach thermal equilibrium in a large magnetic field, perturbed by radio-frequency pulses resonant with the Zeeman transitions in order to induce an observable electromagnetic response, and allowed to return to thermal equilibrium before the process is repeated. Under most circumstances, the behaviour of the spin system is described by a differential equation which is usually known as the *inhomogeneous master equation* (IME) and is given by [22, 28–38]

$$\frac{d}{dt}\rho(t) = -i[H_{\text{coh}}(t), \rho(t)] + \hat{\Gamma}(\rho(t) - \rho_{\text{eq}}). \quad (2.1)$$

The term H_{coh} is the *coherent part* of the spin Hamiltonian, which is uniform for all spin ensemble members. The relaxation of the spin system is described by a *relaxation superoperator*, denoted $\hat{\Gamma}$. The relaxation superoperator is constructed from the *fluctuating part* of the spin Hamiltonian, which is in general different for each member of the ensemble at a given point in time. The fluctuating part represents the interaction between ensemble members and their environment.

The last term in equation 2.1 depends on the deviation of the spin density operator from its thermal equilibrium value, and causes the density operator to reach thermal equilibrium when left unperturbed for a long time. This situation is similar to the modified Bloch equation 1.9.

Equation 2.1 has been a fixture in spin dynamical theory for a long time and its limitations have remained unnoticed for almost the same time period. In the derivation in his 1957 paper [29], Redfield used the following phrase at a key step of the derivation: “unless the system is prepared in an unusual way”.

So what is “a system prepared in an unusual way”? The discussion in the Redfield paper makes it clear that the term implies a large deviation of the density operator from thermal equilibrium, such that the density operator ventures outside the *high-temperature*

and *weak-order* approximation (see reference 30, page 288)

$$\|\hbar H_{\text{coh}}/k_B T\| \ll 1 \quad \text{and} \quad \|\rho - N^{-1}\mathbb{1}\| \ll 1, \quad (2.2)$$

where the Frobenius norm of an operator is defined by $\|A\| = \sum_{r,s} |\langle r|A|s\rangle|^2$.

In other words, equation 2.1 only applies in the high-temperature limit for spin systems which remain close to equilibrium at all times, and this restriction was well-known at the time this equation was first developed.

There is great current interest in the preparation of nuclear spin systems “in an unusual way”, i.e. far from equilibrium. Such preparations include hyperpolarised spin systems with a large level of Zeeman polarisation, enhanced with respect to thermal equilibrium polarisation by many orders of magnitude [8–19]. Typical hyperpolarisation methods include dynamic nuclear polarisation (DNP) [8–11, 39] and optical pumping [12–15]. In addition, nuclear spin systems may be prepared in states corresponding to non-equilibrium spin isomer distributions, such as hydrogen enriched in the *para* spin isomer and rapidly rotating methyl groups prepared with non-equilibrium distributions of populations between the spin isomers of the three equivalent protons [40–42]. In some circumstances these different modes of non-equilibrium spin order interconvert, leading for example to the phenomena of parahydrogen-induced hyperpolarisation, in which the non-equilibrium singlet spin order of *para*-enriched hydrogen gives rise to large magnetization components after a chemical reaction [16–19, 43], and quantum-rotor-induced polarisation (QRIP) in which non-equilibrium methyl rotor order also gives rise to enhanced NMR signals [40–42].

The IME suffers from (at least) two distinct sets of problems. For spin dynamical calculations

- the inhomogeneous character of the IME is awkward to deal with.

From a thermodynamic point of view

- the IME is restricted to the high-temperature and weak-order regime.
- the IME does not correctly predict the observed build-up of longitudinal magnetization for spin systems that are far from equilibrium.
- the IME does not handle the relaxation of coherences correctly.

To overcome at least some of these issues several alternative master equations have been proposed, each of which have the form of a *homogeneous* differential equation, of the type:

$$\frac{d}{dt}\rho(t) = -i[H_{\text{coh}}(t), \rho(t)] + \hat{\Gamma}^\theta \rho(t), \quad (2.3)$$

where $\hat{\Gamma}^\theta$ is a “thermalised” variant of the relaxation superoperator $\hat{\Gamma}$, adjusted in such a way that the spin density operator ρ tends to the correct thermal equilibrium value

ρ_{eq} in thermal equilibrium with the environment [44–47].

However as shown below the proposed solutions are not able to resolve all the raised issues. The aim of this chapter is to discuss the construction of an alternative HME which does not suffer from these restrictions and most importantly retains validity for spin systems far from equilibrium. In order to achieve this, a departure from the *semi-classical* approach to relaxation theory, which is almost universal in standard texts on magnetic resonance, is considered [22, 33–37].

2.1 Theoretical Background

The theoretical background of NMR relaxation theory is reviewed briefly in order to establish the notation and to resolve ambiguities in some of the key terms.

2.1.1 Liouville space

While the state $|\psi\rangle$ of a system is an element of a Hilbert space \mathcal{H} , the density operator ρ is an element of the space of linear operators on \mathcal{H} denoted by \mathcal{L} and referred to as *Liouville space*. The description of NMR relaxation phenomena is most easily carried out within Liouville space. The dimension of the corresponding Liouville space is $N_{\mathcal{L}} = N_{\mathcal{H}}^2$. An operator O may then be then regarded as a vector of length $N_{\mathcal{L}}$ in this space and is denoted $|O\rangle$. The inner product between any two operators (called the *Liouville bracket*) is defined as follows:

$$(M|N) = \text{Tr}\{M^\dagger N\}. \quad (2.4)$$

One may always choose a set of orthonormal $N_{\mathcal{L}}$ basis operators $\{|O_p\rangle\}$ with $p \in \{1, 2 \dots N_{\mathcal{L}}\}$

$$(O_p|O_q) = \delta_{pq}. \quad (2.5)$$

Such a set of operators constitutes a basis for \mathcal{L} .

2.1.1.1 Superoperators

In analogy to operators a superoperator \hat{A} transforms an operator $|Q\rangle$ into a different operator $|Q'\rangle$ [44, 48]. The following superoperators play a particular important role in relaxation theory:

1. The *left-multiplication superoperator* is denoted here by $M\bullet$, where the bullet symbol \bullet is a placeholder for an operator argument. The superoperator $M\bullet$ multiplies its operand by an operator from the left, as follows:

$$(M\bullet)|O\rangle = |MO\rangle. \quad (2.6)$$

2. The *right-multiplication superoperator* is denoted here by $\bullet M$, and multiplies its operand by an operator from the right, as follows:

$$(\bullet M)|O\rangle = |OM\rangle. \quad (2.7)$$

3. The *commutation superoperator* is defined as follows:

$$\hat{M} = (M\bullet) - (\bullet M) \quad (2.8)$$

such that

$$\hat{M}|N\rangle = |[M, N]\rangle = |MN - NM\rangle. \quad (2.9)$$

In the following discussion, a symbol of the form \hat{M} implies a general superoperator of unspecified type, unless M is already defined as the symbol for an operator, in which case \hat{M} implies the commutation superoperator of the operator M .

The matrix representation of a superoperator in a particular operator basis has matrix elements defined as follows:

$$[\hat{M}]_{rs} = (O_r|\hat{M}|O_s) = \text{Tr}[O_r^\dagger \hat{M} O_s]. \quad (2.10)$$

2.1.2 Spin Hamiltonian

Section 1.3 discussed some of the more relevant nuclear spin interactions. For the purposes of NMR relaxation theory these interactions are organised as shown in figure 2.1. The spin Hamiltonian is then expressed as a sum of *coherent* and *fluctuating* contributions:

$$H(t) = H_{\text{coh}}(t) + H_{\text{fluc}}(t). \quad (2.11)$$

The coherent part is assumed to be the same for each member of the ensemble, whereas the fluctuating part may differ for ensemble members at a given point in time, and is responsible for the relaxation of the system. For typical solution-state NMR experiments the coherent part consists of Zeeman, chemical shift and scalar coupling interactions.

2.1.2.1 Coherent Hamiltonian

The discussion below makes extensive use of a division of the coherent Hamiltonian into three parts, called H_A , H_B and H_C , as follows:

$$H_{\text{coh}}(t) = H_A + H_B + H_C(t). \quad (2.12)$$

The properties of these three terms are as follows:

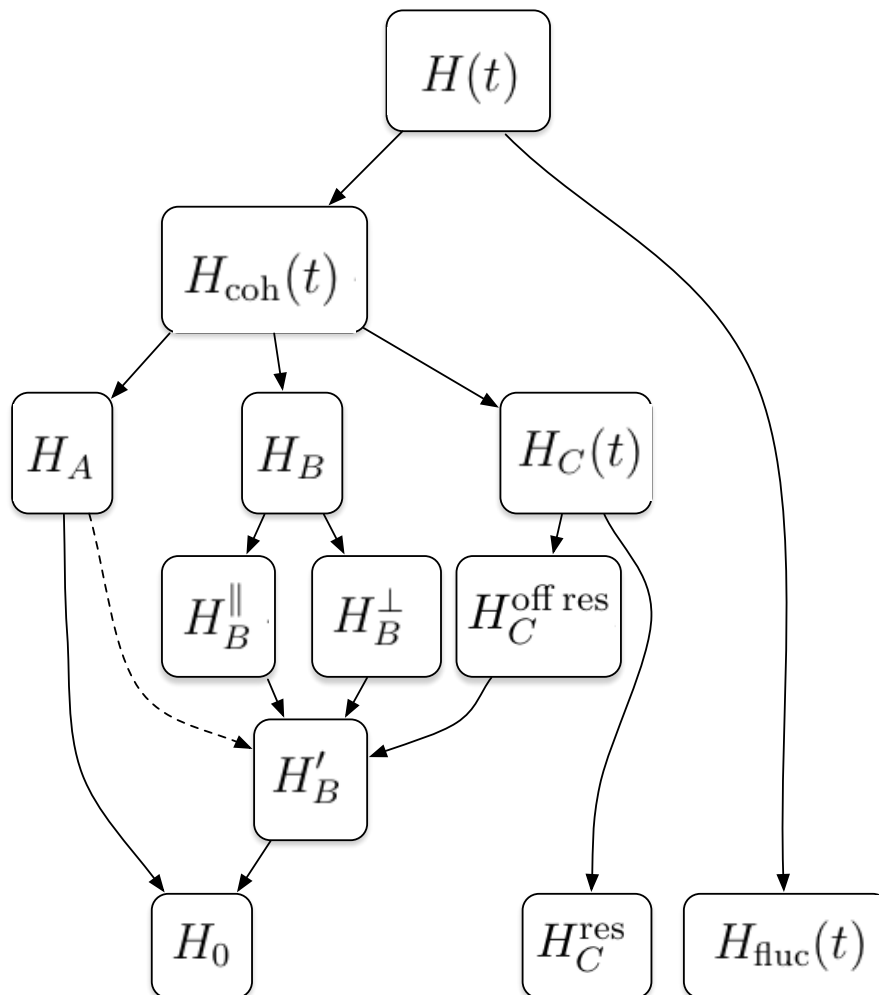


FIGURE 2.1: The organisation of spin Hamiltonian terms used in this article. The Hamiltonian $H(t)$ consists of a coherent term $H_{\text{coh}}(t)$ and a fluctuating term $H_{\text{fluc}}(t)$. The coherent term contains a dominant part H_A , a static (or quasi-static) perturbation H_B , and a time-dependent perturbation $H_C(t)$. The static perturbation may be decomposed into a secular part H_B^{\parallel} which commutes with H_A , and a non-secular part H_B^{\perp} , which does not. The time-dependent perturbation H_C may be divided into a resonant part H_C^{res} and an off-resonant part $H_C^{\text{off res}}$. Standard approximations lead to a corrected perturbation H'_B which commutes with H_A . The main coherent Hamiltonian H_0 is constructed by adding H_A and H'_B .

- *The dominant Hamiltonian H_A .* The term H_A is much larger than the H_B , H_C and H_{fluc} terms:

$$\|H_A\| \gg \|H_B\|, \|H_C\|, \|H_{\text{fluc}}\|. \quad (2.13)$$

The operators H_B and H_C may therefore be regarded as perturbations to the dominant Hamiltonian H_A . To proceed with the discussion the eigenvalues of H_A are assumed to be either degenerate or widely spaced compared to the corresponding matrix elements of the perturbations H_B and H_C in the eigenbasis of H_A (see figure 2.2). This strong constraint on the eigenvalue spectrum of H_A is very important and underpins much of the theory described below. The eigenvalues and

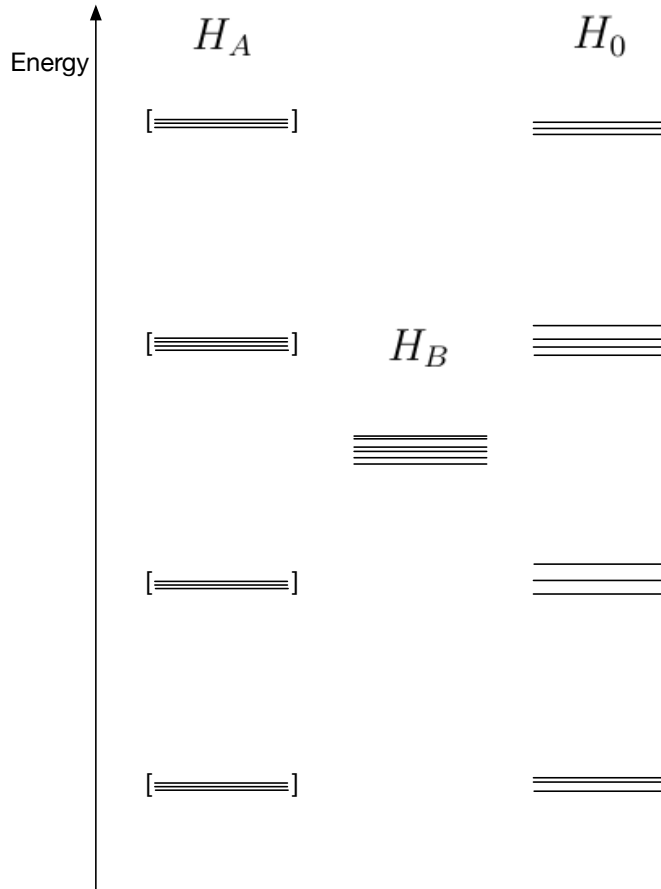


FIGURE 2.2: Schematic eigenvalue spectra of the coherent Hamiltonian terms H_A and H_B . Degenerate eigenvalues are indicated by square brackets. The eigenvalue spectrum of H_A consists of degenerate or widely-spaced eigenvalues, such that the eigenvalue spacing is large compared to $\|H_B\|$, and also $\|H_C\|$ and $\|H_{\text{fluc}}\|$ (not shown). Degeneracy is broken when H_0 is constructed by combining H_A and H_B , after correction for non-secular and off-resonant contributions (equation 2.22).

eigenstates of the dominant term H_A are denoted by ω_r^A and $|r\rangle^A$ respectively

$$H_A |r\rangle^A = \omega_r^A |r\rangle^A. \quad (2.14)$$

The perturbations H_B and H_C are both assumed to fulfill the following condition

$$\langle r|^A H_B |s\rangle^A, \langle r|^A H_C(t) |s\rangle^A \ll |\omega_r^A - \omega_s^A| \quad \forall \omega_r^A \neq \omega_s^A. \quad (2.15)$$

Equation 2.15 implies that the matrix representations of H_B and H_C , expressed in the eigenbasis of H_A , has off-diagonal terms which are either between degenerate states of H_A , or which are always small in magnitude compared to the corresponding separation of non-degenerate H_A eigenvalues.

In typical high-field NMR experiments, H_A represents the dominant Zeeman interaction with a strong external magnetic field. However in some cases, a different Hamiltonian, such as an exchange interaction, is assigned to the H_A term.

- *The (quasi)static perturbation term H_B .* The term H_B is assumed to be small in magnitude with respect to H_A (equation 2.13) and either time-independent or with a slow time-dependence. The latter condition may be written as follows:

$$\left| \frac{d}{dt} \langle r |^A H_B | s \rangle^A \right| \ll |\omega_r^A - \omega_s^A| \quad \forall \omega_r^A \neq \omega_s^A. \quad (2.16)$$

In typical high-field NMR applications, the term H_B contains spin-spin couplings, chemical shift terms, and interactions with time-varying fields such as magnetic field gradient pulses. In solid-state NMR, anisotropic spin interactions such as chemical shift anisotropies, quadrupolar interactions, and dipole-dipole couplings are also included. These terms may acquire a slow time-dependence satisfying equation 2.16 through sample rotation. Since the eigenvalues of H_A are combinations of the Larmor frequencies for the nuclides in the spin system, equation 2.15 implies the validity of a high-field approximation for the nuclear spin Hamiltonian.

The H_B term may be further subdivided into a “secular” term H_B^{\parallel} and a “non-secular” term H_B^{\perp} :

$$H_B = H_B^{\parallel} + H_B^{\perp}, \quad (2.17)$$

where H_B^{\parallel} commutes with H_A

$$[H_A, H_B^{\parallel}] = 0, \quad (2.18)$$

while H_B^{\perp} does not

$$[H_A, H_B^{\perp}] \neq 0. \quad (2.19)$$

- *The time-dependent perturbation term $H_C(t)$.* The term H_C is also small in magnitude with respect to H_A (equation 2.13) but has a rapid time-dependence such that the following condition is satisfied

$$\left| \frac{d}{dt} \langle r |^A H_C(t) | s \rangle^A \right| \not\ll |\omega_r^A - \omega_s^A| \quad \forall \omega_r^A \neq \omega_s^A. \quad (2.20)$$

In typical NMR experiments, $H_C(t)$ includes the interaction of the spin system with a radio-frequency field. The $H_C(t)$ term may be further divided into the resonant term $H_C^{\text{res}}(t)$ and the off-resonant term $H_C^{\text{off res}}(t)$.

Since equation 2.15 is assumed to be satisfied, the “non-secular” term H_B^{\perp} may either be ignored, or treated approximately by a small correction to the eigenvalues of H_B^{\parallel} . The off-resonant term $H_C^{\text{off res}}(t)$ also gives rise to small shifts which may be taken into account through a small correction to H_B . For simplicity it is assumed that any non-secular corrections induced by H_B^{\perp} , and any off-resonance shifts induced by $H_C^{\text{off res}}$ (for example, Bloch-Siegert shifts [49]), are incorporated into a corrected version of H_B ,

denoted H'_B , which commutes with H_A

$$[H_A, H'_B] = 0. \quad (2.21)$$

The main part of the coherent Hamiltonian, denoted here H_0 , is now constructed by combining the H_A and H'_B terms

$$H_0 = H_A + H'_B. \quad (2.22)$$

Since the operators H_A and H_0 commute

$$[H_A, H_0] = 0, \quad (2.23)$$

it is possible to define a set of states that form a simultaneous eigenbasis of both operators. The states which form this simultaneous eigenbasis are denoted $\{|1\rangle \dots |N_{\mathcal{H}}\rangle\}$, where $N_{\mathcal{H}}$ is the dimension of \mathcal{H} . The corresponding eigenequations are as follows:

$$H_0 |r\rangle = \omega_r |r\rangle, \quad H_A |r\rangle = \omega_r^A |r\rangle. \quad (2.24)$$

Note that although the eigenvalues ω_r^A of H_A are the same as in equation 2.14, the set of eigenstates $|r\rangle$ may not be identical to the set of eigenstates $|r\rangle^A$, since eigenstates belonging to degenerate subspaces of H_A may be mixed by the H_B term.

The H_0 eigenstates may be used to define a set of transition operators (or shift operators) X_{rs} , as follows:

$$X_{rs} = |r\rangle\langle s|, \quad (2.25)$$

where the states $|r\rangle$ satisfy equation 2.24. The operator X_{rs} converts the state $|s\rangle$ into the state $|r\rangle$. There are $N_{\mathcal{L}} = N_{\mathcal{H}}^2$ transition operators since the indices r and s both run from 1 to $N_{\mathcal{H}}$.

The set of all eigenstate transition operators $\{X_{rs}\}$ forms an orthonormal operator basis of Liouville space, being orthonormal in both indices

$$(X_{rs}|X_{kl}) = \delta_{rk}\delta_{sl}. \quad (2.26)$$

The eigenstate transition operators X_{rs} are eigenoperators of the commutation superoperator of H_0

$$\hat{H}_0 |X_{rs}) = \omega_{rs} |X_{rs}) \quad (2.27)$$

and the transition frequencies are given by

$$\omega_{rs} = \omega_r - \omega_s. \quad (2.28)$$

The eigenstate transition operators X_{rs} are also eigenoperators of the commutation superoperator of H_A , but with different eigenvalues

$$\hat{H}_A |X_{rs}\rangle = \omega_{rs}^A |X_{rs}\rangle, \quad (2.29)$$

where

$$\omega_{rs}^A = \omega_r^A - \omega_s^A. \quad (2.30)$$

In the case that H_A is chosen to be the Zeeman Hamiltonian for the spin system, the eigenvalues ω_{rs}^A are given by linear combinations of the nuclear Larmor frequencies of the relevant nuclides.

The transition operators X_{rs} have inconvenient rotational properties which derive from the complexity and low rotational symmetry of the operator H_B . It proves convenient to define a new orthonormal eigenoperator basis for \hat{H}_A , with operators $|A_\alpha\rangle$ satisfying the eigenequation

$$\hat{H}_A |A_\alpha\rangle = \omega_\alpha^A |A_\alpha\rangle. \quad (2.31)$$

The eigenvalues are denoted ω_α^A with $\alpha \in \{0, 1 \dots N_{\mathcal{L}}\}$. Each eigenvalue ω_α^A corresponds to one of the frequencies ω_{rs}^A in equation 2.30, and each eigenoperator may be expressed as a linear superposition of transition operators with the same eigenvalue of \hat{H}_A

$$|A_\alpha\rangle = \sum_{r=1}^{N_{\mathcal{H}}} \sum_{s=1}^{N_{\mathcal{H}}} |X_{rs}\rangle (X_{rs} |A_\alpha\rangle) \times \delta(\omega_{rs}^A - \omega_\alpha^A), \quad (2.32)$$

where $\delta(x) = 1$ for $x = 0$ and 0 otherwise.

It is desirable to choose eigenoperators $\{|A_1\rangle \dots\}$ which have convenient properties under three-dimensional rotations of the nuclear spin angular momenta. Whether this is possible depends on the commutation properties of the dominant Hamiltonian H_A .

In high-field NMR, the dominant Hamiltonian H_A is usually identified with the Zeeman Hamiltonian, ignoring any chemical shifts or other perturbations:

$$\text{high-field NMR:} \quad H_A = H_Z, \quad (2.33)$$

$$H_Z = \sum_{i=1}^N \omega_i^0 I_{iz}. \quad (2.34)$$

The commutation properties of H_A are different for homonuclear and heteronuclear systems:

- In *homonuclear* systems (all nuclides of the same type), all Larmor frequency terms ω_i^0 are identical, and hence H_A is proportional to the total angular momentum operator along the z -axis, $I_z = \sum_{i=1}^N I_{iz}$. In this case H_A commutes with the

total spin angular momentum along the field, and also the total square angular momentum of all nuclei

$$[H_A, I_z] = [H_A, I^2] = 0, \quad (2.35)$$

where $I^2 = I_x^2 + I_y^2 + I_z^2$ and $I_\nu = \sum_{i=1}^N I_{i\nu}$; $\nu \in \{x, y, z\}$. Hence, each eigenoperator $|A_\alpha\rangle$ may be identified with an *irreducible spherical tensor operator* (ISTO) $|T_{\lambda\mu}^\alpha\rangle$

$$|A_\alpha\rangle = c_\alpha |T_{\lambda\mu}^\alpha\rangle \quad (2.36)$$

obeying the following standard eigenequations:

$$\begin{aligned} \hat{I}^2 |T_{\lambda\mu}^\alpha\rangle &= \lambda_\alpha(\lambda_\alpha + 1) |T_{\lambda\mu}^\alpha\rangle, \\ \hat{I}_z |T_{\lambda\mu}^\alpha\rangle &= \mu_\alpha |T_{\lambda\mu}^\alpha\rangle, \\ \hat{I}^2 &= (\hat{I}_x)^2 + (\hat{I}_y)^2 + (\hat{I}_z)^2. \end{aligned} \quad (2.37)$$

Here \hat{I}_x is the commutation superoperator of the total angular momentum along the x -axis, $I_x = \sum_{i=1}^N I_{ix}$, and similarly for the y and z -operators [44]. Note that $(\hat{I}_x)^2$ is *not* the same superoperator as $\sum_{i=1}^N \hat{I}_{ix}^2$. The rotational rank and azimuthal quantum number of the eigenoperator $|A_\alpha\rangle$ are denoted λ_α and μ_α respectively. The normalization factor c_α in equation 2.36 ensures that $\langle A_\alpha | A_\alpha \rangle = 1$.

- In *heteronuclear* systems, the Zeeman Hamiltonian does not commute with the total square angular momentum operator of all spins but with the total square angular momentum operators of individual groups of spins, organized by their isotopic types $\{I, S, \dots\}$. If the numbers of spins of the different isotopic types are denoted $\{N_I, N_S, \dots\}$, the relevant z -angular momentum operators are denoted $I_z = \sum_{i=1}^{N_I} I_{iz}$, $S_z = \sum_{s=1}^{N_S} S_{sz}$, etc. and the total-square angular momentum operators by:

$$I^2 = \sum_{i=1}^{N_I} (I_{ix}^2 + I_{iy}^2 + I_{iz}^2), \quad S^2 = \sum_{s=1}^{N_S} (S_{sx}^2 + S_{sy}^2 + S_{sz}^2). \quad (2.38)$$

The following commutation relationships apply:

$$\begin{aligned} [H_A, I_z] &= [H_A, I^2] = [H_A, S_z] = [H_A, S^2] = 0 \quad \dots, \\ [I_z, S_z] &= [I^2, S^2] = 0 \quad \dots \end{aligned} \quad (2.39)$$

An appropriate set of \hat{H}_A eigenoperators is given by the tensor product of the individual spherical tensor operator sets

$$\{A_\alpha\} = \{T_{\lambda,\mu}^I\} \otimes \{T_{\lambda,\mu}^S\} \otimes \dots \quad (2.40)$$

Each eigenoperator has the form

$$|A_\alpha\rangle = c_\alpha \left| T_{\lambda,\mu}^{I,\alpha} T_{\lambda,\mu\dots}^{S,\alpha} \right\rangle, \quad (2.41)$$

with a set of rotational ranks $\{\lambda_\alpha^I, \lambda_\alpha^S \dots\}$ and azimuthal quantum numbers $\{\mu_\alpha^I, \mu_\alpha^S \dots\}$ for the spin species $\{I, S \dots\}$.

2.1.2.2 Fluctuating Hamiltonian

The fluctuating Hamiltonian H_{fluc} , which is responsible for spin relaxation, typically contains contributions from several different nuclear spin interactions

$$H_{\text{fluc}}(t) = H_{\text{fluc}}^{\Lambda_1}(t) + H_{\text{fluc}}^{\Lambda_2}(t) + \dots \quad (2.42)$$

The interactions $\{\Lambda_1, \Lambda_2 \dots\}$ typically include nuclear dipole-dipole interactions, chemical shift anisotropies, etc. The random fluctuations of these interactions, due to molecular motion, are responsible for nuclear spin relaxation. In general, the fluctuations of different interactions are correlated with each other.

Each fluctuating Hamiltonian term may be expressed as a superposition of \hat{H}_A eigenoperators, as follows:

$$|H_{\text{fluc}}^\Lambda(t)\rangle = \sum_\alpha F_\alpha^\Lambda(t) |A_\alpha\rangle, \quad (2.43)$$

where the coefficients are defined as follows:

$$F_\alpha^\Lambda(t) = (A_\alpha | H_{\text{fluc}}^\Lambda(t)) \quad (2.44)$$

and have the following *correlation functions*:

$$G_{\alpha\alpha'}^{\Lambda\Lambda'}(\tau) = \overline{F_\alpha^{\Lambda*}(t+\tau) F_{\alpha'}^{\Lambda'}(t)} \quad (2.45)$$

The overbar indicates the ensemble average. The correlation functions $G_{\alpha\alpha'}^{\Lambda\Lambda'}(\tau)$ are assumed to be independent of t (stationary assumption)

$$G_{\alpha\alpha'}^{\Lambda\Lambda'}(\tau) = G_{\alpha\alpha'}^{\Lambda\Lambda'}(0) g_{\alpha\alpha'}^{\Lambda\Lambda'}(\tau) \quad \text{with} \quad g_{\alpha\alpha'}^{\Lambda\Lambda'}(0) = 1 \quad (2.46)$$

and to decay monotonically with increasing τ . For most physical situations the correlation functions become vanishingly small for τ larger than an interval called the *correlation time* denoted τ_c . In general the correlation time may be different for different mechanisms, but this complication will be overlooked, for the sake of simplicity.

In the case of rotational diffusion, the correlation functions may be shown to decay approximately exponentially [50], with the following form

$$g_{\alpha\alpha'}^{\Lambda\Lambda'}(\tau) \simeq \exp\{-|\tau|/\tau_c\} \quad \text{with} \quad \tau_c > 0. \quad (2.47)$$

For simplicity we assume that the correlation time is independent of the interaction and eigenoperator indices.

The spectral density functions is defined as the Fourier transform of the correlation functions

$$j_{\alpha\alpha'}^{\Lambda\Lambda'}(\omega) = \int_{-\infty}^{\infty} g_{\alpha\alpha'}^{\Lambda\Lambda'}(\tau) \exp\{i\omega\tau\} d\tau. \quad (2.48)$$

For an exponential correlation function (equation 2.47), the real part of the spectral density has the simple form of an absorption-mode Lorentzian

$$\text{Re}\{j_{\alpha\alpha'}^{\Lambda\Lambda'}(\omega)\} = \frac{2\tau_c}{1 + \omega^2\tau_c^2}. \quad (2.49)$$

An alternative approach is to expand the fluctuating Hamiltonian in transition operators as follows:

$$|H_{\text{fluc}}^{\Lambda}(t)\rangle = \sum_{r,s} \langle r| H_{\text{fluc}}^{\Lambda}(t)|s\rangle |X_{rs}\rangle. \quad (2.50)$$

The correlation functions of the fluctuating matrix elements are defined as follows:

$$G_{ijkl}^{\Lambda\Lambda'}(\tau) = \overline{\langle i| H_{\text{fluc}}^{\Lambda}(t+\tau)|j\rangle \langle k| H_{\text{fluc}}^{\Lambda'}(t)|l\rangle}, \quad (2.51)$$

which are again assumed to be independent of t due to stationarity. The spectral density functions of the transition matrix elements are defined as follows:

$$J_{ijkl}(\omega) = \sum_{\Lambda,\Lambda'} J_{ijkl}^{\Lambda\Lambda'}(\omega), \quad (2.52)$$

from which the contributions of the individual correlation functions are given by

$$J_{ijkl}^{\Lambda\Lambda'}(\omega) = \int_{-\infty}^{\infty} G_{ijkl}^{\Lambda\Lambda'}(\tau) \exp\{i\omega\tau\} d\tau. \quad (2.53)$$

Their real parts are again proportional to absorption-mode Lorentzians, as in equation 2.49.

2.1.3 Equation of Motion

The time evolution for a single member of the ensemble in Liouville space may be expressed as follows:

$$\frac{d}{dt} |\sigma(t)\rangle = -i\hat{H}(t) |\sigma(t)\rangle, \quad \hat{H}(t) = \hat{H}_0 + \hat{H}_C^{\text{res}} + \hat{H}_{\text{fluc}}(t) \quad (2.54)$$

and the solution is given by a time-ordered exponential superoperator

$$|\sigma(t)\rangle = \hat{U}(t) |\sigma(0)\rangle, \quad \hat{U}(t) = \hat{T} \exp \left\{ -i \int_0^t \hat{H}(s) ds \right\}. \quad (2.55)$$

The evolution of the ensemble may be determined by performing an ensemble average. After the ensemble average the evolution of the system may be approximated by an equation of the type [51]

$$|\rho(t)\rangle = \hat{V}(t) |\rho(0)\rangle, \quad (2.56)$$

but the propagation superoperator \hat{V} is in general not unitary. The primary aim of relaxation theory is the systematic construction of \hat{V} valid within appropriate limits. [28–30, 51–58]

2.2 Semi-classical relaxation theory

The semi-classical relaxation theory of nuclear spin systems is widely covered in the standard literature [28, 30, 32–37]. To underpin the later discussion however a concise overview of the basic concepts and key approximations is necessary.

2.2.1 Semi-classical relaxation superoperator

In order to prepare for the application of second-order perturbation theory, the spin Hamiltonian is expressed in the interaction frame of the dominant part of the coherent Hamiltonian H_A

$$\tilde{H}(t) = \exp\{+i\hat{H}_A t\} H(t). \quad (2.57)$$

In the case that H_A is identified with the Zeeman Hamiltonian the interaction frame is the usual rotating frame.

The LvN equation, in the interaction frame, is given by

$$\frac{d}{dt} |\tilde{\sigma}(t)\rangle = -i\tilde{H}(t) |\tilde{\sigma}(t)\rangle, \quad \tilde{H}(t) = \tilde{H}_{\text{coh}} + \tilde{H}_{\text{fluc}}(t), \quad (2.58)$$

with the interaction-frame fluctuating Hamiltonian

$$\tilde{H}_{\text{fluc}}(t) = \exp\{+i\hat{H}_A t\} H_{\text{fluc}}(t) \quad (2.59)$$

and the interaction-frame coherent Hamiltonian

$$\tilde{H}_{\text{coh}}(t) = H_0 - H_A + \tilde{H}_C^{\text{res}}(t). \quad (2.60)$$

The solution to the LvN equation for the time evolution of individual ensemble members may be approximated by time-dependent perturbation theory [26, 30, 32–37, 59]. The following standard approximations and assumptions are made:

- The density operator and the fluctuating contributions are statistically independent (uncorrelated).
- The ensemble average of the fluctuating contributions vanishes.
- The fluctuating contributions represent a weakly stationary process, so that two-time correlations only depend on their time difference $t' - t = \tau$.
- There exists a correlation time τ_C such that the ensemble average of the random fluctuations becomes negligible for time differences $\tau \gg \tau_C$.
- The terms H_B , H_C and H_{fluc} are all sufficiently small that $\|H_B\tau_C\| \ll 1$, $\|H_C\tau_C\| \ll 1$ and $\|H_{\text{fluc}}\tau_C\| \ll 1$, so that the interaction frame density operator does not change significantly over the timescale of τ_C .

It is important to note that the set of assumptions above do *not* include the spin system being close to equilibrium. So even if the spin system is far from equilibrium the evolution of the ensemble-average density operator in the interaction frame may be approximated by

$$\frac{d}{dt} |\tilde{\rho}(t)\rangle = \hat{\mathcal{L}}_{\text{SC}}(t) |\tilde{\rho}(t)\rangle, \quad (2.61)$$

where the semi-classical Liouvillian superoperator, in the interaction frame, is given by

$$\hat{\mathcal{L}}_{\text{SC}} = -i\hat{H}_{\text{coh}} + \hat{U}_A^\dagger(t) \hat{\Gamma}_{\text{SC}}^{\text{lab}} \hat{U}_A(t) \quad (2.62)$$

and the relaxation superoperator in the laboratory frame is as follows [28, 29]:

$$\hat{\Gamma}_{\text{SC}}^{\text{lab}} = - \int_{-\infty}^0 \overline{\hat{H}_{\text{fluc}}(0) \hat{H}_{\text{fluc}}(\tau)} d\tau. \quad (2.63)$$

If small *dynamic frequency shifts* are neglected [26, 28–30, 59], this may be written as follows:

$$\hat{\Gamma}_{\text{SC}}^{\text{lab}} = -\frac{1}{2} \sum_{\Lambda, \Lambda'} \sum_{\alpha, \alpha'} J_{\alpha\alpha'}^{\Lambda\Lambda'}(\omega_{\alpha'}^A) \hat{A}_\alpha \hat{A}_{\alpha'}^\dagger. \quad (2.64)$$

An alternative expression, making use of the transition operators between the eigenstates of the Hamiltonian H_0 , is as follows:

$$\hat{\Gamma}_{\text{SC}}^{\text{lab}} = -\frac{1}{2} \sum_{i,j,k,l} J_{ijkl}(\omega_{kl}) \hat{X}_{ij} \hat{X}_{kl}^\dagger, \quad (2.65)$$

where the spectral densities are given in equation 2.52, and the differences ω_{kl}^A between eigenvalues of the dominant Hamiltonian H_A are defined in equation 2.30.

The interaction-frame Liouvillian given in equation 2.62 is difficult to use, because of the time-dependent terms $\hat{U}_A(t)$. This problem is avoided by making another approximation. The laboratory frame relaxation superoperator is expanded in eigenoperators of \hat{H}_A

$$\hat{\Gamma}_{\text{SC}}^{\text{lab}} = \sum_{\alpha, \alpha'} |A_\alpha\rangle \langle A_{\alpha'}| \times (A_\alpha | \hat{\Gamma}_{\text{SC}}^{\text{lab}} | A_{\alpha'}). \quad (2.66)$$

This allows the second term in equation 2.62 to be written as follows:

$$\hat{U}_A^\dagger(t) \hat{\Gamma}_{\text{SC}}^{\text{lab}} \hat{U}_A(t) = \sum_{\alpha, \alpha'} |A_\alpha\rangle \langle A_{\alpha'}| \times (A_\alpha | \hat{\Gamma}_{\text{SC}}^{\text{lab}} | A_{\alpha'}) \exp\{i(a_\alpha - a_{\alpha'})t\}. \quad (2.67)$$

The rapidly oscillating terms in this equation may be ignored under the assumption that the relaxation rate constants are small compared to the eigenvalue separation of the dominant Hamiltonian H_A . This approximation is reasonable since the eigenvalues of H_A are assumed to be either degenerate or widely spaced. The omission of rapidly oscillating components in equation 2.67 allows use of the following *secularized relaxation superoperator* in the interaction frame

$$\tilde{\hat{\Gamma}}_{\text{SC}}^{\text{sec}} \simeq \sum_{\alpha, \alpha'} |A_\alpha\rangle \langle A_{\alpha'}| \times (A_\alpha | \hat{\Gamma}_{\text{SC}}^{\text{lab}} | A_{\alpha'}) \delta(a_\alpha - a_{\alpha'}), \quad (2.68)$$

where $\delta(x) = 1$ if $x = 0$ and $\delta(x) = 0$ otherwise. The Liouvillian superoperator in the interaction frame of H_A is therefore given, to a very good approximation, by

$$\tilde{\hat{\mathcal{L}}}_{\text{SC}} \simeq -i\tilde{\hat{H}}_{\text{coh}} + \tilde{\hat{\Gamma}}_{\text{SC}}^{\text{sec}}, \quad (2.69)$$

where $\tilde{\hat{\Gamma}}_{\text{SC}}^{\text{sec}}$ is time-independent. Spin dynamical calculations may therefore be conducted in the interaction frame of the dominant Hamiltonian H_A , using the interaction-frame coherent Hamiltonian $\tilde{\hat{H}}_{\text{coh}}$ and the secularized semi-classical relaxation superoperator $\tilde{\hat{\Gamma}}_{\text{SC}}^{\text{sec}}$ of equation 2.68.

For homonuclear spin systems in liquid-state high field NMR experiments, H_A may be chosen to equal the dominant Zeeman interaction. In this case, selection rules on the rotational correlation functions [60] render the secularization procedure in equation 2.68 unnecessary, since the matrix elements $(A_\alpha | \hat{\Gamma}_{\text{SC}}^{\text{lab}} | A_{\alpha'})$ vanish in any case for $a_\alpha \neq a_{\alpha'}$. However, this is not always true for heteronuclear spin systems. An example of the relaxation superoperator secularization in heteronuclear systems may be found in reference 61.

For simplicity, the secularized relaxation superoperator in the interaction frame is now denoted as $\hat{\Gamma}$

$$\hat{\Gamma} = \tilde{\hat{\Gamma}}_{\text{SC}}^{\text{sec}}. \quad (2.70)$$

From the definition of $\hat{\Gamma}_{\text{SC}}^{\text{sec}}$, this superoperator is identical when expressed in the laboratory frame

$$[\hat{H}_A, \hat{\Gamma}] = 0 \quad \implies \quad \hat{\Gamma}^{\text{lab}} = \hat{U}_A \hat{\Gamma} \hat{U}_A^\dagger = \hat{\Gamma}. \quad (2.71)$$

2.2.2 Transition probabilities

The transition probability per unit time from an eigenstate $|r\rangle$ of H_0 to a different eigenstate $|s\rangle$ may be derived from the secularized relaxation superoperator as follows [32]:

$$W_{r \rightarrow s} = -(X_{ss} | \hat{\Gamma} | X_{rr}) = J_{sr sr}(\omega_{sr}). \quad (2.72)$$

The semi-classical approach leads to identical rate coefficients for forward and backward transitions, as sketched in figure 2.3(a):

$$W_{r \rightarrow s} = W_{s \rightarrow r}. \quad (2.73)$$

As is well-known, symmetrical transition probabilities are incompatible with the establishment of thermal equilibrium at a finite temperature [22, 28–38].

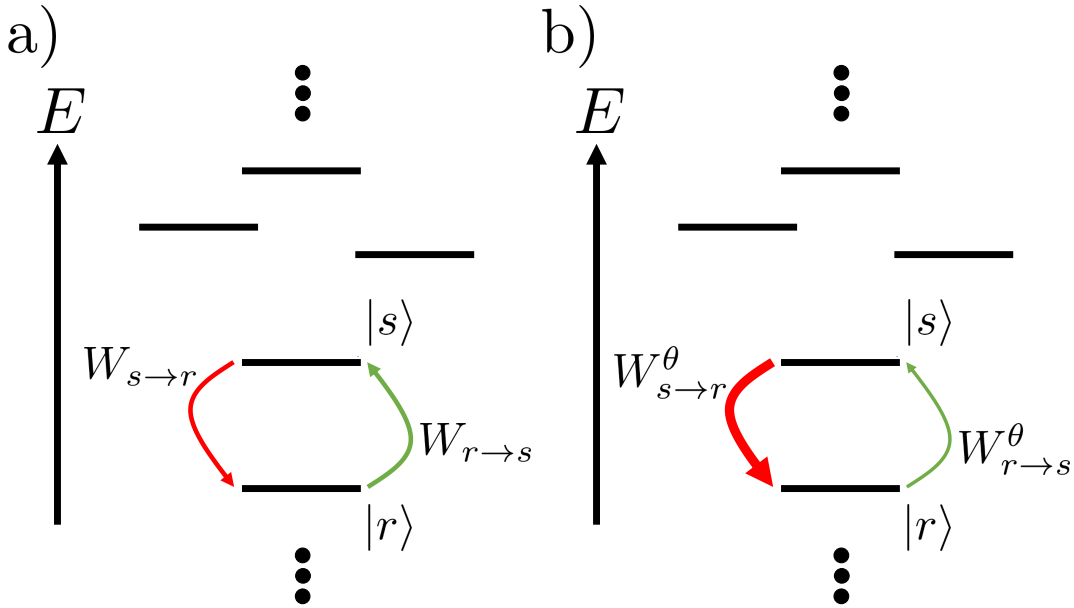


FIGURE 2.3: A section of the energy level structure of an arbitrary quantum system. Relaxation phenomena induce transitions between the states $|r\rangle$ and $|s\rangle$. Transitions that cause the system to gain energy are indicated in green, transitions that cause the system to lose energy are indicated in red. (a) Semi-classical transition probabilities. The “upwards” and “downwards” transition probabilities $W_{r \rightarrow s}$ and $W_{s \rightarrow r}$ are equal. (b) After thermalisation, the “downwards” transition probability $W_{s \rightarrow r}^\theta$ (thick arrow) is larger than the “upwards” transition probability $W_{r \rightarrow s}^\theta$ (thin arrow).

2.2.3 Coherence decay rate constants

The decay rate constant for a coherence between the eigenstates $|r\rangle$ and $|s\rangle$ of the coherent Hamiltonian H_0 may be expressed as

$$\lambda_{rs} = -(X_{rs}|\hat{\Gamma}|X_{rs}), \quad (2.74)$$

which may be written as the sum of an "adiabatic" and "non-adiabatic" contributions [30, 32–36]

$$\lambda_{rs} = \lambda_{rs}^{\text{ad}} + \lambda_{rs}^{\text{na}} \quad (2.75)$$

with

$$\begin{aligned} \lambda_{rs}^{\text{ad}} &= \int_{-\infty}^0 \overline{(\langle r|\tilde{H}_{\text{fluc}}(0)|r\rangle - \langle s|\tilde{H}_{\text{fluc}}(0)|s\rangle)(\langle r|\tilde{H}_{\text{fluc}}(\tau)|r\rangle - \langle s|\tilde{H}_{\text{fluc}}(\tau)|s\rangle)} d\tau \\ &= \frac{1}{2} \sum_{\Lambda, \Lambda'} \left(J_{rrrr}^{\Lambda\Lambda'}(0) - J_{rrss}^{\Lambda\Lambda'}(0) - J_{ssrr}^{\Lambda\Lambda'}(0) + J_{ssss}^{\Lambda\Lambda'}(0) \right) \end{aligned} \quad (2.76)$$

and

$$\lambda_{rs}^{\text{na}} = \frac{1}{2} \left(\sum_{k \neq r} W_{r \rightarrow k} + \sum_{k \neq s} W_{s \rightarrow k} \right). \quad (2.77)$$

The adiabatic contributions are due to random fluctuations of the energy levels. The non-adiabatic contributions arise from the finite lifetimes of the spin states, due to transitions to other states. As an illustrative example, the non-adiabatic contribution for an arbitrary three-level system is illustrated in figure 2.4(a). The coherence between states $|2\rangle$ and $|3\rangle$ is indicated by a wavy line. The non-adiabatic contribution to the decay of this coherence is due to all transitions out of the states $|2\rangle$ and $|3\rangle$.

2.2.4 Semi-classical equation of motion

The master equation for the dynamics of the spin density operator within the semi-classical approach is therefore given by

$$\frac{d}{dt} |\rho\rangle = \hat{\mathcal{L}}_{\text{SC}} |\rho\rangle, \quad (2.78)$$

where the Liouvillian is

$$\hat{\mathcal{L}}_{\text{SC}} \simeq -i\{\hat{H}_0 + \hat{H}_C^{\text{res}}(t)\} + \hat{\Gamma}_{\text{SC}} \quad (2.79)$$

and the secularized semi-classical relaxation superoperator is given by equation 2.68.

Since the semi-classical relaxation superoperator predicts equal probabilities for transitions gaining and losing energy (equation 2.73), the true thermal equilibrium state of the spin density operator is not correctly predicted by equations 2.78 and 2.79. This

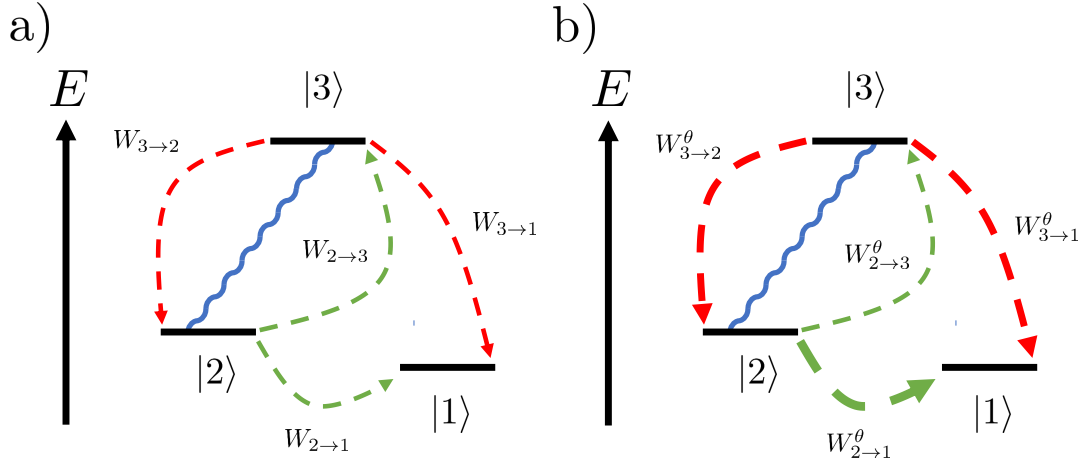


FIGURE 2.4: Energy levels of a three-level quantum system. A coherence between the states $|2\rangle$ and $|3\rangle$ is indicated by a blue wavy line. The non-adiabatic contribution to the coherence decay process is given by the summed transition probability for all transitions out of the states $|2\rangle$ and $|3\rangle$ as indicated by the arrows. **(a)** In the semi-classical treatment, “upwards” and “downwards” transition probabilities are equal. **(b)** At finite temperature the non-adiabatic contributions to the coherence decay rate must be adjusted to reflect the different transition probabilities in the two directions.

problem is often addressed by arbitrarily introducing a thermal equilibrium term in the relaxation part, leading to the widely used inhomogeneous master equation (IME) of the form [22, 28–38]

$$\frac{d}{dt} |\rho\rangle = -i(\hat{H}_0 + \hat{H}_C^{\text{res}}(t)) |\rho\rangle + \hat{\Gamma}_{\text{SC}}(|\rho\rangle - |\rho_{\text{eq}}\rangle). \quad (2.80)$$

Strictly speaking the introduction of the thermal equilibrium term may be justified within the high-temperature and weak-order approximation so that equation 2.80 necessarily gives incorrect results for spin systems which are far from equilibrium.

2.3 Thermalisation

The semi-classical relaxation superoperator of equation 2.64 fails to predict the correct thermal equilibrium state, since the transition probabilities are symmetric, as in eq. 2.73. Instead the *state of complete disorder* represents the stationary distribution of $\hat{\Gamma}_{\text{SC}}$ and lies in its null-space

$$\hat{\Gamma}_{\text{SC}} |1\rangle = |0\rangle. \quad (2.81)$$

The semi-classical relaxation superoperator $\hat{\Gamma}_{\text{SC}}$ therefore drives the system to the unphysical state of infinite temperature. In the following several of the existing techniques to account for this problem will be examined with an emphasis on their weaknesses.

2.3.1 Thermal Corrections

The correct thermal equilibrium state may be forced into the null-space of $\hat{\Gamma}_{\text{SC}}$ by adjusting the semi-classical relaxation superoperator using a procedure known as “thermalisation”. Most techniques [44–47] achieve this by multiplying the SC-relaxation superoperator by a thermal correction superoperator $\hat{\Theta}$

$$\hat{\Gamma}^\theta = \hat{\Gamma}_{\text{SC}}\hat{\Theta}, \quad (2.82)$$

with the resulting property

$$\hat{\Gamma}^\theta|\rho_{\text{eq}}\rangle = |0\rangle. \quad (2.83)$$

Here, the state $|0\rangle$ represents the zero element of \mathcal{L} . The thermalised equation of motion for the density operator is then given by

$$\frac{d}{dt}|\rho\rangle = (-i\hat{H}_{\text{coh}} + \hat{\Gamma}^\theta)|\rho\rangle, \quad (2.84)$$

where \hat{H}_{coh} is the commutation superoperator of the coherent Hamiltonian H_{coh} .

Any thermalised relaxation superoperator should have the following properties:

- **preserves the trace:** This condition captures the fact that the sum of all populations should be a constant of motion. Populations are free to be redistributed among each other, but there is no “loss” of populations

$$\frac{d}{dt}(\mathbb{1}|\rho(t)) = (\mathbb{1}|\frac{d}{dt}\rho(t)) = (\mathbb{1}|\hat{\Gamma}^\theta|\rho(t)) = 0. \quad (2.85)$$

- **preserves hermiticity:** The density matrix must remain hermitian at all points in time to be in agreement with the statistical interpretation of quantum mechanics

$$\frac{d}{dt}\rho_{rs}(t) = \frac{d}{dt}\rho_{sr}^*(t). \quad (2.86)$$

- **obeys detailed balance:** At thermal equilibrium the detailed balance condition applies [26, 59]. The transition probabilities of $\hat{\Gamma}^\theta$ should therefore fulfill the following condition:

$$\frac{\rho_{\text{eq}}^{ss}}{\rho_{\text{eq}}^{rr}} = \frac{\hat{\Gamma}_{ssrr}^\theta}{\hat{\Gamma}_{rrss}^\theta} = \frac{W_{r\rightarrow s}^\theta}{W_{s\rightarrow r}^\theta} = \exp(\beta_\theta\omega_{rs}). \quad (2.87)$$

The detailed balance condition indicates that transitions from higher energy states to lower energy states are slightly more likely than vice versa. It follows that $|\rho_{\text{eq}}\rangle$ is a stationary distribution and lies in the null-space of $\hat{\Gamma}^\theta$ [62].

- **predict consistent coherence decay rates:** The thermalised coherence decay rate constants are composed of adiabatic and non-adiabatic contributions

$$\lambda_{rs}^\theta = \lambda_{rs}^{\theta,\text{ad}} + \lambda_{rs}^{\theta,\text{na}}. \quad (2.88)$$

The adiabatic contributions to the coherence decay rate constants should be independent of the thermal correction

$$\lambda_{rs}^{\theta,\text{ad}} = \lambda_{rs}^{\text{ad}}. \quad (2.89)$$

The non-adiabatic contributions, on the other hand, depend on the transition probabilities and should be adjusted according to the detailed balance condition, as follows

$$\lambda_{rs}^{\theta,\text{na}} = \frac{1}{2} \left(\sum_{k \neq r} W_{r \rightarrow k}^\theta + \sum_{k \neq s} W_{s \rightarrow k}^\theta \right). \quad (2.90)$$

A variety of methods have been proposed for the thermalisation of the relaxation superoperator. Their properties and limitations are summarized in table 2.1.

TABLE 2.1: The methods for treating nuclear spin relaxation discussed in this paper, and their properties in the context of a finite-temperature molecular environment. The following abbreviations are used: SC = semi-classical relaxation theory; IME = inhomogeneous Master equation; Jeener = Jeener’s thermalised relaxation superoperator [44]; LdB = Levitt-di Bari method for thermalising the relaxation superoperator [45–47]; sLdB = simplified Levitt-di Bari method as implemented in *SpinDynamica* 3.2 software [63]; LB = Lindblad method.

	SC	IME	Jeener	LdB	sLdB	LB
correct thermal equilibrium	×	✓	✓	✓	✓	✓
valid outside high-temperature regime	×	×	✓	✓	×	✓
valid outside weak-order regime	×	×	✓	✓	×	✓
transition probabilities fulfil detailed balance	×	×	✓	✓	×	✓
coherence decay rates: correct adiabatic contributions	✓	✓	×	✓	✓	✓
coherence decay rates: correct non-adiabatic contributions	×	×	×	×	×	✓
equation number	2.68	2.1,2.80	2.92	2.103	2.109	2.125
references	28, 29	28–30	44	45, 46	45–47	this work

2.3.1.1 Jeener's Method

Jeener's seminal article on superoperators in magnetic resonance [44] contains a proposed thermalisation method for relaxation superoperators. This is based on the *energy superoperator* $\hat{\mathcal{E}}$ defined as follows:

$$\hat{\Theta}_J = \exp(\beta_\theta \hat{\mathcal{E}}), \quad \hat{\mathcal{E}} = \frac{1}{2}(\hat{H}_0 \bullet + \bullet \hat{H}_0). \quad (2.91)$$

The thermally corrected relaxation superoperator is given by

$$\hat{\Gamma}_J^\theta = \hat{\Gamma}_{SC} \hat{\Theta}_J = \hat{\Gamma}_{SC} \exp(\beta_\theta \hat{\mathcal{E}}). \quad (2.92)$$

The method works by transforming the thermal equilibrium density operator $|\rho_{\text{eq}}\rangle$ into $|\mathbb{1}\rangle$. This may be seen as follows: The action of the energy superoperator on a population operator of the coherent Hamiltonian is given by

$$\hat{\mathcal{E}} |X_{kk}\rangle = \omega_k |X_{kk}\rangle. \quad (2.93)$$

The thermal equilibrium density operator may be expressed in terms of the population operators

$$|\rho_{\text{eq}}\rangle = Z^{-1} \sum_k \exp(-\beta_\theta \omega_k) |X_{kk}\rangle, \quad Z = \sum_k \exp(-\beta_\theta \omega_k). \quad (2.94)$$

According to equations 2.93 and 2.94, the result of applying the total energy superoperator to the thermal equilibrium density operator is given by

$$\hat{\mathcal{E}} |\rho_{\text{eq}}\rangle = Z^{-1} \sum_k \omega_k \exp(-\beta_\theta \omega_k) |X_{kk}\rangle. \quad (2.95)$$

It is then straightforward to show that Jeener's thermal correction superoperator transforms the thermal equilibrium state into the state of total disorder

$$\begin{aligned} \hat{\Theta}_J |\rho_{\text{eq}}\rangle &= Z^{-1} \sum_k \exp(-\beta_\theta \omega_k) \sum_n \frac{(\beta_\theta \omega_k)^n}{n!} |X_{kk}\rangle \\ &= Z^{-1} \sum_k \exp(-\beta_\theta \omega_k) \exp(\beta_\theta \omega_k) |X_{kk}\rangle \\ &= Z^{-1} |\mathbb{1}\rangle. \end{aligned} \quad (2.96)$$

Since the state of total disorder lies within the null-space of the SC-relaxation superoperator, $|\rho_{\text{eq}}\rangle$ lies in the null-space of $\hat{\Gamma}_J^\theta$

$$\hat{\Gamma}_J^\theta |\rho_{\text{eq}}\rangle = Z^{-1} \hat{\Gamma} |\mathbb{1}\rangle = |0\rangle. \quad (2.97)$$

The transition probabilities per unit time are modified in the following way:

$$W_{r \rightarrow s}^{\theta, J} = (X_{ss} | \hat{\Gamma}_J^\theta | X_{rr}) = (X_{ss} | \hat{\Gamma} \exp(\beta_\theta \hat{\mathcal{E}}) | X_{rr}) = \exp(\beta_\theta \omega_r) W_{r \rightarrow s} \quad (2.98)$$

and the ratio between forward and backwards transition probabilities is given by

$$\frac{W_{r \rightarrow s}^{\theta, J}}{W_{s \rightarrow r}^{\theta, J}} = \exp(\beta_\theta \omega_{rs}), \quad (2.99)$$

showing that the thermalised transition probabilities obey the detailed balance condition (equation 2.87).

However, Jeener's method does not handle the coherence decay rate constants correctly. The thermalised decay rate constants of a particular coherence are given by

$$\begin{aligned} \lambda_{rs}^{\theta, J} &= (X_{rs} | \hat{\Gamma}_J^\theta | X_{rs}) = \exp(\beta_\theta (\omega_r + \omega_s)) \lambda_{rs}, \\ \lambda_{sr}^{\theta, J} &= (X_{sr} | \hat{\Gamma}_J^\theta | X_{sr}) = \exp(\beta_\theta (\omega_r + \omega_s)) \lambda_{sr}. \end{aligned} \quad (2.100)$$

The equality $\lambda_{rs}^{\theta, J} = \lambda_{sr}^{\theta, J}$ follows from $\lambda_{rs} = \lambda_{sr}$ and maintains the hermiticity of the density operator. However, there is still a problem. The adiabatic and non-adiabatic contributions to the coherence decay rate constants are given in Jeener's method by

$$\begin{aligned} \lambda_{rs}^{\theta, \text{ad}, J} &= \exp\left(\frac{1}{2} \beta_\theta (\omega_r + \omega_s)\right) \lambda_{rs}^{\text{ad}}, \\ \lambda_{rs}^{\theta, \text{na}, J} &= \exp\left(\frac{1}{2} \beta_\theta (\omega_r + \omega_s)\right) \lambda_{rs}^{\text{na}}, \end{aligned} \quad (2.101)$$

where the adiabatic and non-adiabatic rate constants are given by equations 2.76 and 2.77 respectively. The terms $\lambda_{rs}^{\theta, \text{ad}, J}$ and $\lambda_{rs}^{\theta, \text{na}, J}$ are both in conflict with the requirements of equations 2.89 and 2.90. In particular, Jeener's method adjusts the adiabatic contributions to the coherence decay rates, which does not make physical sense, since the adiabatic contributions are not related to state transitions and are energy-preserving.

The properties of the Jeener method are summarized in table 2.1. The Jeener method fulfils most of the required conditions of a thermalisation method, but does not treat the coherence decay rate constants correctly.

2.3.1.2 Levitt-di Bari and Levante-Ernst method

An alternative thermalisation technique was proposed by Levitt and di Bari [45, 46] and further developed by Levante and Ernst [47]. This method is termed here the LdB method and uses projection superoperators onto the population operators of the coherent Hamiltonian, weighted by the eigenvalue of the associated eigenstate

$$\hat{\omega} = \sum_k \omega_k |X_{kk}\rangle \langle X_{kk}|. \quad (2.102)$$

The superoperator $\hat{\omega}$ is therefore simply the projection of $\hat{\mathcal{E}}$ onto the population subspace of H_0 . Similarly to equation 2.92 the thermal correction superoperator is then given by

$$\hat{\Theta}_{\text{LdB}} = \exp(-\beta_\theta \hat{\omega}) \quad (2.103)$$

and the action of $\hat{\omega}$ onto the thermal equilibrium density operator is identical to the action of $\hat{\mathcal{E}}$ (compare with equation 2.95)

$$\hat{\omega}|\rho_{\text{eq}}\rangle = Z^{-1} \sum_k \omega_k \exp(-\beta_\theta \omega_k) |X_{kk}\rangle. \quad (2.104)$$

As a result $\hat{\Theta}_{\text{LdB}}$ transforms the thermal equilibrium density operator into the state of total disorder

$$\hat{\Theta}_{\text{LdB}}|\rho_{\text{eq}}\rangle = Z^{-1} |\mathbb{1}\rangle \quad (2.105)$$

and ρ_{eq} lies in the null-space of $\hat{\Gamma}_{\text{LdB}}^\theta$

$$\hat{\Gamma}_{\text{LdB}}^\theta|\rho_{\text{eq}}\rangle = |0\rangle. \quad (2.106)$$

The modification of the transition probabilities is identical to Jeener's method

$$W_{r \rightarrow s}^{\theta, \text{LdB}} = (X_{ss} | \hat{\Gamma}_{\text{LdB}}^\theta | X_{rr}) = (X_{ss} | \hat{\Gamma}_{\text{SC}} \exp(\beta_\theta \hat{\omega}) | X_{rr}) = \exp(\beta_\theta \omega_r) W_{r \rightarrow s}, \quad (2.107)$$

so that the transition probabilities of $\hat{\Gamma}_{\text{LdB}}^\theta$ obey the detailed balance condition.

A defect of the LdB method is that the coherence decay rates are not adjusted at all, since the coherence operators lie in the null-space of $\hat{\omega}$.

$$\begin{aligned} \hat{\omega}|X_{rs}\rangle = |0\rangle &\implies \exp(\beta_\theta \hat{\omega})|X_{rs}\rangle = |X_{rs}\rangle, \\ \lambda_{rs}^{\theta, \text{LdB}} = (X_{rs} | \hat{\Gamma}_{\text{SC}} \exp(\beta_\theta \hat{\omega}) | X_{rs}) &= (X_{rs} | \hat{\Gamma}_{\text{SC}} | X_{rs}) = \lambda_{rs}. \end{aligned} \quad (2.108)$$

Hence the Levitt-di Bari method obeys the condition of equation 2.89 for the adiabatic decay rate contribution, but not that of 2.90 for the non-adiabatic contribution.

A simplified version of the LdB method (sLdB), which employs the high-temperature and weak-order approximations, is currently implemented in version 3.3.2 of the *SpinDynamica* software package [63]. This method uses the following thermalisation correction:

$$\hat{\Theta}_{\text{sLdB}} = \hat{\mathbb{I}} - |\rho_{\text{eq}}\rangle\langle\mathbb{1}|. \quad (2.109)$$

The thermally adjusted transition probabilities are given by

$$W_{r \rightarrow s}^{\theta, \text{sLdB}} = W_{r \rightarrow s} - \sum_j W_{j \rightarrow s} \langle j | \rho_{\text{eq}} | j \rangle, \quad (2.110)$$

whereas the coherence decay rates remain unchanged

$$\lambda_{rs}^{\theta, \text{sLdB}} = \lambda_{rs}. \quad (2.111)$$

The sLdB method generates the correct thermal equilibrium density operator in the high-temperature approximation but does not obey detailed balance in general, and fails to handle coherence decay rate constants correctly.

The sLdB method is in fact the IME in superoperator form. This is easy to see by applying $\hat{\Gamma}_{\text{sLdB}}^\theta$ to an arbitrary density operator $|\rho\rangle$

$$\begin{aligned} \hat{\Gamma}_{\text{sLdB}}^\theta |\rho\rangle &= \hat{\Gamma} \hat{\Theta}_{\text{sLdB}} |\rho\rangle \\ &= \hat{\Gamma} \{ \hat{\mathbb{1}} - |\rho_{\text{eq}}\rangle\langle\mathbb{1}| \} |\rho\rangle \\ &= \hat{\Gamma} \{ |\rho\rangle - \text{Tr}\{\rho\} |\rho_{\text{eq}}\rangle \} \\ &= \hat{\Gamma} \{ |\rho\rangle - |\rho_{\text{eq}}\rangle \}, \end{aligned} \quad (2.112)$$

where the last equality follows from the fact that $\text{Tr}\{\rho\} = 1$ for a valid density operator. This shows that the sLdB method has the same defects as the IME, most notably the requirement that the density operator $|\rho\rangle$ has to fulfill the weak-order *and* high-temperature approximation.

2.4 Lindblad thermalisation

Here an alternative thermalisation method, called the Lindblad (LB) method, is suggested [28, 64–66]. The method is fundamentally different to existing techniques as it requires quantum mechanical corrections to the spectral densities to account for the finite sample temperature. As a consequence the LB method does not lead to a relaxation superoperator which may be expressed as the product of the semi-classical relaxation superoperator and a thermal correction superoperator, as in equation 2.82. Instead one has to perform thermal corrections to the individual components of the relaxation superoperator.

The Lindbladian formulation of relaxation processes has been extensively used in quantum optics, quantum computing, laser physics and quantum information theory [56, 58]. In the field of quantum information theory the Lindblad formulation takes a central role in the characterisation of dissipative processes. In particular, the characterisation of Markovian and non-Markovian completely positive and trace preserving (CPTP) dynamics is of fundamental importance. Roughly speaking, a CPTP process indicates evolution of a valid density operator into another valid density operator, and hence captures all physically reasonable evolutions [26]. Recently, it has been shown that any evolution generated by a CPTP Markovian process may be obtained by application of some time-dependent Lindblad generator [67, 68].

The above implies that if a given relaxation process may not be described in terms of a Lindblad formulation it can not be considered a valid Markovian quantum process. One could therefore argue that the reformulation of the NMR master equation in terms of Lindblad generators is not simply a mathematical exercise, but rather a necessary criterion to ensure that the resulting dynamics do indeed describe a valid Markovian process.

Nevertheless, it might be for such reasons that the NMR community has mainly considered the Lindblad formulation an over-elaborate tool and disregarded its fundamental physical importance. As a consequence its application to magnetic resonance relaxation phenomena is rarely found within the NMR literature [69, 70].

2.4.1 Quantum-Mechanical Spectral Densities

The starting point of the Lindblad method is to treat both the environment and the spin system quantum mechanically [26, 28, 31, 59]. The fluctuating contributions are replaced by a Hamiltonian of the following type

$$H_{\text{fluc}}^{\Lambda} = \sum_{\alpha} A_{\alpha} \otimes B_{\alpha}^{\Lambda}, \quad (2.113)$$

where individual eigenoperators A_{α} of the system are being coupled (represented by \otimes) to environmental ("bath") operators B_{α}^{Λ} .

The environment represents a thermal reservoir with sufficient heat capacity to always remain close to thermal equilibrium due to its size and complexity, and is described by a density operator $\rho_{\text{eq}}^{\text{bath}}$. It is not necessary to assume that the *spin system* remains close to equilibrium. The combined density operator of the spin system and the environment is assumed to be of the form:

$$\rho_{\text{tot}}(t) = \rho(t) \otimes \rho_{\text{eq}}^{\text{bath}}. \quad (2.114)$$

The "quantum-mechanical" relaxation superoperator may be derived by substituting the expression for H_{fluc} from equation 2.113 into equation 2.63, and taking the trace over the environmental degrees of freedom [26, 30, 59]. Following Hubbard [31], the quantum mechanical relaxation superoperator is obtained:

$$\begin{aligned} \hat{\Gamma}_{\text{QM}}^{\text{lab}} &= - \sum_{\Lambda, \Lambda'} \sum_{\alpha, \alpha'} \int_{-\infty}^0 (A_{\alpha} \bullet A_{\alpha'}^{\dagger} - \bullet A_{\alpha'}^{\dagger} A_{\alpha}) \langle B_{\alpha'}^{\Lambda'}(\tau) B_{\alpha}^{\Lambda}(0) \rangle \exp(i\omega_{\alpha'}^{\Lambda} \tau) \\ &= - \sum_{\Lambda, \Lambda'} \sum_{\alpha, \alpha'} \int_{-\infty}^0 (A_{\alpha'}^{\dagger} \bullet A_{\alpha} - A_{\alpha} A_{\alpha'}^{\dagger} \bullet) \langle B_{\alpha}^{\Lambda}(0) B_{\alpha'}^{\Lambda'}(\tau) \rangle \exp(i\omega_{\alpha'}^{\Lambda} \tau). \end{aligned} \quad (2.115)$$

Here $\langle B_{\alpha'}^{\Lambda'\dagger}(\tau)B_{\alpha}^{\Lambda}(0) \rangle$ are quantum-mechanical correlation functions, defined as follows:

$$\langle B_{\alpha'}^{\Lambda'\dagger}(\tau)B_{\alpha}^{\Lambda}(0) \rangle = \text{Tr}_{\text{bath}} \left\{ U_{\text{bath}}(\tau)B_{\alpha'}^{\Lambda'\dagger}U_{\text{bath}}^{\dagger}(\tau)B_{\alpha}^{\Lambda}\rho_{\text{eq}}^{\text{bath}} \right\} = \langle B_{\alpha'}^{\Lambda'\dagger}(0)B_{\alpha}^{\Lambda}(-\tau) \rangle. \quad (2.116)$$

Since the system-bath interaction is hermitian it is permissible to replace the second part of equation 2.115 by its hermitian conjugate

$$\begin{aligned} \hat{\Gamma}_{\text{QM}}^{\text{lab}} &= - \sum_{\Lambda, \Lambda'} \sum_{\alpha, \alpha'} \int_{-\infty}^0 (A_{\alpha} \bullet A_{\alpha'}^{\dagger} - \bullet A_{\alpha'}^{\dagger} A_{\alpha}) \langle B_{\alpha'}^{\Lambda'\dagger}(\tau)B_{\alpha}^{\Lambda}(0) \rangle \exp(i\omega_{\alpha'}^A \tau) \\ &= - \sum_{\Lambda, \Lambda'} \sum_{\alpha, \alpha'} \int_{-\infty}^0 (A_{\alpha'} \bullet A_{\alpha}^{\dagger} - A_{\alpha}^{\dagger} A_{\alpha'} \bullet) \langle B_{\alpha}^{\Lambda\dagger}(0)B_{\alpha'}^{\Lambda'}(\tau) \rangle \exp(-i\omega_{\alpha'}^A \tau). \end{aligned} \quad (2.117)$$

The sum is invariant under the exchange of the labels ($\alpha \leftrightarrow \alpha'$) and ($\Lambda \leftrightarrow \Lambda'$) which we perform on the second part

$$\begin{aligned} \hat{\Gamma}_{\text{QM}}^{\text{lab}} &= - \sum_{\Lambda, \Lambda'} \sum_{\alpha, \alpha'} \int_{-\infty}^0 (A_{\alpha} \bullet A_{\alpha'}^{\dagger} - \bullet A_{\alpha'}^{\dagger} A_{\alpha}) \langle B_{\alpha'}^{\Lambda'\dagger}(\tau)B_{\alpha}^{\Lambda}(0) \rangle \exp(i\omega_{\alpha'}^A \tau) \\ &= - \sum_{\Lambda, \Lambda'} \sum_{\alpha, \alpha'} \int_{-\infty}^0 (A_{\alpha} \bullet A_{\alpha'}^{\dagger} - A_{\alpha'}^{\dagger} A_{\alpha} \bullet) \langle B_{\alpha'}^{\Lambda'\dagger}(-\tau)B_{\alpha}^{\Lambda}(0) \rangle \exp(-i\omega_{\alpha'}^A \tau). \end{aligned} \quad (2.118)$$

A simple transformation of variables ($\tau \mapsto -\tau$) in the second sum leads to the following expression:

$$\begin{aligned} \hat{\Gamma}_{\text{QM}}^{\text{lab}} &= - \sum_{\Lambda, \Lambda'} \sum_{\alpha, \alpha'} \int_{-\infty}^0 (A_{\alpha} \bullet A_{\alpha'}^{\dagger} - \bullet A_{\alpha'}^{\dagger} A_{\alpha}) \langle B_{\alpha'}^{\Lambda'\dagger}(\tau)B_{\alpha}^{\Lambda}(0) \rangle \exp(i\omega_{\alpha'}^A \tau) \\ &\quad - \sum_{\Lambda, \Lambda'} \sum_{\alpha, \alpha'} \int_0^{\infty} (A_{\alpha} \bullet A_{\alpha'}^{\dagger} - A_{\alpha'}^{\dagger} A_{\alpha} \bullet) \langle B_{\alpha'}^{\Lambda'\dagger}(\tau)B_{\alpha}^{\Lambda}(0) \rangle \exp(i\omega_{\alpha'}^A \tau). \end{aligned} \quad (2.119)$$

By considering only the secular contributions $\omega_{\alpha} = \omega_{\alpha'}$ and neglecting dynamical frequency shifts, the two sums may be combined to form a complete Fourier transform (see Appendix A.1)

$$\hat{\Gamma}_{\text{QM}}^{\text{sec}} = \sum_{\Lambda, \Lambda'} \sum_{\alpha, \alpha'} \hat{\mathcal{D}}[A_{\alpha}, A_{\alpha'}^{\dagger}] K_{\alpha\alpha'}^{\Lambda\Lambda'}(\omega_{\alpha'}^A) \delta(\omega_{\alpha}^A - \omega_{\alpha'}^A), \quad (2.120)$$

where the quantum-mechanical spectral densities are given by

$$K_{\alpha\alpha'}^{\Lambda\Lambda'}(\omega) = \int_{-\infty}^{\infty} \langle B_{\alpha'}^{\Lambda'\dagger}(\tau)B_{\alpha}^{\Lambda}(0) \rangle \exp(i\omega\tau) d\tau \quad (2.121)$$

and $\hat{\mathcal{D}}$ defines the so-called Lindbladian dissipator [26, 59]

$$\hat{\mathcal{D}}[A, B] = A \bullet B - \frac{1}{2} (BA \bullet + \bullet BA). \quad (2.122)$$

In contrast to the classical correlation functions, the quantum mechanical correlation functions are not symmetric with respect to frequency, i.e. $K(\omega) \neq K(-\omega)$. In thermal equilibrium they obey the Kubo-Martin-Schwinger(KMS)-condition [26, 59]

$$K_{\alpha\alpha'}^{\Lambda\Lambda'}(\omega) = K_{\alpha'\alpha}^{\Lambda\Lambda'}(-\omega) \exp(\beta\theta\omega). \quad (2.123)$$

Detailed knowledge of the quantum mechanical spectral densities is rarely available. Nevertheless they may be approximated by classical spectral densities by invoking an appropriate quantum mechanical correction [71]. One possibility is given by the Schofield method [72]

$$K_{\alpha\alpha'}^{\Lambda\Lambda'}(\omega) \mapsto J_{\alpha\alpha'}^{\Lambda\Lambda'}(\omega) \exp(-\frac{1}{2}\beta\theta\omega). \quad (2.124)$$

Corrections of this form have been previously used in the description of vibrational relaxation effects [73].

This leads to the following expression for the secularized relaxation superoperator

$$\hat{\Gamma}_{\text{LB}}^{\theta} = \sum_{\Lambda, \Lambda'} \sum_{\alpha, \alpha'} \hat{\mathcal{D}}[A_{\alpha}, A_{\alpha'}^{\dagger}] J_{\alpha\alpha'}^{\Lambda\Lambda'}(\omega_{\alpha}^A) \exp(-\frac{1}{2}\beta\theta\omega_{\alpha}^A) \delta(\omega_{\alpha} - \omega_{\alpha'}), \quad (2.125)$$

where $J_{\alpha\alpha'}^{\Lambda\Lambda'}(\omega)$ are the classical spectral densities defined in equation 2.52.

Equation 2.125 is the central result of this section. It has a clear relationship with the semiclassical form of equation 2.64. The double commutation superoperator is replaced by a Lindbladian dissipator (multiplied by -1/2), and thermal correction factors $\exp(\frac{1}{2}\beta\theta\omega_{\alpha}^A)$ are introduced.

The Lindblad dissipators have a clear relationship with the physical picture of figure 2.3. They may be understood as inducing forward and backward transition processes as illustrated below:

$$(X_{ss} | \hat{\mathcal{D}}[X_{ij}, X_{ij}^{\dagger}] | X_{rr}) = \delta_{is} \delta_{jr}, \quad (X_{ss} | \hat{\mathcal{D}}[X_{ij}^{\dagger}, X_{ij}] | X_{rr}) = \delta_{js} \delta_{ir}. \quad (2.126)$$

Terms $\hat{\mathcal{D}}[X_{ij}, X_{ij}^{\dagger}]$ and $\hat{\mathcal{D}}[X_{ij}^{\dagger}, X_{ij}]$ are associated with relaxation processes across the same pair of H_0 eigenstates but in opposite directions. The transition probabilities per unit time are given by

$$W_{r \rightarrow s}^{\theta, \text{LB}} = (X_{ss} | \hat{\Gamma}_{\text{LB}}^{\theta} | X_{rr}) = \exp(-\frac{1}{2}\beta\theta\omega_{sr}) W_{r \rightarrow s}. \quad (2.127)$$

Hence the transition probabilities for the forward and backwards processes are related as follows

$$W_{r \rightarrow s}^{\theta, \text{LB}} = W_{s \rightarrow r}^{\theta, \text{LB}} \exp(-\beta\theta\omega_{sr}), \quad (2.128)$$

in agreement with the detailed balance condition and the physical picture in figure 2.3.

The Lindbladian formalism also handles the coherence decay rate constants correctly. The adiabatic contributions to the coherence decay rates are unaffected by thermalisation, as should be the case:

$$\lambda_{rs}^{\theta,\text{ad}} = \lambda_{rs}^{\text{ad}} \quad (2.129)$$

The non-adiabatic contributions to the coherence decay rate constants are sums of thermalised transition probabilities. This is also physically reasonable (see figure 2.4)

$$\begin{aligned} \lambda_{rs}^{\theta,\text{na}} &= \frac{1}{2} \left(\sum_{k \neq r} \exp(-\frac{1}{2}\beta\theta\omega_{kr}) W_{r \rightarrow k} + \sum_{k \neq s} \exp(-\frac{1}{2}\beta\theta\omega_{ks}) W_{s \rightarrow k} \right) \\ &= \frac{1}{2} \left(\sum_{k \neq r} W_{r \rightarrow k}^{\theta,\text{LB}} + \sum_{k \neq s} W_{s \rightarrow k}^{\theta,\text{LB}} \right). \end{aligned} \quad (2.130)$$

To summarise, the thermalised Lindblad representation of equation 2.125 preserves the trace and hermiticity of the density operator, obeys the detailed balance condition, and handles coherence decay processes correctly.

2.5 Defect of Double Commutators

It is important to note that the double-commutator form of the relaxation superoperator which results from semi-classical relaxation theory (equation 2.64) does *not* provide a clear separation of the forward and backwards transition probabilities and hence is incompatible with detailed balance at finite temperature, even after the inclusion of thermal corrections. It is only at infinite temperature that the Lindblad formalism and double commutator formalism coincide.

This may be demonstrated by making use of the eigenoperator formulation of the relaxation superoperator as presented in equation 2.65. An attempt at thermally adjusting the secularized double-commutation form of the relaxation superoperator is as follows:

$$\hat{\Gamma}^{\theta} = -\frac{1}{2} \sum_{ij} \exp(-\frac{1}{2}\beta\theta\omega_{ij}) J_{ijij}(\omega_{ij}) \hat{X}_{ij} \hat{X}_{ij}^{\dagger}. \quad (2.131)$$

The transition probability per unit time $W_{k \rightarrow l}$ from the eigenstate $|k\rangle$ to the eigenstate $|l\rangle$ of the Hamiltonian H_A may be identified with the following matrix element

$$W_{k \rightarrow l} = \langle X_{ll} | \hat{\Gamma}^{\theta} | X_{kk} \rangle = -\frac{1}{2} \sum_{ij} \exp(-\frac{1}{2}\beta\theta\omega_{ij}) J_{ijij}(\omega_{ij}) (\delta_{li}\delta_{ki} - \delta_{li}\delta_{kj} - \delta_{lj}\delta_{ki} + \delta_{lj}\delta_{kj}). \quad (2.132)$$

The collection of Kronecker deltas above indicate that a double-commutator mixes forward and backward processes. Similarly one may calculate the transition probability for

the reverse process

$$W_{l \rightarrow k} = \langle X_{kk} | \hat{\Gamma}^\theta | X_{ll} \rangle = -\frac{1}{2} \sum_{ij} \exp(-\frac{1}{2}\beta_\theta \omega_{ij}) J_{ijij}(\omega_{ij}) (\delta_{ki}\delta_{li} - \delta_{ki}\delta_{lj} - \delta_{kj}\delta_{li} + \delta_{kj}\delta_{lj}). \quad (2.133)$$

Clearly these two transition probabilities are equal

$$W_{k \rightarrow l} = W_{l \rightarrow k}, \quad (2.134)$$

so that forward and backward transitions are equally likely. This violates the detailed balance condition. It follows that thermal correction of the spectral density functions within the double commutator formalism cannot lead to a valid thermalised relaxation superoperator, at finite temperature.

It is only at infinite temperature that the Lindblad formalism and the double commutator formalism coincide. This is simply because the spectral densities become temperature-independent. The relaxation superoperator in the double-commutator formalism at infinite temperature may be written as shown below:

$$\hat{\Gamma}^\theta = -\frac{1}{2} \sum_{ij} J_{ijij}(\omega_{ij}) \{ \frac{1}{2} (\hat{X}_{ij} \hat{X}_{ij}^\dagger + \hat{X}_{ji} \hat{X}_{ji}^\dagger) \}, \quad (2.135)$$

since $\exp(-\frac{1}{2}\beta_\theta \omega_{ij}) = 1$ for $T \rightarrow \infty$. To proceed the following identity is employed

$$\frac{1}{2} (\hat{X}_{ij} \hat{X}_{ij}^\dagger + \hat{X}_{ji} \hat{X}_{ji}^\dagger) = -(\hat{\mathcal{D}}[X_{ij}, X_{ij}^\dagger] + \hat{\mathcal{D}}[X_{ji}, X_{ji}^\dagger]). \quad (2.136)$$

The relaxation superoperator in the double-commutator formalism is then readily expressed in Lindblad form

$$\begin{aligned} \hat{\Gamma}^\theta &= \frac{1}{2} \sum_{ij} J_{ijij}(\omega_{ij}) (\hat{\mathcal{D}}[X_{ij}, X_{ij}^\dagger] + \hat{\mathcal{D}}[X_{ji}, X_{ji}^\dagger]) \\ &= \frac{1}{2} \sum_{ij} J_{ijij}(\omega_{ij}) \hat{\mathcal{D}}[X_{ij}, X_{ij}^\dagger] + J_{ijij}(\omega_{ij}) \hat{\mathcal{D}}[X_{ji}, X_{ji}^\dagger] \\ &= \frac{1}{2} \sum_{ij} J_{ijij}(\omega_{ij}) \hat{\mathcal{D}}[X_{ij}, X_{ij}^\dagger] + J_{jiji}(\omega_{ji}) \hat{\mathcal{D}}[X_{ji}, X_{ji}^\dagger] \\ &= \sum_{ij} J_{ijij}(\omega_{ij}) \hat{\mathcal{D}}[X_{ij}, X_{ij}^\dagger] \end{aligned} \quad (2.137)$$

by noticing that $J_{ijij}(\omega_{ij}) = J_{jiji}(\omega_{ji})$ at infinite temperature.

2.6 Case Studies

In this section the Lindblad approach is applied to three simple cases. The first two cases concern “ordinary” high-field NMR in the high-temperature and weak-order approximation, where the LB formulation reproduces well-known results which may also be derived using the inhomogeneous master equation. In the last example we consider a spin system far from equilibrium, where the conventional IME equation breaks down.

2.6.1 Homonuclear spin-1/2 pairs

Consider an ensemble of rigid molecules undergoing rotational diffusion, with each molecule containing a homonuclear spin-1/2 pair. The electronic environments of the two spins are distinct (chemical inequivalence). The nuclear spin relaxation is assumed to be dominated by dipole-dipole relaxation where the rotational correlation time is denoted by τ_C .

In the presence of resonant radiofrequency irradiation, the coherent Hamiltonian is given in the laboratory frame, by

$$H_{\text{coh}} = H_A + H_B + H_C. \quad (2.138)$$

The dominant part of the Hamiltonian (see section 2.1.2.1) in the laboratory frame is given by

$$H_A = \omega^0(1 + \delta_{\text{ref}})(I_{1z} + I_{2z}), \quad (2.139)$$

while the terms H_B and H_C are given in the interaction frame of H_A (rotating frame) by

$$H_B = \Omega_1 I_{1z} + \Omega_2 I_{2z} + 2\pi J_{12} \mathbf{I}_1 \cdot \mathbf{I}_2, \quad H_C = \omega_{\text{nut}}(I_x \cos(\phi_I) + I_y \sin(\phi_I)). \quad (2.140)$$

Here the *chemical shift offsets* are given by $\Omega_i = \omega^0(\delta_{\text{iso}}^i - \delta_{\text{ref}})$, where $\{\delta_1, \delta_2\}$ are the chemical shifts of the two sites and δ_{ref} is the chemical shift position of the carrier frequency of the radio-frequency irradiation.

These choices of H_A , H_B and H_C fulfil the constraints in section 2.1.2.1: The eigenvalues of H_A are either degenerate or spaced by multiples of the spectrometer reference frequency $|\omega^0(1 + \delta_{\text{ref}})|$, which is much larger than the matrix elements of H_B and H_C .

Following equation 2.36, the eigenoperators of the commutation superoperator \hat{H}_A are proportional to the irreducible spherical tensor operators, as in equation 2.37. The corresponding eigenvalues of \hat{H}_A are given by

$$\omega_\alpha^A = \mu_\alpha \omega^0. \quad (2.141)$$

The fluctuating part of the spin Hamiltonian, which is responsible for the dipole-dipole relaxation, takes the form [32]

$$H_{\text{fluc}}(t) = \sum_{m=-2}^{+2} F_m^{2,*}(\Omega_{\text{PL}}^{(12)}(t)) T_{2m}^{(12)}, \quad (2.142)$$

where $T_{2m}^{(12)}$ indicates a component of the second-rank irreducible spherical tensor operator for the coupling of spins I_1 and I_2 as defined in Appendix A.1. The spatial components F_{2m} depend on the Euler angles $\Omega_{\text{PL}}^{(12)}(t)$ that relate the principal axis system of the dipole-dipole coupling to the laboratory frame. This transformation is time-dependent due to rotational diffusion of the molecule. Assuming a single exponential decay for the corresponding correlation functions as indicated by equation 2.47 the spectral densities are given by Lorentzians.

Following the recipe of equation 2.125, and assuming isotropic rotational diffusion, the secular and thermalised relaxation superoperator may be expressed as follows

$$\hat{\Gamma}_{\text{LB}}^\theta = \frac{6}{5} b_{12}^2 \sum_{m=-2}^{+2} \hat{\mathcal{D}}[T_{2m}^{(12)}, T_{2m}^{(12)\dagger}] J^\theta(m\omega^0), \quad (2.143)$$

where the thermally corrected spectral density functions are given by

$$J^\theta(\omega) = \exp(-\frac{1}{2}\beta_\theta\omega) J(\omega) \quad (2.144)$$

and

$$J(\omega) = \frac{2\tau_C}{1 + \omega^2\tau_C^2}. \quad (2.145)$$

The thermalised relaxation superoperator may be represented as a 16×16 matrix in a basis of orthogonal operators. One possible basis involves all ket-bra products for the singlet and triplet states of the 2-spin-1/2 system, defined as follows:

$$\begin{aligned} |S_0\rangle &= 2^{-1/2}(|\alpha\beta\rangle - |\beta\alpha\rangle), & |T_{+1}\rangle &= |\alpha\alpha\rangle, \\ |T_0\rangle &= 2^{-1/2}(|\alpha\beta\rangle + |\beta\alpha\rangle), & |T_{-1}\rangle &= |\beta\beta\rangle. \end{aligned} \quad (2.146)$$

The 4×4 block involving the population operators for these states is as follows:

$$\left[\hat{\Gamma}_{\text{LB}}^\theta \right]_{4 \times 4} = \frac{6}{5} b_{12}^2 \times$$

$ S_0\rangle \langle S_0 $	$ T_+\rangle \langle T_+ $	$ T_0\rangle \langle T_0 $	$ T_-\rangle \langle T_- $
0	0	0	0
0	$-\frac{1}{8}J^\theta(-\omega^0) - \frac{1}{4}J^\theta(-2\omega^0)$	$\frac{1}{8}J^\theta(\omega^0)$	$\frac{1}{4}J^\theta(2\omega^0)$
0	$\frac{1}{8}J^\theta(-\omega^0)$	$-\frac{1}{8}(J^\theta(-\omega^0) + J^\theta(\omega^0))$	$\frac{1}{8}J^\theta(\omega^0)$
0	$\frac{1}{4}J^\theta(-2\omega^0)$	$\frac{1}{8}J^\theta(-\omega^0)$	$-\frac{1}{8}J^\theta(\omega^0) - \frac{1}{4}J^\theta(2\omega^0)$

(2.147)

The row and column of zeros indicate that the singlet population is disconnected from the triplet populations under dipole-dipole relaxation processes. The population of the singlet state is therefore a long-lived state [74–80], in the case that coherent Hamiltonian terms mixing the singlet and triplet states are suppressed. In the current example, the relevant singlet-triplet mixing term is proportional to the chemical shift frequency difference $|\Omega_1 - \Omega_2|$. The long-lived nature of the singlet population is revealed by suppressing this mixing term, either by transporting the sample to a region of low magnetic field [74], or by applying a resonant radiofrequency field [78].

The thermalised relaxation superoperator $\hat{\Gamma}_{\text{LB}}^\theta$ may also be used to treat well-known relaxation phenomena such as the transient and steady-state nuclear Overhauser (NOE) effects [22, 37]. The simulations shown in Figure 2.5 were performed by integrating the homogeneous equation of motion in the interaction frame (equation 2.84) using *SpinDynamica* software [63].

Figure 2.5(a) shows a transient NOE effect in which inversion of the magnetization of one set of spins induces a transient increase in the magnetization of the second set of spins through dipole-dipole cross-relaxation. Figure 2.5(b) shows a steady-state NOE effect. Saturation of the longitudinal magnetization of one set of spins by a continuous resonant rf field establishes a steady state in which the magnetization of the second set of spins is enhanced with respect to thermal equilibrium.

These phenomena are well understood and the simulated trajectories using the Lindblad method agree with the literature [45, 46]. For the steady-state NOE it is straightforward to show that within the fast motion limit ($\omega^0 \tau_C \ll 1$) and high-temperature approximation the maximal achievable polarisation enhancement on the passive spin is given by $\epsilon_{\text{NOE}}^{\text{SS}} = \frac{3}{2}$ which is in agreement with figure 2.5(b) [22, 37].

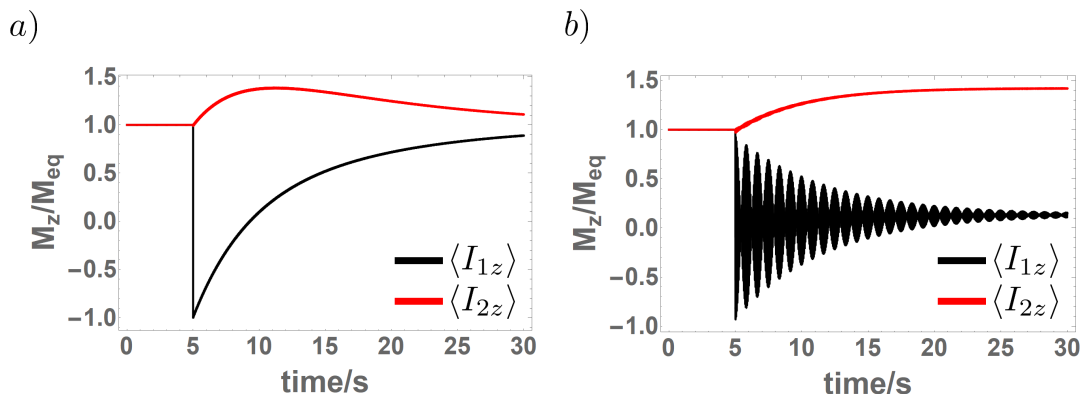


FIGURE 2.5: Simulations of nuclear Overhauser effects (NOE) in a system of homonuclear proton pairs at a temperature of 300 K and a magnetic field of 11.75 T using the Lindbladian form of the relaxation superoperator (equation 2.143). The vertical scales correspond to the ratio of the longitudinal spin magnetization M_z to its thermal equilibrium value M_{eq} . (a) Simulation of the transient NOE. Starting from thermal equilibrium, a selective π -rotation is applied to one set of spins at time point $t = 5$ s, and the expectation values of the z -magnetization components tracked in the subsequent interval. No resonant rf field is applied ($\omega_{\text{nut}} = 0$). (b) Simulation of the steady-state NOE. Starting at $t = 5$ s, a continuous rf irradiation with nutation frequency $\omega_{\text{nut}} = 2\pi \times 2.5$ Hz is applied to a thermal equilibrium state. The simulation parameters are as follows: $\Omega_1 = 0$, $\Omega_2 = 2\pi \times 200$ Hz, $J_{12} = 15$ Hz, $b_{12} = -2\pi \times 30$ kHz, and $\tau_C = 10$ ps. The resulting T_1 time constant is 5.64 s.

2.6.2 Heteronuclear spin-1/2 pairs

In the case of heteronuclear spin pairs (one I -spin coupled to one S -spin, with magnetogyric ratios γ_I and γ_S), the dominant part of the coherent Hamiltonian, in the laboratory frame, is given by

$$H_A = \omega_I^0(1 + \delta_{\text{ref}}^I)I_z + \omega_S^0(1 + \delta_{\text{ref}}^S)S_z, \quad (2.148)$$

where $\omega_I^0 = -\gamma_I B^0$ and $\omega_S^0 = -\gamma_S B^0$ are the Larmor frequencies of the two species, and $\{\delta_{\text{ref}}^I, \delta_{\text{ref}}^S\}$ are the chemical shifts of the two spectrometer reference frequencies.

The H_B and H_C components of the coherent spin Hamiltonian have the following form in the interaction frame of H_A

$$\begin{aligned} H_B &= \Omega_I I_z + \Omega_S S_z + 2\pi J_{IS} I_z S_z \\ H_C &= \omega_{\text{nut}}^I (I_x \cos \phi_I + I_y \sin \phi_I) + \omega_{\text{nut}}^S (S_x \cos \phi_S + S_y \sin \phi_S). \end{aligned} \quad (2.149)$$

The chemical shift offset frequencies for the two isotopes are given by $\Omega_I = \omega_I^0(\delta_I - \delta_{\text{ref}}^I)$ and $\Omega_S = \omega_S^0(\delta_S - \delta_{\text{ref}}^S)$, where δ_I and δ_S are the chemical shifts of the two spin species. Resonant radiofrequency fields applied to the two spin species have amplitudes corresponding to the nutation frequencies $\{\omega_{\text{nut}}^I, \omega_{\text{nut}}^S\}$, and phases $\{\phi_I, \phi_S\}$.

According to Equation 2.40, the eigenoperators of H_A are given in the heteronuclear case by products of spherical tensor operators. These may be labelled by their individual total and z -angular momentum ($T_{k_1 k_2 m_1 m_2}^{(ij)}$). The relevant eigenoperators for heteronuclear dipolar relaxation are given by column $(k_1, k_2) = (1, 1)$ of table A.2. The thermalised relaxation superoperator for the heteronuclear case may be expressed as follows:

$$\hat{\Gamma}_{\text{LB}}^\theta = \frac{6}{5} b_{12}^2 \sum_{m'_1, m'_2=-2}^{+2} \sum_{m_1, m_2=-2}^{+2} \hat{\mathcal{D}}[T_{11m_1 m_2}^{(12)}, T_{11m_1 m_2}^{(12)\dagger}] J^\theta(\omega_{m_1 m_2}^A) \delta(\omega_{m_1 m_2}^A - \omega_{m'_1 m'_2}^A). \quad (2.150)$$

The relaxation dynamics of the Zeeman spin state populations are governed by the following matrix:

$$[\hat{\Gamma}_{\text{LB}}^\theta]_{4 \times 4} = \frac{6}{5} b_{12}^2 \times$$

$ \alpha\alpha\rangle \langle\alpha\alpha $	$ \beta\alpha\rangle \langle\beta\alpha $	$ \alpha\beta\rangle \langle\alpha\beta $	$ \beta\beta\rangle \langle\beta\beta $
$-\frac{1}{16} J^\theta(-\omega_I^0)$ $-\frac{1}{16} J^\theta(-\omega_S^0)$ $-\frac{1}{4} J^\theta(-(\omega_I^0 + \omega_S^0))$	$\frac{1}{16} J^\theta(\omega_I^0)$	$\frac{1}{16} J^\theta(\omega_S^0)$	$\frac{1}{4} J^\theta(\omega_I^0 + \omega_S^0)$
$\frac{1}{16} J^\theta(-\omega_I^0)$	$-\frac{1}{16} J^\theta(\omega_I^0)$ $-\frac{1}{16} J^\theta(-\omega_S^0)$ $-\frac{1}{24} J^\theta(\omega_I^0 - \omega_S^0)$	$\frac{1}{24} J^\theta(-\omega_I^0 + \omega_S^0)$	$\frac{1}{16} J^\theta(\omega_S^0)$
$\frac{1}{16} J^\theta(-\omega_S^0)$	$\frac{1}{24} J^\theta(\omega_I^0 - \omega_S^0)$	$-\frac{1}{16} J^\theta(-\omega_I^0)$ $-\frac{1}{16} J^\theta(\omega_S^0)$ $-\frac{1}{24} J^\theta(-\omega_I^0 + \omega_S^0)$	$\frac{1}{16} J^\theta(\omega_I^0)$
$\frac{1}{4} J^\theta(-(\omega_I^0 + \omega_S^0))$	$\frac{1}{16} J^\theta(-\omega_S^0)$	$\frac{1}{16} J^\theta(-\omega_I^0)$	$-\frac{1}{16} J^\theta(\omega_I^0)$ $-\frac{1}{16} J^\theta(\omega_S^0)$ $-\frac{1}{4} J^\theta(\omega_I^0 + \omega_S^0)$

(2.151)

Simulations of the z -magnetisation dynamics during heteronuclear transient-NOE and steady-state-NOE experiments [22, 37] involving pairs of ^{13}C and ^1H spins are shown in figure 2.6. The trajectories were generated by *SpinDynamica* software [63] using equation 2.150. The maximum achievable enhancement of the ^{13}C magnetization for a coupled ^{13}C - ^1H pair in the steady-state NOE experiment is given by $\epsilon \simeq 3$. The numerical simulations of figure 2.6(b) confirm that this well-known result [22, 37] may be reproduced by using the Lindbladian relaxation superoperator.

2.6.3 Singlet-Triplet conversion

As a concluding example the build-up of longitudinal magnetization in a system of magnetically equivalent (or near-equivalent) spin-1/2 pairs fully populated in their singlet

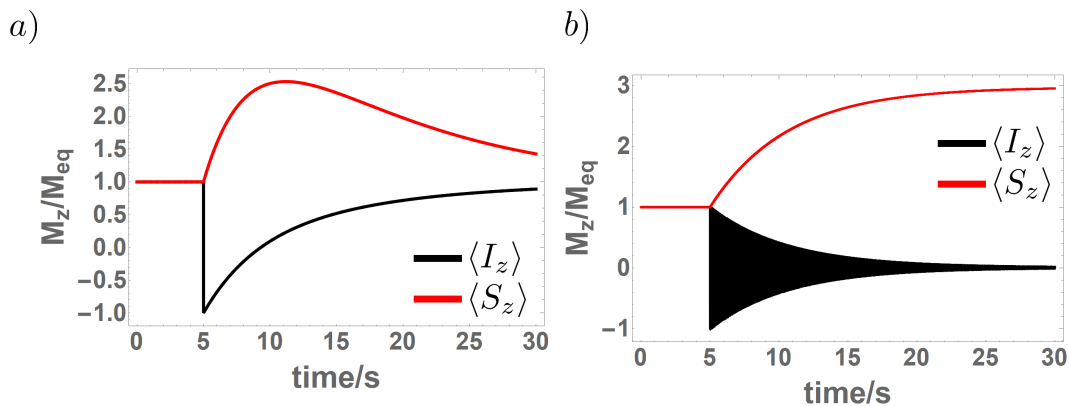


FIGURE 2.6: Simulations of heteronuclear Overhauser effects (NOE) in a system of ^1H - ^{13}C pairs at a temperature of 300 K and a magnetic field of 11.75 T using the Lindbladian form of the relaxation superoperator (equation 2.143). The black curves show the ratio of the ^1H (I -spin) magnetization M_z^I to its thermal equilibrium value M_{eq}^I . The red curves show the ratio of the ^{13}C (S -spin) magnetization M_z^S to its thermal equilibrium value M_{eq}^S . (a) Simulation of the transient NOE. Starting from thermal equilibrium, a selective π -rotation is applied to the ^1H spins at time point $t = 5$ s and the expectation values of the z -angular momentum components of both spin species tracked in the subsequent interval. No resonant rf field is applied ($\omega_{\text{nut}}^I = \omega_{\text{nut}}^S = 0$). (b) Simulation of the steady-state NOE. Starting from a thermal equilibrium state, continuous rf irradiation with nutation frequency $\omega_{\text{nut}}^I = 2\pi \times 100$ Hz is applied to the ^1H spins, starting at time point $t = 5$ s. No rf field is applied to the ^{13}C spins ($\omega_{\text{nut}}^S = 0$). The dipolar relaxation was treated using equation 2.150. The simulation parameters are as follows: $\Omega_I = \Omega_S = 0$, $\tau_C = 10$ ps, $b_{12} = -2\pi \times 30$ kHz. For this choice of parameters the ^1H and ^{13}C T_1 time constants are $T_1^I = T_1^S = 5.62$ s.

state is considered. Under normal conditions this represents a system that has been prepared “in an unusual way” (the experimental verification will be given in the following section).

The dominant and perturbative parts of the coherent Hamiltonian in the absence of resonance rf fields are given by:

$$H_A = \omega^0(I_{1z} + I_{2z}), \quad H_B = 2\pi J_{12}\mathbf{I}_1 \cdot \mathbf{I}_2, \quad (2.152)$$

so that spherical tensor operators may be used as the eigenoperators of \hat{H}_A .

The relaxation of the system may be modelled as a superposition of the dipole-dipole (DD) and fluctuating random field (ran) mechanisms [39]. The fluctuating random field mechanism may include spin-rotation interactions as well as external random fields deriving from, for example, paramagnetic species in solution. The DD mechanism does not induce spin-isomer conversion, which is entirely driven by uncorrelated random fields. The relaxation superoperator in the Lindblad formalism is therefore written as

$$\hat{\Gamma}_{\text{LB}}^\theta = \hat{\Gamma}_{\text{LB}}^{\theta, \text{DD}} + \hat{\Gamma}_{\text{LB}}^{\theta, \text{ran}}. \quad (2.153)$$

The DD Lindbladian relaxation superoperator $\hat{\Gamma}_{\text{LB}}^{\theta, \text{DD}}$ is given by equation 2.143. A suitable relaxation superoperator for the fluctuating random fields is given by the following expression

$$\hat{\Gamma}_{\text{LB}}^{\theta, \text{ran}} = \sum_{i,j=1}^2 \kappa_{ij} \omega_{\text{rms}}^{(i)} \omega_{\text{rms}}^{(j)} \sum_{m=-1}^{+1} \hat{\mathcal{D}}[T_{1m}^{(i)}, T_{1m}^{(j)\dagger}] J_{\text{ran}}^{\theta}(m\omega^0), \quad (2.154)$$

where

$$J_{\text{ran}}^{\theta}(\omega) = J_{\text{ran}}(\omega) \exp(-\frac{1}{2}\beta_{\theta}\omega) \quad (2.155)$$

and

$$J_{\text{ran}}(\omega) = \frac{2\tau_{\text{ran}}}{1 + \omega^2\tau_{\text{ran}}^2}. \quad (2.156)$$

Here $J_{\text{ran}}(\omega)$ represents the spectral density for the external random field fluctuations, $\omega_{\text{rms}}^{(j)}$ is the root-mean-square amplitude of the local field fluctuations, assumed to be isotropic and the same for the two sites ($\omega_{\text{rms}} = \omega_{\text{rms}}^{(1)} = \omega_{\text{rms}}^{(2)}$). The coefficient $-1 \leq \kappa_{12} \leq 1$ describes the correlation between random field fluctuations at spin sites (i) and (j). By definition, $\kappa_{11} = \kappa_{22} = 1$. Perfectly correlated random fields are described by $\kappa_{12} = 1$ while uncorrelated random fields have $\kappa_{12} = 0$.

In the extreme narrowing limit, the spectral density functions are frequency-independent ($J(\omega) \simeq 2\tau_C$). The relaxation rate constant R_1 is given by

$$R_1 = R_1^{\text{DD}} + R_1^{\text{ran}}, \quad (2.157)$$

where the individual contributions to R_1 are given by the following matrix elements

$$\begin{aligned} R_1^{\text{DD}} &= -\frac{\langle I_z | \hat{\Gamma}_{\text{LB}}^{\theta, \text{DD}} | I_z \rangle}{\langle I_z | I_z \rangle} = \frac{3}{10} b_{12}^2 \tau_C (\cosh(\frac{1}{2}\beta_{\theta}\omega^0) + 4 \cosh(\beta_{\theta}\omega^0)), \\ R_1^{\text{ran}} &= -\frac{\langle I_z | \hat{\Gamma}_{\text{LB}}^{\theta, \text{ran}} | I_z \rangle}{\langle I_z | I_z \rangle} = 2\omega_{\text{rms}}^2 \tau_{\text{ran}} \cosh(\frac{1}{2}\beta_{\theta}\omega^0). \end{aligned} \quad (2.158)$$

In the Lindblad formalism, the temperature-dependence of the spin-lattice relaxation rate constants derives not only from the temperature-dependence of the correlation time τ_C and τ_{ran} , but also from the explicit temperature dependence of the hyperbolic functions in equation 2.158.

The relaxation rate constant for singlet order (the mean population difference between the singlet and triplet states) is given by the following matrix element

$$R_S = R_S^{\text{ran}} = -\frac{\langle \mathbf{I}_1 \cdot \mathbf{I}_2 | \hat{\Gamma}_{\text{LB}}^{\theta, \text{ran}} | \mathbf{I}_1 \cdot \mathbf{I}_2 \rangle}{\langle \mathbf{I}_1 \cdot \mathbf{I}_2 | \mathbf{I}_1 \cdot \mathbf{I}_2 \rangle} = \frac{4}{3} \omega_{\text{rms}}^2 \tau_{\text{ran}} (1 - \kappa_{12}) (1 + 2 \cosh(\frac{1}{2}\beta_{\theta}\omega^0)). \quad (2.159)$$

In the high-temperature limit, which is applicable to NMR at ordinary temperatures, these expressions are given by:

$$R_1^{\text{DD}} \simeq \frac{3}{2} b_{12}^2 \tau_C, \quad R_1^{\text{ran}} \simeq 2\omega_{\text{rms}}^2 \tau_{\text{ran}}, \quad R_S^{\text{ran}} \simeq 4\omega_{\text{rms}}^2 \tau_{\text{ran}} (1 - \kappa_{12}). \quad (2.160)$$

The relaxation rate constant for singlet order R_S vanishes for perfectly correlated random fields ($\kappa_{12} = 1$).

As shown in Appendix A.3, the trajectory of the z -magnetisation is well approximated within the fast-motion and high-temperature limit by the following expression

$$\langle I_z(t) \rangle / \langle I_z \rangle_{\text{eq}} \simeq 1 - A_1 \exp(-R_1 t) - A_S \exp(-R_S t), \quad (2.161)$$

where the coefficients are

$$A_1 = \frac{R_S}{2(R_1 - R_S)}, \quad A_S = \frac{-2R_1 + R_S}{2(R_1 - R_S)}. \quad (2.162)$$

The first exponential in equation 2.161 represents the fast equilibration of the outer triplet states due to T_1 processes. The second exponential represents the singlet-triplet conversion process. The coefficients approach $A_1 \rightarrow 0$ and $A_S \rightarrow -1$ in the limit $R_1 \gg R_S$, in which case the recovery of z -magnetization is dominated by the small rate constant R_S for the singlet-triplet conversion.

A numerical comparison between the IME and the Lindblad approach is shown figure 2.7. As figure 2.7 shows there is great disagreement between the IME and the Lindblad approach. This may be rationalised as follows. Because the singlet and triplet states are approximately eigenstates of the dominant Hamiltonian, the conversion between the $I = 0$ and $I = 1$ manifold is rather inefficient. The corresponding time scale of the process is described by a time constant $T_S = R_S^{-1}$ (see figure 2.7a top). However, the triplet manifold rapidly magnetizes in the magnetic field due to spin-lattice relaxation, leading to the establishment of a Boltzmann distribution between its Zeeman-split energy levels (see figure 2.7a middle). The spin-lattice relaxation time constant T_1 is therefore much smaller than the time constant T_S for singlet-to-triplet conversion. It is therefore reasonable to assume that the rate of magnetization build-up is limited by the slowest process, which is the singlet-to-triplet conversion. Hence, the magnetization should build up along the field with the slow time constant of the order of T_S rather than T_1 (see figure 2.7a bottom).

The IME however predicts a recovery of the z -magnetisation with a time constant T_1 . It follows that the IME completely fails to capture the physical picture. This is a direct consequence of the initial density operator being far from equilibrium. The IME is simply not suited to treat these cases.

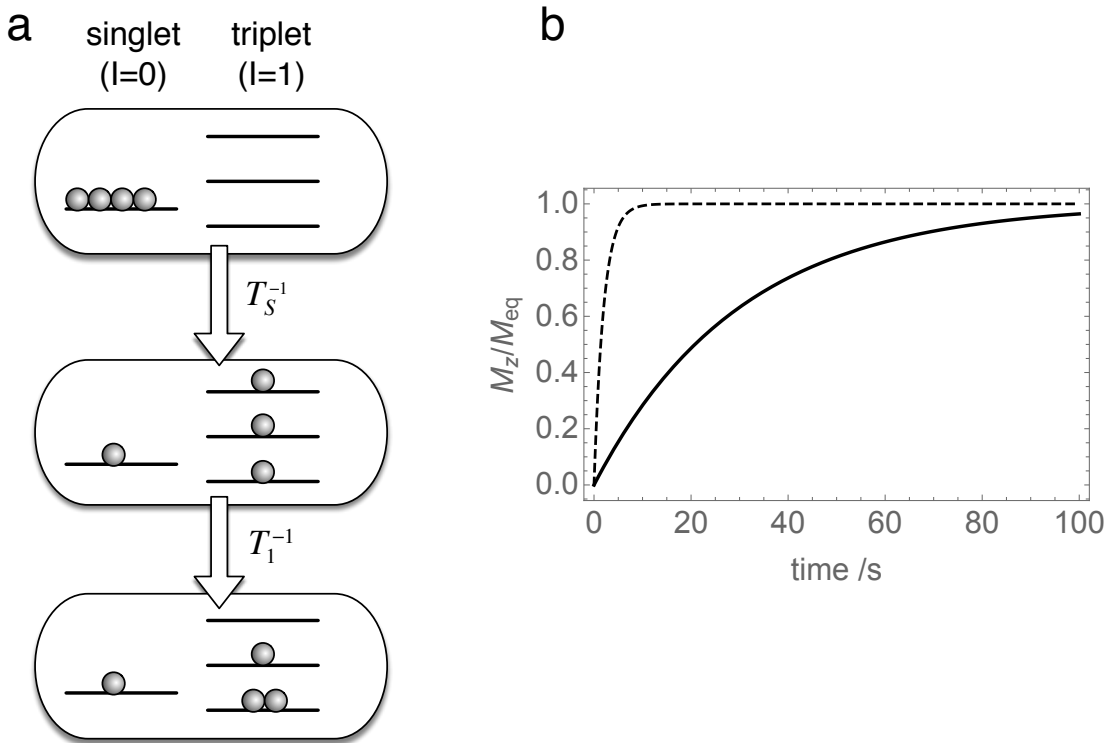


FIGURE 2.7: A particular example which illustrates the failure of the IME for spin systems far from equilibrium. The horizontal lines represent the Hamiltonian eigenvalues (energy levels) and the balls represent state populations. (a) An ensemble of spin-1/2 pairs is prepared so that only the non-magnetic ($I = 0$) singlet state is populated. Conversion from the singlet state to the magnetic triplet states ($I = 1$) occurs with a time constant T_S . The triplet manifold reaches thermal equilibrium in a magnetic field with time constant T_1 , such that $T_1 \ll T_S$. (b) Trajectories of the spin magnetization along the field M_z , normalized to the thermal equilibrium value. The IME predicts recovery of M_z with time constant T_1 (dashed line), which is physically unreasonable. The Lindblad trajectory (solid line) has been simulated using equations 2.143 and 2.154. The simulations were performed using the parameters: $\omega_{\text{rms}} = 2\pi \times 10$ kHz, $\tau_{\text{ran}} = 60.31$ ps, $\kappa_{12} = 0.955$, $\tau_C = 107$ fs and $b_{12} = -2\pi \times 34.88$ kHz, resulting in relaxation time constants: $T_1 = 2$ s and $T_S = 22.5$ s.

The Lindblad method on the other correctly captures the physical picture and describes the recovery of the longitudinal magnetization with the long time constant $T_S \gg T_1$, as indicated by the (approximate) analytic solution of equation 2.161.

2.7 Fullerene-encapsulated water ($\text{H}_2\text{O}@\text{C}_{60}$)

The following discussion is based on references 39 and 81.

Modern NMR techniques routinely generate far from equilibrium systems. Many of these systems may not be adequately described within a semi-classical approach. Instead more sophisticated thermalisation techniques such as the Lindblad method become relevant. A particular example where this is true, is given by *fullerene-encapsulated* water molecules ($\text{H}_2\text{O}@\text{C}_{60}$) as shown in figure 2.8a.

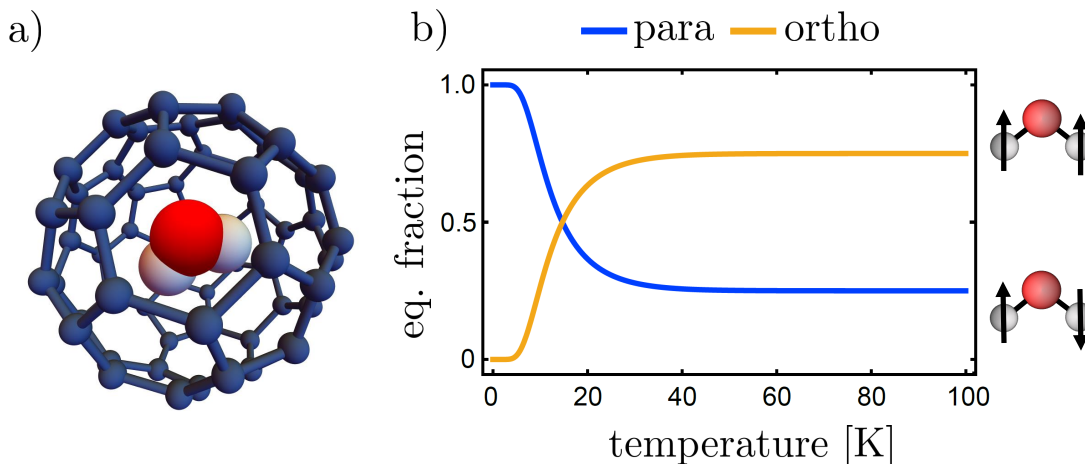


FIGURE 2.8: **a)** Schematic representation of a fullerene-encapsulated water molecule (not to scale). **b)** The two protons of the $\text{H}_2\text{O}@\text{C}_{60}$ molecules may occupy either a nuclear singlet or one of its triplet states. The fractional population of these two spin-states depends significantly on the temperature of the environment.

The C_{60} framework acts as an isolating cage for the water molecule reducing the effect of external influences, most notably proton exchange. Inside the fullerene cage the water molecule undergoes unhindered rotation and behaves like a *molecular quantum rotor*. The rotational motion of the water molecule is therefore quantised and may be characterised by the corresponding quantum numbers. In a *rigid rotor* approximation the energy levels (see figure 2.9) are given by [82, 83]

$$E_J = \frac{J(J+1)\hbar^2}{2I_M}, \quad (2.163)$$

where each energy level is $(2J+1)$ -times degenerate and I_M denotes the *moment of inertia* of the water molecule. In some way the encapsulated water molecule thus behaves similarly to water in the gas phase.

The $\text{H}_2\text{O}@\text{C}_{60}$ molecules exhibit interesting magnetic properties due to *Pauli principle* [84]. The overall wave function of a molecule may be denoted by $\psi(\vec{r}, \vec{s})$ with \vec{r} describing all spatial degrees of freedom and \vec{s} describing all spin degrees of freedom.

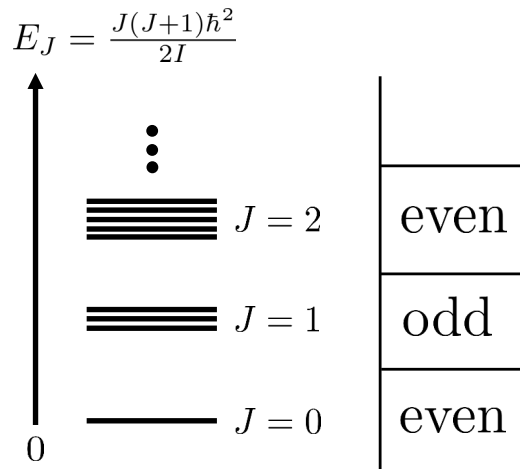


FIGURE 2.9: Rotational energy levels of a quantum rigid rotor (left) and the particle exchange symmetry of the associated eigenstate (right).

For the $\text{H}_2\text{O}@C_{60}$ molecules the vector \vec{r} describes rotational degrees of freedom. The Pauli principle states that the total wave function (for fermions) has to remain anti-symmetric under exchange of any two particles

$$(P_{ij}\psi)(\vec{r}, \vec{s}) = -\psi(P_{ij}\vec{r}, P_{ij}\vec{s}), \quad (2.164)$$

where P_{ij} represents the exchange operator for the particles i and j . A common simplification assumes that the total wave function may be decomposed into a direct product of spatial and spin degrees of freedom [82]

$$\psi(\vec{r}, \vec{s}) = \phi(\vec{r})\chi(\vec{s}). \quad (2.165)$$

It follows that the Pauli principle may only be fulfilled if either the spatial part or the spin part is anti-symmetric under particle exchange, but never both. The ladder in figure 2.9 indicates that rotational wave functions described by an even rotational quantum number $J = 2n$ are symmetric, whereas rotational wave functions characterised by odd rotational quantum number $J = 2n + 1$ are anti-symmetric under particle exchange. This suggests the following pattern for the combination of rotational and spin wave functions:

	$\phi(\vec{r})$	$\chi(\vec{s})$
$\psi(\vec{r}, \vec{s})$	even	odd
$\psi(\vec{r}, \vec{s})$	odd	even

TABLE 2.2: Possible permutation symmetries of spatial and spin wave functions under the exchange of any two particles in order to fulfill the Pauli Principle.

Symmetric rotational states may therefore only combine with anti-symmetric spin states and anti-symmetric rotational states may only combine with symmetric spin states.

This leads to the concept of *spin isomerism* describing the idea that encapsulated H₂O molecules may exclusively exist in a *para*-state ($I=0$) or *ortho*-state ($I=1$). To a good approximation the populations of the *ortho*- and *para*-states are governed by a rotational Boltzmann-distribution. Experimental observations indicate that the equilibrium fraction of *ortho* and *para* H₂O@C₆₀ follow the Boltzmann-distribution indicated in figure 2.8b [85, 86]. At low temperatures only the non-magnetic *para* state is accessible as it couples to the rotational ground state with $J = 0$. Sample cooling below $T < 10$ K therefore provides an experimental way to prepare the system in a pure *para*-state.

The following discussion will be based on H₂¹⁶O@C₆₀ and H₂¹⁷O@C₆₀ molecules. Both isotopologues behave as quantum rotors at low temperatures. The H₂¹⁶O@C₆₀ molecules represent an easy model system to study, whereas H₂¹⁷O@C₆₀ molecules are slightly more interesting from an NMR point of view. The H₂¹⁷O@C₆₀ molecules display surprisingly rich spectral properties even if the system is initially prepared in a thermal equilibrium state. The spectral discussion will be followed up by a description of the spin isomer conversion phenomenon at room temperature for both the H₂¹⁶O@C₆₀ and the H₂¹⁷O@C₆₀ molecules.

2.7.1 Proton line shape factors

The H₂O@C₆₀ molecules have been synthesised by molecular surgery techniques, a detailed description of the synthesis can be found in references 87–89. The starting material may either consist of H₂¹⁶O or H₂¹⁷O molecules leading to H₂¹⁶O@C₆₀ or H₂¹⁷O@C₆₀, respectively.

Spectral properties of the H₂¹⁷O@C₆₀ molecules have been analysed by dissolving 26.77 mg of the material in 1 mL of ortho-dichlorobenzene-d₄ (ODCB-d₄). Before acquisition the sample has been thoroughly degassed by several standard freeze-pump-cycles to reduce the content of dissolved molecular oxygen. The determination of the line shapes proceeded by simple pulse excitation of equilibrium spin-order. The relevant portion of the resulting H₂¹⁷O@C₆₀ proton spectrum is shown in figure 2.10.

The proton spectrum shows a clear sextet structure with a small H₂¹⁶O@C₆₀ impurity at its center. The sextet structure follows from the non-zero scalar coupling of the two protons to the ¹⁷O nucleus. The ¹⁷O nucleus possesses spin $S = 5/2$ with $(2 \times 5/2 + 1 = 6)$ different ¹⁷O spin states. These split the proton signal of the ¹H_{*a*} into a sextet. Clearly by symmetry the signal of the second proton ¹H_{*b*} is also split into a sextet in exactly the same fashion. The resonance frequencies for the ¹H_{*a*} and ¹H_{*b*} are thus identical and

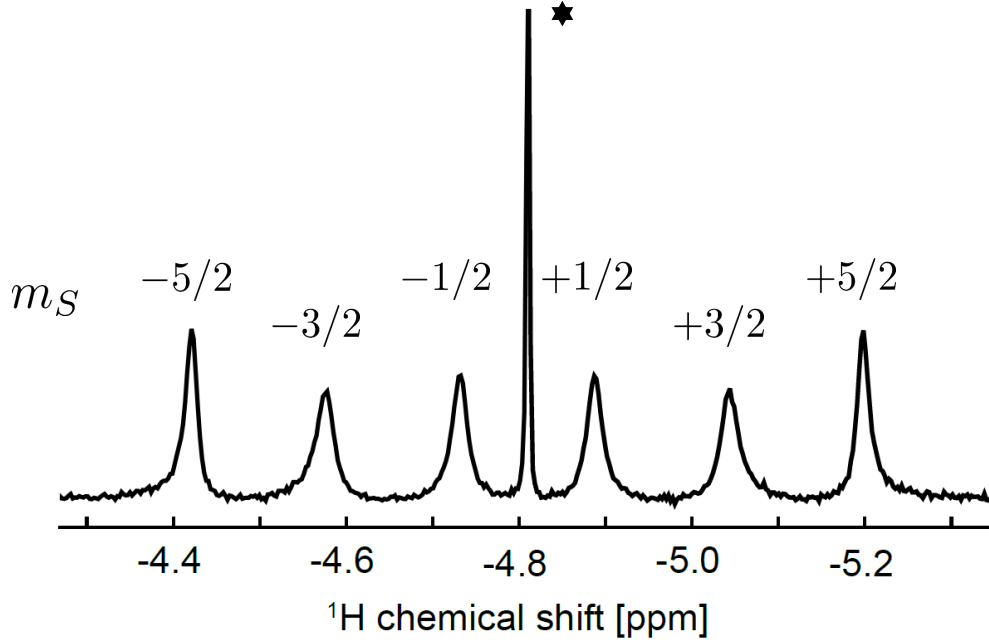


FIGURE 2.10: Relevant region of the $\text{H}_2^{17}\text{O}@C_{60}$ proton spectrum after simple pulse excitation. Sample was dissolved in ODCB-d4 with a final concentration of 36.2 mM. The proton resonances are split into a sextet structure. Individual peaks may be associated with the z -angular momentum quantum number m_S of the ^{17}O . The assignment assumes a negative scalar coupling constant. The central resonance (indicated by a star) may be attributed to $\text{H}_2^{16}\text{O}@C_{60}$ impurities. Spectral integration indicates that 88% of the fullerenes are occupied by H_2^{17}O molecules and the remaining 12% with H_2^{16}O . The peak linewidths of the sextet display the ratios (15:23:18:18:23:15).

overlap with each other. The individual peaks of the sextet may therefore be associated with one of the projection quantum numbers m_S of the ^{17}O spin (see figure 2.10 top).

The laboratory frame coherent Hamiltonian for this system may be expressed as follows:

$$H_{\text{coh}}^{\text{lab}} = \omega_1^0(I_{1z} + I_{2z}) + \omega_S^0 S_z + 2\pi J_{\text{IS}}(I_{1z}S_z + I_{2z}S_z) = \omega_1^0 I_z + \omega_S^0 S_z + 2\pi J_{\text{IS}} I_z S_z, \quad (2.166)$$

where ω_1^0 represents the Larmor frequency of the protons, ω_S^0 the Larmor frequency of the oxygen and J_{IS} their mutual scalar coupling constant. The z -angular momentum operators I_{jz} refer to the z -angular momentum of the protons and the z -angular momentum operator S_z refers to the z -angular momentum of the oxygen. The scalar coupling between the protons has been omitted as these do not contribute to the NMR signal [22]. The resulting rotating frame Hamiltonian is given by a single scalar coupling interaction

$$H_{\text{coh}} = 2\pi J_{\text{IS}} I_z S_z. \quad (2.167)$$

The splitting of the proton lines is rather unremarkable and may be explained by standard NMR theory. But the linewidth behaviour of the proton resonances is surprising and requires more careful analysis. The proton peaks highlighted in figure 2.10 display identical peak areas, but rather different proton linewidths (here defined as the full width at a peaks half maximum height). The linewidths for the proton peaks are 9.1 ± 0.3 Hz ($m_S = \pm 5/2$), 13.2 ± 0.3 Hz ($m_S = \pm 3/2$) and 10.7 ± 0.1 Hz ($m_S = \pm 1/2$) leading to ratios (15:23:18:18:23:15). In general the linewidth of a Lorentzian is related to its relaxation rate constant λ_j . The real part of a complex Lorentzian (see equation 1.13) takes the form

$$\text{Re}\{S_j(\omega)\} = M_{\text{eq}}^0 \times \frac{\lambda_j}{\lambda_j^2 + (\omega - \omega_j)^2}, \quad (2.168)$$

where λ_j and ω_j represent generic relaxation rate constants and resonance frequencies. The half maximum peak height of a real Lorentzian occurs at $(\omega_j \pm \lambda_j)$

$$\text{Re}\{S_j(\omega_j - \lambda_j)\} = \text{Re}\{S_j(\omega_j + \lambda_j)\} = M_{\text{eq}}^0 \frac{1}{2\lambda_j} \propto \frac{1}{2\lambda_j}, \quad (2.169)$$

so that the peak linewidth is proportional to twice relaxation rate constant ($\propto 2\lambda_j$). This means that the resonances of the ^1H spectrum with $m_S = \pm 5/2$, $m_S = \pm 3/2$ and $m_S = \pm 1/2$ all relax at different rates.

In general there are several relaxation mechanisms that may contribute to the spectral line shape. Common relaxation mechanisms for small molecules, such as the encapsulated H_2O molecules, are fluctuating dipolar fields, external random fields and chemical shift anisotropy modulation [36]. These however are incapable of explaining the peculiar peak linewidth pattern of figure 2.10. Instead numerical simulations suggest that the proton line shape is completely dominated by the quadrupolar relaxation of the oxygen spin. A comparison between the experimental spectrum (figure 2.10) and a *SpinDynamica* simulation including only quadrupolar relaxation of the oxygen is shown in figure 2.11 [63].

The spectral simulation assumed a semi-classical expression for the quadrupolar relaxation superoperator and the coherent Hamiltonian given by equation 2.166. Within the fast motion limit the quadrupolar relaxation superoperator takes the following form [36]

$$\hat{\Gamma}_{\text{SC}}^{\text{Q}} = -\frac{\tau_C}{5} \left\| A_{\text{Q}}^{(3)} \right\|^2 \sum_{m=-2}^2 (-1)^m \hat{T}_{2m}^{(3)} \hat{T}_{2-m}^{(3)} \quad \text{with} \quad \left\| A_{\text{Q}}^{(3)} \right\|^2 = (C_{\text{Q}}^{(3)})^2 \text{Tr}(W_{\text{Q}}^{(3)\dagger} \cdot W_{\text{Q}}^{(3)}). \quad (2.170)$$

Explicit expressions for the quadrupolar ISTO are given in appendix A.2. Good agreement between the experimental and simulated spectrum was found for $J_{\text{IS}} = -77.9$ Hz, $\tau_C = 107$ fs. The norm of the quadrupole tensor $\left\| A_{\text{Q}}^{(3)} \right\|/2\pi = 0.675$ MHz has been calculated previously using quantum chemistry techniques [90].

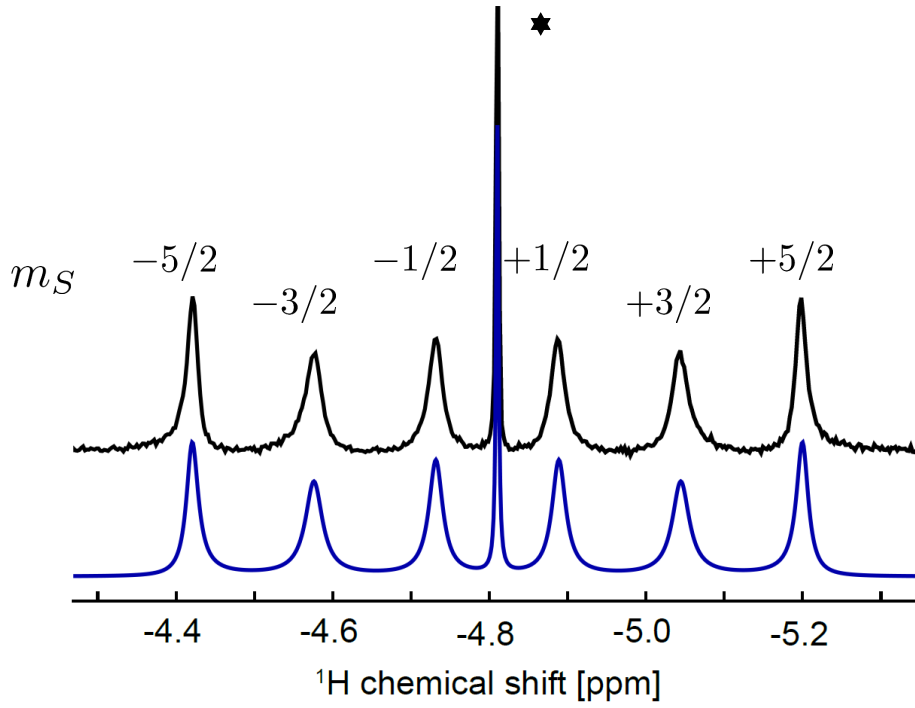


FIGURE 2.11: Comparison between the experimental (black) and simulated (blue) proton spectrum of the $\text{H}_2^{17}\text{O}@C_{60}$ molecules after simple pulse excitation. The proton line shape is completely dominated by quadrupolar relaxation of the oxygen and other relaxation mechanisms have been neglected. The simulation parameters are $J_{\text{IS}} = -77.9$ Hz, $\tau_C = 107$ fs and $\|A_Q^{(3)}\|/2\pi = 0.675$ MHz.

For the line shape determination it is not necessary to employ the Lindblad formalism since the initial state of the system represents equilibrium spin order. Instead it is sufficient to consider the following Liouvillian

$$\hat{L} \approx -i\hat{H}_{\text{coh}} + \hat{\Gamma}_{\text{SC}}^{\text{Q}}, \quad (2.171)$$

with \hat{H}_{coh} representing the commutation superoperator of the coherent Hamiltonian given by equation 2.167. Choosing a particular set of basis operators the Liouvillian may be represented by a $(N_{\mathcal{H}}^2 \times N_{\mathcal{H}}^2)$ dimensional matrix. The dimensionality of the problem quickly grows with an increasing number of spins and larger spin angular momenta. For the line shape problem however it is not necessary to consider the complete matrix of the Liouvillian. The subspace spanned by the following set of orthogonal spin operators contains all the necessary information

$$\{(I_1^- + I_2^-) \otimes |S, m_S\rangle\langle m_S, S|\}, \quad m_S \in \{-S, -S+1, \dots, +S+1, +S\}. \quad (2.172)$$

For the $\text{H}_2^{17}\text{O}@C_{60}$ case with $S = 5/2$ the line shape information is contained within a (6×6) dimensional subspace. The projected matrix block takes the following form:

$$\begin{bmatrix} -i\frac{5}{2}J_{\text{IS}} - 12\tau_Q & 8\tau_Q & 4\tau_Q & 0 & 0 & 0 \\ 8\tau_Q & -i\frac{3}{2}J_{\text{IS}} - \frac{92}{5}\tau_Q & \frac{16}{5}\tau_Q & \frac{36}{5}\tau_Q & 0 & 0 \\ 4\tau_Q & \frac{16}{5}\tau_Q & -i\frac{1}{2}J_{\text{IS}} - \frac{72}{5}\tau_Q & 0 & \frac{36}{5}\tau_Q & 0 \\ 0 & \frac{36}{5}\tau_Q & 0 & i\frac{1}{2}J_{\text{IS}} - \frac{72}{5}\tau_Q & \frac{16}{5}\tau_Q & 4\tau_Q \\ 0 & 0 & \frac{36}{5}\tau_Q & \frac{16}{5}\tau_Q & i\frac{3}{2}J_{\text{IS}} - \frac{92}{5}\tau_Q & 8\tau_Q \\ 0 & 0 & 0 & 4\tau_Q & 8\tau_Q & i\frac{5}{2}J_{\text{IS}} - 12\tau_Q \end{bmatrix}$$

$$\text{with } \tau_Q = \left\| A_Q^{(3)} \right\|^2 \tau_C. \quad (2.173)$$

For sufficiently slow proton relaxation, which is usually the case in such systems, the condition $1/T_{1\text{H}} \ll 2\pi J_{\text{IS}}$ is well satisfied. In this regime the off-diagonal matrix elements become negligible in the sense of first order perturbation theory [25]. The line widths of the proton peaks are then given by the real part of the diagonal elements.

Since similar setups are frequently encountered in the context of nuclear long-lived spin states one may generalise the considerations above to a generic third spin S . To determine the line shape factors for a generic spin S one may first observe that the quadrupolar relaxation superoperator only acts on spin S . The required matrix elements indicated by equation 2.172 are then fully determined by a set of single spin commutators

$$\hat{T}_{2m}^{(3)} |P_{m_1, m_2}^S\rangle = [T_{2m}^{(3)}, P_{m_1, m_2}^S], \quad (2.174)$$

where the operators P_{m_1, m_2}^S are defined as follows:

$$P_{m_1, m_2}^S = |S, m_1\rangle\langle S, m_2|. \quad (2.175)$$

As indicated in appendix A.2 the spherical tensor operators $T_{2,m}^{(3)}$ may be expressed in terms of shift and z -angular momentum operators. Their action onto an angular momentum state for the quadrupolar spin is given by the following expressions:

$$\begin{aligned} \hat{S}^+ |S, m_i\rangle &= C_{S, m_i}^+ |S, m_i + 1\rangle = \sqrt{S(S+1) - m_i(m_i + 1)} |S, m_i + 1\rangle, \\ \hat{S}^- |S, m_i\rangle &= C_{S, m_i}^- |S, m_i - 1\rangle = \sqrt{S(S+1) - m_i(m_i - 1)} |S, m_i - 1\rangle, \\ \hat{S}_z |S, m_i\rangle &= m_i |S, m_i\rangle. \end{aligned} \quad (2.176)$$

The relations above may be used to determine the general expression for the commutators in equation 2.174

$$\begin{aligned}
[T_{22}^{(3)}, P_{m_1, m_2}^S] &= +\frac{1}{2}(C_{S, m_1}^+ C_{S, m_1+1}^+ P_{m_1+2, m_2}^S - C_{S, m_2}^- C_{S, m_2-1}^- P_{m_1, m_2-2}^S), \\
[T_{21}^{(3)}, P_{m_1, m_2}^S] &= -\frac{1}{2}(m_1 C_{S, m_1}^+ P_{m_1+1, m_2}^S - (m_2 - 1) C_{S, m_2}^- P_{m_1, m_2-1}^S \\
&\quad + (m_1 + 1) C_{S, m_1}^+ P_{m_1+1, m_2}^S - m_2 C_{S, m_2}^- P_{m_1, m_2-1}^S), \\
[T_{20}^{(3)}, P_{m_1, m_2}^S] &= +\sqrt{\frac{3}{2}}(m_1 - m_2)^2 P_{m_1, m_2}^S.
\end{aligned} \tag{2.177}$$

Within the projected subspace of equation 2.172 the spherical tensor operators of opposite projections additionally commute

$$[T_{2m}^{(3)}, T_{2-m}^{(3)}] = 0, \tag{2.178}$$

so that a matrix element for a generic spin S reduces to the sum of three contributions

$$\begin{aligned}
(P_{m_1, m_1}^S | \hat{\Gamma}_{\text{SC}}^{\text{Q}} | P_{m_2, m_2}^S) &= -\frac{\tau_C}{5} \|A_{\text{Q}}^{(3)}\|^2 \left\{ 2(P_{m_1, m_1}^S | \hat{T}_{2-2}^{(3)} \hat{T}_{22}^{(3)} | P_{m_2, m_2}^S) \right. \\
&\quad \left. + 2(P_{m_1, m_1}^S | \hat{T}_{2-1}^{(3)} \hat{T}_{21}^{(3)} | P_{m_2, m_2}^S) + (P_{m_1, m_1}^S | \hat{T}_{20}^{(3)} \hat{T}_{20}^{(3)} | P_{m_2, m_2}^S) \right\}.
\end{aligned} \tag{2.179}$$

The commutator relations of equation 2.177 may then be substituted into equation 2.179. If the projection quantum numbers are restricted to $m_1 \leq m_2$ the symbolic software package *Mathematica* may be used to reduce the matrix elements to the following algebraic expressions [91]

$$\begin{aligned}
(P_{m_1, m_1}^S | \hat{\Gamma}_{\text{SC}}^{\text{Q}} | P_{m_2, m_2}^S) &= \\
\tau_C \|A_{\text{Q}}^{(3)}\|^2 \left\{ -\frac{1}{5} \delta_{m_1, m_2} (S(S+1)(S+S^2-1) + 2S(S+1)m_1^2 - 3m_1^4) \right. \\
&\quad + \frac{1}{10} \delta_{m_1, m_2+1} (S-m_2)(S+m_2+1)((2m_2+1)^2) \\
&\quad \left. + \frac{1}{10} \delta_{m_1, m_2+2} (1-2m_2)^2 (S-m_2+1)(S+m_2) \right\}.
\end{aligned} \tag{2.180}$$

And since the semi-classical relaxation superoperator is symmetric, the remaining matrix elements for $m_1 > m_2$ are simply obtained by interchanging the projection numbers m_1 and m_2 .

As argued earlier for slow proton relaxation the line shape factors may be determined by considering the diagonal elements with $m_1 = m_2$. The relaxation rate constant $\lambda(m_1)$ of the proton peak associated with the projection quantum number m_1 of the S spin is then simply given by the expression below:

$$\lambda(m_1) = (P_{m_1, m_1}^S | \hat{\Gamma}_{\text{SC}}^{\text{Q}} | P_{m_1, m_1}^S) = \frac{\tau_C}{5} \|A_{\text{Q}}^{(3)}\|^2 (3m_1^4 + S - 2m_1^2 S(S+1) - S^3(S+2)). \tag{2.181}$$

For the case that $S = 5/2$ the following ratios for the peak linewidths are obtained

$$\frac{23}{\lambda(\pm 3/2)} \{\lambda(\pm 5/2), \lambda(\pm 3/2), \lambda(\pm 1/2)\} = \{15, 23, 18\}, \quad (2.182)$$

which matches the peak linewidths of the experimental spectrum shown in figure 2.10 exactly.

2.7.2 $\text{H}_2\text{O}@C_{60}$ spin isomer conversion

The observation of *para-to-ortho* conversion for the $\text{H}_2\text{O}@C_{60}$ molecules at room temperature is enabled by a technique known as bullet DNP [11]. A schematic overview of the bullet DNP setup is given in figure 2.12.

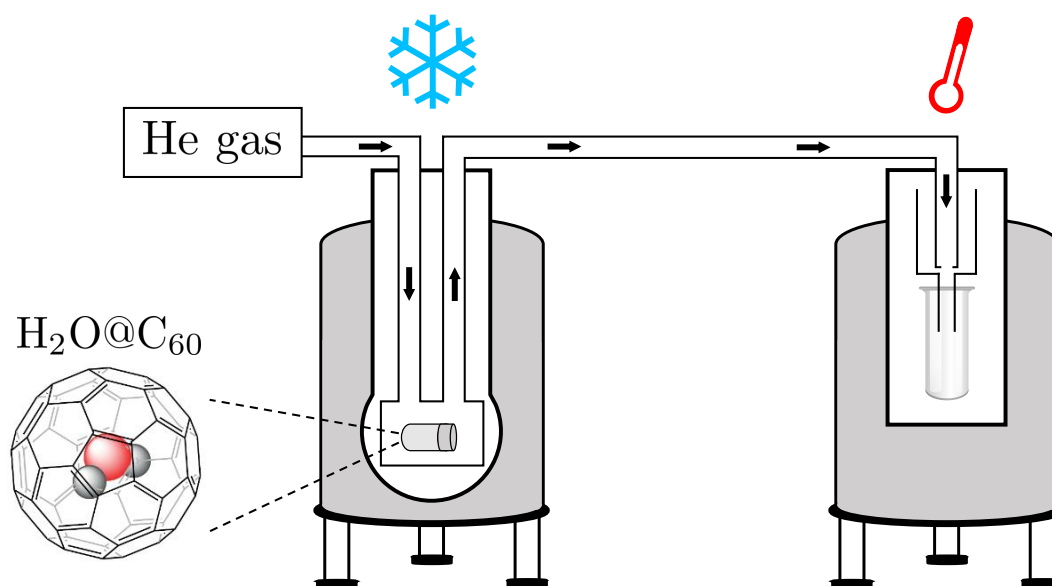


FIGURE 2.12: The bullet DNP setup makes use of two NMR magnets. The first magnet is equilibrated at low temperatures ($T < 10$ K), the second magnet is a conventional high-field NMR magnet at room temperature. The two magnets are connected via a transfer tube. Initially a bullet casing is loaded with a frozen sample solution and placed inside the cooling magnet. The bullet may be transferred to the room temperature magnet via the transfer tubing. The rapid transfer process is driven by pressurised Helium gas. On its way to the detection magnet the bullet hits a receiver before it reaches the sample region. On impact the frozen sample solution is released from the bullet casing and drops into hot solvent of a conventional NMR tube. This leads to a quick dissolution process. After the dissolution process the sample may be manipulated by means of standard high-field NMR techniques.

The *para-to-ortho* conversion dynamics for both $\text{H}_2^{16}\text{O}@C_{60}$ and $\text{H}_2^{17}\text{O}@C_{60}$ have been observed in separate experiments but under identical conditions. Initially a 17 mM solution of $\text{H}_2\text{O}@C_{60}$ in ODCB-d4 has been prepared. The bullet casing was loaded with 50 μL of the 17 mM solution. The freezing process has been performed by exposing

the loaded bullet to liquid nitrogen. Spin isomer enrichment proceeded by keeping the bullet inside the cooling magnet ($\sim 4\text{K}$) for approximately 15 hours. After equilibration pressurised Helium gas at 8 bar has been used for a rapid transport of the sample to the detection magnet. The transfer time was estimated to be around ~ 100 ms. Acquisition of the FID started several seconds before arrival of the sample. After arrival relaxation dynamics of the sample have been monitored by acquisition of a ^1H -spectra time series via application of 30° flip angle pulses every 250 ms.

To increase the signal-to-noise ratio the $\text{H}_2^{16}\text{O}@C_{60}$ ^1H -spectra have been multiplied by a Lorentzian mask (see figure 2.13a). The processed spectra were subsequently integrated to obtain the proton signal intensity as a function of time. The resulting recovery of the z -magnetisation is shown in figure 2.13b.

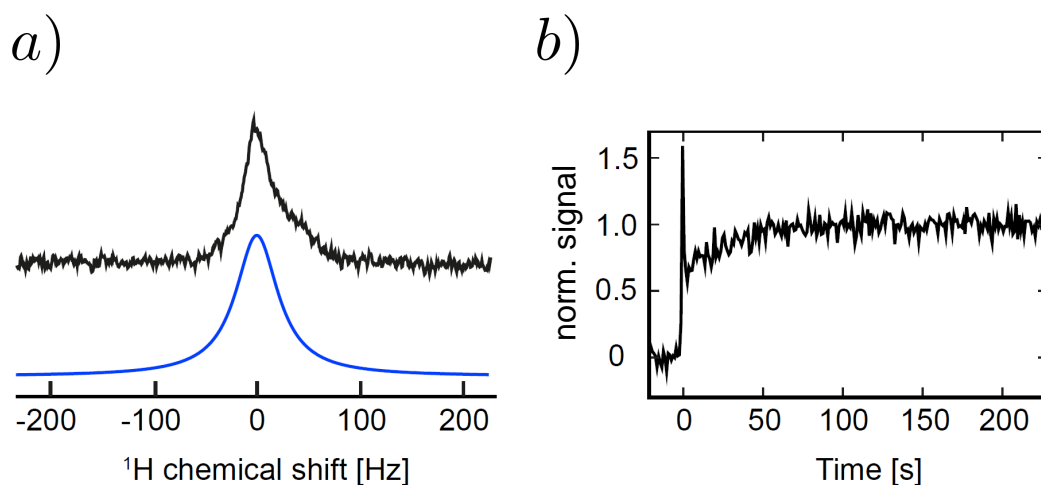


FIGURE 2.13: **a)** $\text{H}_2^{16}\text{O}@C_{60}$ thermal equilibrium proton spectrum in black. Lorentzian mask is indicated in blue. Experimental spectrum has been obtained 8 minutes after the dissolution process and is averaged over 8 transients. **b)** Normalised proton signal as a function of time. The time origin has been chosen to coincide with the arrival of the sample ($t = 0$). Relaxation dynamics have been monitored by a series of ^1H -spectra acquired every 250 ms by simple 30° pulse excitation. Resulting spectra have been integrated after multiplication by a Lorentzian mask and normalised with respect to the steady-state equilibrium magnetisation.

The z -magnetisation trajectory shows a sharp peak at the start of the recovery process. This peak results from observable Zeeman polarisation and is related to a residual magnetic *ortho*- $\text{H}_2^{16}\text{O}@C_{60}$ fraction. It is therefore likely that the equilibration process was not fully completed even after a 15 hour cooling period at $\sim 4\text{K}$. The Zeeman polarisation however quickly decays with a longitudinal relaxation time constant T_1 of approximately 800 ms and the proton signal intensity drastically decreases below its thermal equilibrium value. This indicates the presence of a persistent non-magnetic *para*- $\text{H}_2^{16}\text{O}@C_{60}$ fraction. After approximately 100 seconds the proton signal intensity has fully recovered to its thermal equilibrium value. The slow recovery of the proton intensity may be attributed to the relatively inefficient *para-to-ortho* spin isomer conversion process.

This process occurs on a much longer time scale than ordinary T_1 processes. Since the spin isomer conversion process is closely related to singlet order decay the recovery of the z -magnetisation may be described by a singlet order relaxation time constant T_S of approximately 30 s. The *para-to-ortho* conversion process is much slower since the transition from a *para* to *ortho* spin state is necessarily accompanied by a change in the permutation symmetry of the spin wave function. Many of the very efficient relaxation mechanisms at high magnetic fields (intra-pair dipolar relaxation for example) are incapable of inducing such transitions and are symmetry-forbidden [74–80]. The only effective relaxation mechanism driving the *para-to-ortho* conversion process are randomly fluctuating fields experienced by the fullerene-encapsulated water molecules [39, 74].

Similar observations have been made for the $\text{H}_2^{17}\text{O}@\text{C}_{60}$ molecules. A time series of individual ^1H -spectra for the $\text{H}_2^{17}\text{O}@\text{C}_{60}$ molecules is shown in figure 2.14a. Each spectrum has been weighted by a Lorentzian mask (see figure 2.14a bottom) and additionally time-averaged over an acquisition time of 5 seconds for further improvements to the signal-to-noise ratio.

Most notably the line shapes of the spectrum undergo substantial changes during the recovery process. This may be further appreciated by the sign changes in the proton magnetisation as indicated in figure 2.14b. The peculiar anti-phase pattern displayed by the first proton spectra is characteristic for quantum rotor induced polarisation (QRIP) effects. A full discussion of this effect goes beyond the scope of this work and a detailed explanation may be found in references 61, 92 and 93.

In contrast to the $\text{H}_2^{16}\text{O}@\text{C}_{60}$ sample the z -trajectories for the $\text{H}_2^{17}\text{O}@\text{C}_{60}$ molecules do not display any pronounced intensity spikes at the start of the recovery process. The substitution of ^{16}O by ^{17}O introduces additional dipolar and quadrupolar relaxation pathways. This causes the $\text{H}_2^{17}\text{O}@\text{C}_{60}$ *para-to-ortho* equilibration process to proceed faster, and the residual Zeeman polarisation to relax quicker as the sample is being transported to the detection region [39, 86]. It is therefore not too surprising that the $\text{H}_2^{17}\text{O}@\text{C}_{60}$ molecules display a faster spin isomer conversion rate than the $\text{H}_2^{16}\text{O}@\text{C}_{60}$ molecules (compare figures 2.13b and 2.14b). For the $\text{H}_2^{17}\text{O}@\text{C}_{60}$ molecules the spin isomer conversion process is characterised by a time constant T_S of 16 s. So after a period of approximately 50 seconds after dissolution the conversion process is fully completed and the $\text{H}_2^{17}\text{O}@\text{C}_{60}$ molecules have reached thermal equilibrium. The resulting thermal proton spectrum at the bottom of figure 2.11a can be seen to agree with the thermal spectrum shown in figure 2.11.

The observations above indicate that the state of the protons immediately after dissolution may be approximated by the following density operator $\rho_{\text{H}}(a, b)$

$$\rho_{\text{H}}(a, b) \approx (\mathbb{1} + 2(1 - a)bI_z - 4a\mathbf{I}_1 \cdot \mathbf{I}_2). \quad (2.183)$$

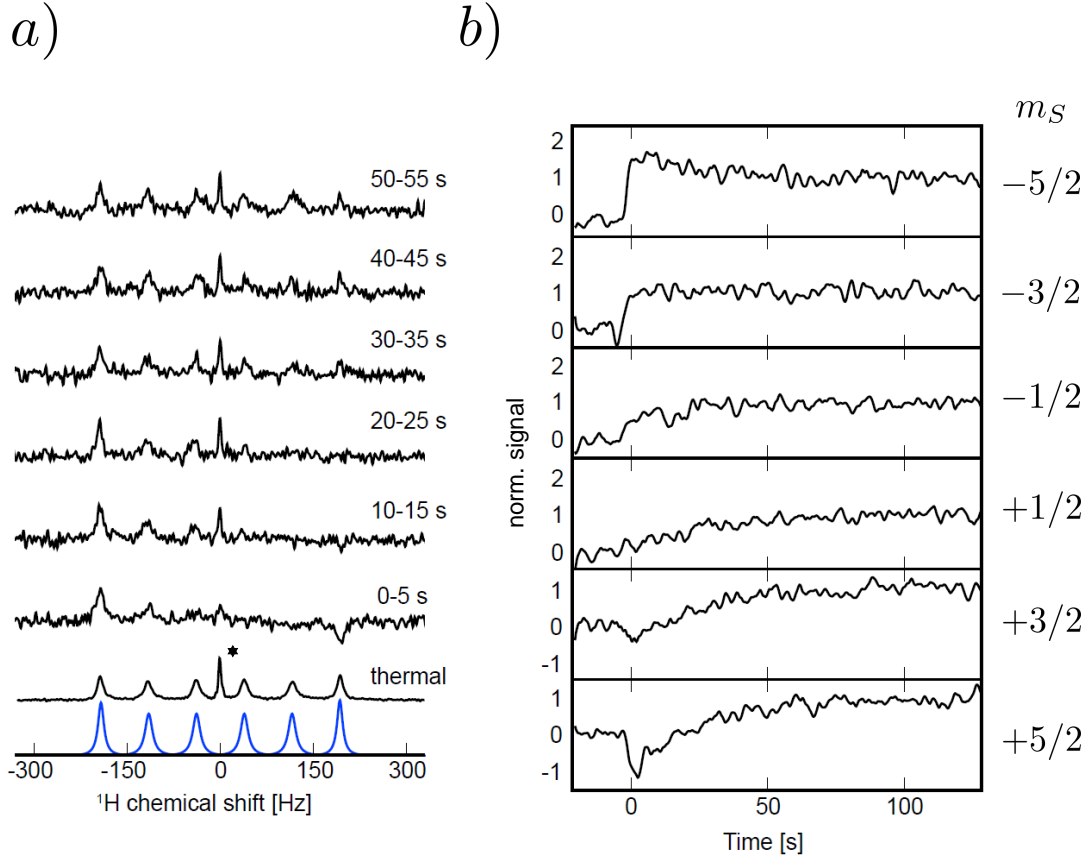


FIGURE 2.14: **a)** $\text{H}_2^{17}\text{O}@C_{60}$ spectral time series after dissolution. A thermal spectrum with small $\text{H}_2^{16}\text{O}@C_{60}$ impurities is indicated at the bottom. The Lorentzian mask is indicated in blue. Time series spectra have been averaged over 5 seconds acquisition time and multiplied by the Lorentzian mask. The initial anti-phase pattern is a result of a QRIP effect displayed by the $\text{H}_2^{17}\text{O}@C_{60}$ molecules. **b)** Normalised $\text{H}_2^{17}\text{O}@C_{60}$ proton signal as a function of time after the dissolution process ($t = 0$). The spectral time series has been acquired 30° pulse excitation every 250 ms and resulting spectra have been integrated after multiplication by a Lorentzian mask. Signal intensity of the individual peaks has been normalised with respect to their steady-state equilibrium value.

Strictly speaking this operator represents the state of the $\text{H}_2^{16}\text{O}@C_{60}$ protons, for the $\text{H}_2^{17}\text{O}@C_{60}$ case one should use the density operator $\rho_{\text{H}}(a, b) \otimes \rho_{\text{O}}(0)$. The degree of singlet polarisation is given by $a \in [0, 1]$ and the degree of residual Zeeman polarisation is characterised by $b \in [0, 1]$. For the limiting cases $(a, b) = (1, 0)$ and $(a, b) = (0, -\frac{1}{2}\beta_{\theta}\omega^0)$ the density operator $\rho_{\text{H}}(a, b)$ reduces to a fully polarised singlet state and a thermally polarised Zeeman state, respectively:

$$\begin{aligned} \rho_{\text{H}}(1, 0) &= |S_0\rangle \langle S_0|, \\ \rho_{\text{H}}(0, -\frac{1}{2}\beta_{\theta}\omega^0) &= \frac{1}{4}(\mathbb{1} - \beta_{\theta}\omega^0 I_z). \end{aligned} \quad (2.184)$$

To avoid confusion it should be noted that for the remainder of this section whenever we compare a system to its thermal equilibrium state, we refer to a thermally polarised Zeeman state at ~ 300 K with thermal equilibrium proton magnetisation M_{eq}^{H} defined

by

$$M_{\text{eq}}^{\text{H}} = \frac{(I_z |\rho_{\text{H}}(0, -\frac{1}{2}\beta\theta\omega^0)|)}{(I_z |I_z|)}. \quad (2.185)$$

For high degrees of singlet polarisation the density operator given by equation 2.183 represents a state far from thermal equilibrium. It is exactly this situation that the bullet DNP experiments aims to create. It should therefore be expected that the relaxation dynamics of the system may not be appropriately described by the IME or related techniques but should employ the Lindblad formulation described in section 2.4.

For the simulations of the relaxation dynamics it has been found that chemical shift contributions are negligible compared to random field, dipolar and quadrupolar (for the H_2^{17}O) contributions. The focus will therefore be on these three mechanisms. For consistency reasons the interactions are first expressed in a common reference frame. It is convenient to choose a frame with the oxygen atom placed at its origin as the common frame. A schematic representation of the reference frame of choice is shown in figure 2.15.

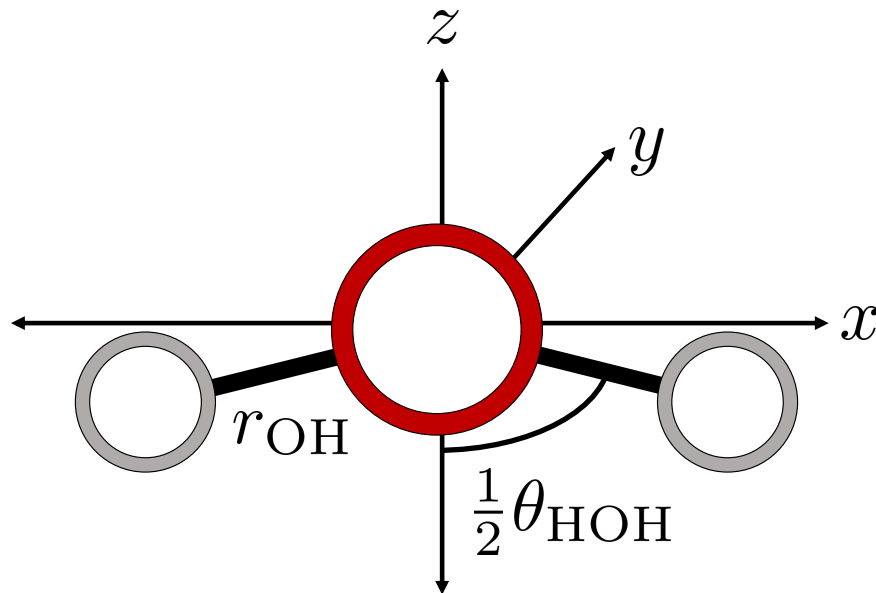


FIGURE 2.15: Molecular reference frame for the $\text{H}_2\text{O}@C_{60}$ molecules. The z -axis is aligned with the symmetry axis of the water molecule. The hydrogen atoms are placed along the x -axis. The distance between the oxygen and a proton atom is indicated by r_{OH} . The angle between the z -axis and the proton-oxygen bond is given by $\frac{1}{2}\theta_{\text{HOH}}$, where θ_{HOH} represents the angle enclosed by both proton-oxygen bonds.

The resulting coordinates for the individual atoms are summarised below:

$$\begin{aligned} \mathbf{r}_1 &= \begin{bmatrix} -\sin(\frac{1}{2}\theta_{\text{HOH}}) & 0 & -\cos(\frac{1}{2}\theta_{\text{HOH}}) \end{bmatrix} r_{\text{OH}}, \\ \mathbf{r}_2 &= \begin{bmatrix} +\sin(\frac{1}{2}\theta_{\text{HOH}}) & 0 & -\cos(\frac{1}{2}\theta_{\text{HOH}}) \end{bmatrix} r_{\text{OH}}, \\ \mathbf{r}_3 &= \begin{bmatrix} 0 & 0 & 0 \end{bmatrix}, \end{aligned} \quad (2.186)$$

where the indices $\{1, 2, 3\}$ refer to the atoms $\{^1\text{H}_a, ^1\text{H}_b, ^{16/17}\text{O}\}$. The proton-oxygen distance is represented by r_{OH} and θ_{HOH} describes the angle enclosed by the two proton-oxygen bonds.

As the $\text{H}_2\text{O}@\text{C}_{60}$ molecules enter the hot solvent bath inside the detection magnet a majority of the previously inaccessible rotational states become accessible. Since rotational transitions are much faster than nuclear transitions we assume a quick equilibration of the rotational states on the NMR timescale [94]. The relaxation process of the fullerene-encapsulated molecules may then be described according to an isotropic diffusion model [50]. It is further reasonable to assume that the rotational diffusion of the cage and the encapsulated water molecules are uncorrelated since the reorientation speed of the water molecules exceeds the reorientation speed of the cage. Experimental observations indicate that the two diffusion constants are separated by approximately three orders of magnitude. This may be established by analysing the relaxation behaviour of single ^{13}C of the C_{60} framework, for example [81].

The diffusion frame of the H_2O may then be assumed to be aligned with the coordinate frame indicated in figure 2.15 and the rotational diffusion process is described by a single diffusion constant τ_C .

The dipolar interaction tensors may then be calculated by making use of equation 1.79 and the atomic coordinates of equation 2.186

$$\begin{aligned}
 W_{12}^{\text{DD}} &= \begin{bmatrix} 2 & 0 & 0 \\ 0 & -1 & 0 \\ 0 & 0 & -1 \end{bmatrix}, & W_{13}^{\text{DD}} &= \begin{bmatrix} \frac{1}{2}(1 - 3 \cos(\theta_{\text{HOH}})) & 0 & \frac{3}{2} \sin(\theta_{\text{HOH}}) \\ 0 & -1 & 0 \\ \frac{3}{2} \sin(\theta_{\text{HOH}}) & 0 & \frac{1}{2}(1 + 3 \cos(\theta_{\text{HOH}})) \end{bmatrix}, \\
 W_{23}^{\text{DD}} &= \begin{bmatrix} \frac{1}{2}(1 - 3 \cos(\theta_{\text{HOH}})) & 0 & -\frac{3}{2} \sin(\theta_{\text{HOH}}) \\ 0 & -1 & 0 \\ -\frac{3}{2} \sin(\theta_{\text{HOH}}) & 0 & \frac{1}{2}(1 + 3 \cos(\theta_{\text{HOH}})) \end{bmatrix},
 \end{aligned} \tag{2.187}$$

so that the dipolar relaxation superoperator (in the fast motion limit) may be expressed as shown below [36]:

$$\hat{\Gamma}_{\text{SC}}^{\text{DD}} = -\frac{\tau_C}{5} \sum_{\substack{i < j \\ k < l}} C_{ij}^{\text{DD}} C_{kl}^{\text{DD}} \text{Tr}(W_{ij}^{\text{DD}\dagger} \cdot W_{kl}^{\text{DD}}) \sum_{m=-2}^{+2} \hat{T}_{2m}^{(ij)} \hat{T}_{2m}^{(kl)\dagger}. \tag{2.188}$$

A thermalised version of the dipolar relaxation superoperator is obtained by streamlining the Lindblad thermalisation method presented in section 2.4. To do so we make use of the following thermalisation superoperator

$$\hat{\Theta}_{\text{LB}} = \exp(-\frac{1}{2}\beta_\theta \hat{H}_{\text{coh}}^{\text{lab}}), \tag{2.189}$$

where $H_{\text{coh}}^{\text{lab}}$ is given by equation 2.166. Additionally we define a projection superoperator $\hat{\mathcal{P}}_{\parallel}$ with the property of projecting out any part of \hat{Q} that commutes with $\hat{H}_{\text{coh}}^{\text{lab}}$

$$[\hat{H}_{\text{coh}}^{\text{lab}}, \hat{\mathcal{P}}_{\parallel}(\hat{Q})] = 0. \quad (2.190)$$

The projection superoperator $\hat{\mathcal{P}}_{\parallel}$ may be realised by first transforming a superoperator \hat{Q} into the eigenbasis of $\hat{H}_{\text{coh}}^{\text{lab}}$ followed by deletion of all matrix elements connecting non-degenerate states. The thermalised dipolar relaxation superoperator in Lindblad form may then be expressed as shown below:

$$\hat{\Gamma}_{\text{LB}}^{\theta, \text{DD}} = \frac{\tau_C}{5} \sum_{\substack{i < j \\ k < l}} C_{ij}^{\text{DD}} C_{kl}^{\text{DD}} \text{Tr}(W_{ij}^{\text{DD}\dagger} \cdot W_{kl}^{\text{DD}}) \sum_{m=-2}^{+2} \hat{\mathcal{P}}_{\parallel}(\hat{\mathcal{D}}[T_{2m}^{(ij)}, \hat{\Theta}_{\text{LB}}(T_{2m}^{(kl)\dagger})]). \quad (2.191)$$

Similar expressions are obtained for the thermalised random field relaxation superoperator

$$\hat{\Gamma}_{\text{LB}}^{\theta, \text{ran}} = \tau_{\text{ran}} \sum_{i,j=1}^3 \kappa_{ij} \omega_{\text{rms}}^{(i)} \omega_{\text{rms}}^{(j)} \sum_{m=-1}^{+1} \hat{\mathcal{P}}_{\parallel}(\hat{\mathcal{D}}[T_{1m}^{(i)}, \hat{\Theta}_{\text{LB}}(T_{1m}^{(j)\dagger})]). \quad (2.192)$$

For the $\text{H}_2^{17}\text{O}@\text{C}_{60}$ molecules we additionally introduce a thermalised quadrupolar relaxation superoperator. With the current choice of reference frame the semi-classical quadrupolar relaxation superoperator coincides with the expression given in equation 2.170. Its thermalised counterpart takes the following form

$$\hat{\Gamma}_{\text{LB}}^{\theta, \text{Q}} = \frac{\tau_C}{5} \|A_{\text{Q}}^{(3)}\|^2 \sum_{m=-2}^{+2} \hat{\mathcal{P}}_{\parallel}(\hat{\mathcal{D}}[T_{2m}^{(3)}, \hat{\Theta}_{\text{LB}}(T_{2m}^{(3)\dagger})]). \quad (2.193)$$

The total relaxation superoperator for the $\text{H}_2^{16}\text{O}@\text{C}_{60}$ and $\text{H}_2^{17}\text{O}@\text{C}_{60}$ cases are then given by the expressions below

$$\hat{\Gamma}_{\text{LB}}^{\theta, (16\text{O})} = \hat{\Gamma}_{\text{LB}}^{\theta, \text{DD}} + \hat{\Gamma}_{\text{LB}}^{\theta, \text{ran}} \quad \hat{\Gamma}_{\text{LB}}^{\theta, (17\text{O})} = \hat{\Gamma}_{\text{LB}}^{\theta, \text{DD}} + \hat{\Gamma}_{\text{LB}}^{\theta, \text{ran}} + \hat{\Gamma}_{\text{LB}}^{\theta, \text{Q}}. \quad (2.194)$$

Evaluation of the corresponding matrix elements shows that the singlet decay constants T_S^{-1} in the fast motion and high-temperature regime is given by the following expressions:

$$\begin{aligned} T_S^{-1}(^{16}\text{O}) &= -\frac{(\mathbf{I}_1 \cdot \mathbf{I}_2 | \hat{\Gamma}_{\text{LB}}^{\theta, (16\text{O})} | \mathbf{I}_1 \cdot \mathbf{I}_2)}{(\mathbf{I}_1 \cdot \mathbf{I}_2 | \mathbf{I}_1 \cdot \mathbf{I}_2)} = 4\tau_{\text{ran}} (1 - \kappa_{12}) \omega_{\text{rms}}^{(1)} \omega_{\text{rms}}^{(2)}, \\ T_S^{-1}(^{17}\text{O}) &= -\frac{(\mathbf{I}_1 \cdot \mathbf{I}_2 | \hat{\Gamma}_{\text{LB}}^{\theta, (17\text{O})} | \mathbf{I}_1 \cdot \mathbf{I}_2)}{(\mathbf{I}_1 \cdot \mathbf{I}_2 | \mathbf{I}_1 \cdot \mathbf{I}_2)} = 35\tau_C C_{13}^{\text{DD}} C_{23}^{\text{DD}} \sin^2(\theta_{\text{HOH}}) + T_S^{-1}(^{16}\text{O}). \end{aligned} \quad (2.195)$$

Agreement between the experimentally observed relaxation rates and the expressions given in equation 2.195 may be obtained by utilising the parameters indicated in table 2.3.

A comparison between the simulated and experimental z -magnetisation recovery for the

T	B^0	r_{OH}	θ_{HOH}	τ_C
300 K	11.75 T	1.00×10^{-10} m	109.64°	107 fs
J_{IS}	$\ A_{\text{Q}}^{(3)}\ /2\pi$	$C_{(12)}^{\text{DD}}/2\pi$	$C_{(13)}^{\text{DD}}/2\pi$	$C_{(23)}^{\text{DD}}/2\pi$
-77.9 Hz	0.675 MHz	-27.48 kHz	16.28 kHz	16.28 kHz
$\omega_{\text{rms}}^{(1)}/2\pi$	$\omega_{\text{rms}}^{(2)}/2\pi$	$\omega_{\text{rms}}^{(3)}/2\pi$	τ_{ran}	
13 kHz	13 kHz	2 kHz	100 ps	
κ_{12}	κ_{13}	κ_{23}		
0.986	0.4	0.4		

TABLE 2.3: NMR parameters for the $\text{H}_2\text{O}@C_{60}$ simulations. Parameters agree with references 39, 81, 90 and 95.

$\text{H}_2^{16}\text{O}@C_{60}$ and $\text{H}_2^{17}\text{O}@C_{60}$ molecules is shown in figure 2.16. All simulations have been performed using *SpinDynamica* [63].

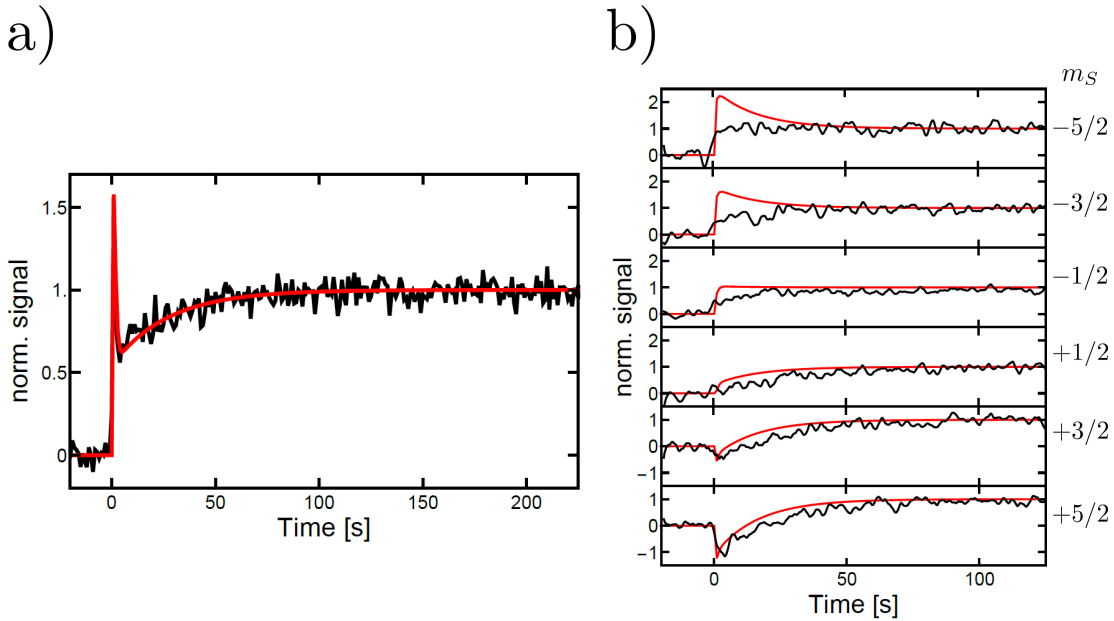


FIGURE 2.16: Comparison between experimental (black) and simulated (red) $\text{H}_2\text{O}@C_{60}$ spin-isomer conversion at 300 K. **a)** Proton magnetisation recovery dynamics for $\text{H}_2^{16}\text{O}@C_{60}$ molecules. The simulations indicate an initial para fraction of 45% and a residual Zeeman enhancement of $20 \times M_{\text{eq}}^{\text{H}}@300\text{K}$. **b)** Proton magnetisation recovery dynamics for the $\text{H}_2^{17}\text{O}@C_{60}$ molecules. Individual proton transitions are associated with the projection number m_S of the ^{17}O . Each resonance displays a different relaxation behaviour due to a small QRIP effect. A rough estimate on the initial para fraction and Zeeman enhancement are 30% and $4 \times M_{\text{eq}}^{\text{H}}@300\text{K}$, respectively. Deviations between experimental data and simulated trajectories are likely due to a combination of post processing (application of a moving time average and Lorentzian mask) and the poor quality of the unprocessed experimental data. Simulation parameters are summarised in table 2.3.

The simulations allowed for a rough estimate of the initial *para* and *ortho* fractions. For the $\text{H}_2^{16}\text{O}@C_{60}$ molecules the experimental data was well matched for $a = 0.45$, $b = 0.48 \times 10^{-3} \approx 20 \times M_{\text{eq}}^{\text{H}}@300\text{K}$, indicating an initial *para* fraction of 45% and slight Zeeman enhancement. The $\text{H}_2^{17}\text{O}@C_{60}$ molecules displayed a smaller initial *para* fraction and Zeeman polarisation. Reasonable agreement was achieved by assuming $a = 0.3$, $b = 0.01 \times 10^{-3} \approx 4 \times M_{\text{eq}}^{\text{H}}@300\text{K}$, indicating an initial *para* fraction of 30%. This is probably due to the presence of the quadrupolar ^{17}O nucleus.

Overall there is excellent agreement between the simulations and the experimental data for the $\text{H}_2^{16}\text{O}@C_{60}$ case. The simulations for the $\text{H}_2^{17}\text{O}@C_{60}$ only agree on a qualitative basis. This might be due to the challenging quality of the raw data. As mentioned previously extraction of the slow conversion process required filtering via a Lorentzian mask and a moving time average of 5 seconds.

Chapter 3

Close to thermal equilibrium

Conventional NMR experiments are performed by coherently manipulating thermally equilibrated systems. For typical high-field NMR setups the thermally equilibrated state is given by a slightly magnetised sample. The extent of magnetisation depends explicitly on the magnetic field strength and the temperature. Following arguments from the previous section, at ordinary temperatures one may safely invoke the high-temperature approximation and represent the high-field density operator as follows:

$$\rho_{\text{eq}} \approx N_{\mathcal{H}}^{-1}(\mathbb{1} - \hbar\omega^0/(k_{\text{B}}T)I_z). \quad (3.1)$$

Since the magnetic energy of the sample is relatively small compared to the average thermal energy ($\hbar\omega^0/(k_{\text{B}}T) \sim 10^{-5}$) the system is only slightly polarised. The application of RF pulses may only influence whatever little Zeeman polarisation is present. For this reason we refer to such systems as being close to thermal equilibrium even under coherent manipulation.

The following section analyses some aspects of coherent manipulation of thermal spin order in coupled spin-1/2 pairs. Special attention will be paid to spin pairs displaying a small difference in their resonance frequency compared to their scalar coupling constant. For such systems, the eigenstates of the coherent Hamiltonian closely resemble the angular momentum singlet and triplet states and efficient coherent manipulation of the angular momentum states becomes relevant.

3.1 Coupled spin-1/2 pairs

Before exploring the coherent manipulation of coupled spin-1/2 pairs some useful tools for the analysis of typical NMR experiments are briefly summarised. The presented pulse sequences are mainly analysed within this framework.

3.1.1 The coherent Hamiltonian

For a generic two-spin-1/2 system in solution, the laboratory frame Hamiltonian may be expressed as follows [22]:

$$H_0 = \omega_1^0 I_{1z} + \omega_2^0 I_{2z} + \omega_J \mathbf{I}_1 \cdot \mathbf{I}_2, \quad \omega_j^0 = -2\pi\gamma_j \mathbf{B}_z^0 (1 + \delta_{\text{iso}}^j), \quad \omega_J = 2\pi J_{12}. \quad (3.2)$$

Using equation 1.63 it is convenient to move into a reference frame rotating at the mean frequency ($\omega_{\text{ref}} = \frac{1}{2}(\omega_1^0 + \omega_2^0)$) of the two spins. In this reference frame the Hamiltonian may be expressed as shown below:

$$H_0 = \frac{1}{2}\omega_\Delta(I_{1z} - I_{2z}) + \omega_J \mathbf{I}_1 \cdot \mathbf{I}_2, \quad \omega_\Delta = \omega_1^0 - \omega_2^0 = 2\pi\Delta. \quad (3.3)$$

This particular representation of the Hamiltonian makes it obvious that the differential chemical shift term is a symmetry breaking contribution and is key in accessing singlet-order in coupled spin-1/2 systems. A measure for the degree of asymmetry is the mixing angle of the Hamiltonian defined as follows:

$$\theta_{\text{mix}} = \arctan(|\Delta/J|). \quad (3.4)$$

The mixing angle ranges over $\theta_{\text{mix}} \in [0, \pi/2]$ with $\theta_{\text{mix}} = 0$ representing nearly-equivalent, $\theta_{\text{mix}} = \pi/4$ intermediate and $\theta_{\text{mix}} = \pi/2$ inequivalent systems.

3.1.2 Single Transition operators

The subsequent treatment of two-spin-1/2 systems makes heavy use of the single transition operator formalism [96–98]. For any two states ($|r\rangle, |s\rangle$) of the system it is possible to construct the following set of operators:

$$\begin{aligned} I_x^{rs} &= \frac{1}{2}(|r\rangle\langle s| + |s\rangle\langle r|), & I_y^{rs} &= \frac{1}{2i}(|r\rangle\langle s| - |s\rangle\langle r|), \\ I_z^{rs} &= \frac{1}{2}(|r\rangle\langle r| - |s\rangle\langle s|), & \mathbb{1}^{rs} &= |r\rangle\langle r| + |s\rangle\langle s|. \end{aligned} \quad (3.5)$$

satisfying the commutation relations below

$$[I_i^{rs}, I_j^{rs}] = \frac{i}{2}\epsilon_{ijk} I_k^{rs} \quad [I_i^{rs}, I_j^{kl}] = 0. \quad (3.6)$$

Single transition operators therefore generate the group SU(2). If the Hamiltonian of the system allows for such a decomposition it is possible to think of the dynamics as being broken up into the motion of several “fictitious”-spin-1/2 particles.

3.1.3 A convenient basis

It is important to note that single transition operators do not only depend on the pair of states, but also on the particular choice of basis. In that sense, there is some flexibility in how to choose these operators. Unless otherwise stated the following basis will be employed for the remainder of this chapter

$$\{|S_0\rangle, |T_0\rangle, \frac{1}{\sqrt{2}}(|T_+\rangle + |T_-\rangle), \frac{1}{\sqrt{2}}(|T_+\rangle - |T_-\rangle)\}. \quad (3.7)$$

This basis has some particular advantages when working with coupled spin-1/2 pairs. Most notably the Hamiltonian of equation 3.3 decouples into three subspaces

$$\begin{aligned} H_0 &= H_0^{12} + H_0^3 + H_0^4 \\ &= \{\omega_\Delta I_x^{12} - \omega_J I_z^{12} - \frac{1}{4}\omega_J \mathbb{1}^{12}\} + \{\frac{1}{4}\omega_J \mathbb{1}^3\} + \{\frac{1}{4}\omega_J \mathbb{1}^4\}. \end{aligned} \quad (3.8)$$

Additionally, the total projection angular momentum operators are contained within two-dimensional subspaces

$$I_x = 2I_x^{23} \quad I_y = -2I_y^{24} \quad I_z = 2I_x^{34}. \quad (3.9)$$

Every possible sequence of free evolution delays and radio frequency pulses may therefore be visualised by simple operations onto fictitious-spin-1/2 particles.

3.2 Generalised magnetisation-to-singlet transfer

Since the first experimental demonstration of nuclear singlet states, and their surprising NMR relaxation properties, the problem of converting magnetisation to singlet-order (or vice versa) has been a topic of great interest [99]. Over the years several methods have been developed to tackle this problem [99–104]. Most of these methods fall into one of three categories.

The first category consists of adiabatic transformations [99–102]. Adiabatic transformations usually transform the eigenstates of the internal Hamiltonian to singlet and triplet states. This is achieved by application of a suitable time-dependent and "slowly" time-varying Hamiltonian. As a consequence, populations of the internal Hamiltonian are adiabatically transformed into singlet and triplet populations.

The second class of magnetisation to singlet order transformations may be summarised as low power methods [103, 104]. These methods exploit avoided crossings in the rotating frame. Application of a low power pulse with a frequency matching the J coupling of the two spins places the eigenenergies of the "singlet" and the "central triplet" state at the center of the avoided crossing. At this point the energy levels are almost degenerate leading to efficient singlet and central triplet mixing.

The third category consists of high power methods that employ strong radio frequency pulses separated by suitable evolution delays [105–110]. In general, most of these sequences have been developed either for strongly coupled ($\Delta \ll J$) or weakly coupled ($\Delta \gg J$) spin systems.

The magnetisation-to-singlet (M2S) sequence (see figure 3.1) is a popular choice for strongly coupled spin systems [107]. Its efficiency however quickly drops off in the in-

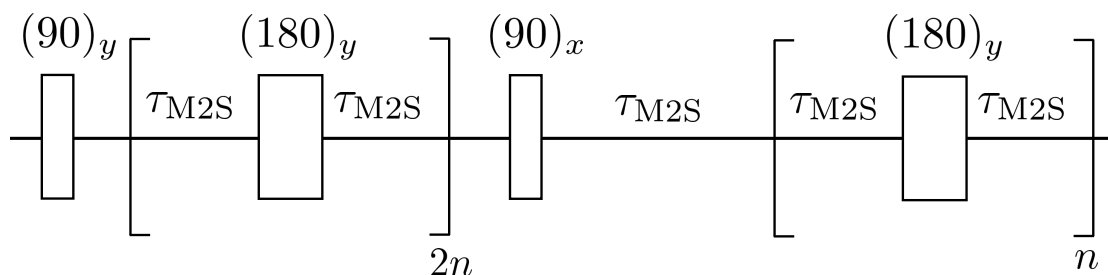


FIGURE 3.1: Schematic representation of the M2S pulse sequence. In the strong coupling limit the evolution delay, τ_{M2S} , is given by $1/(4J)$ and the echo number, n , is determined by the defining equation: $2n \tan^{-1}(\omega_{\Delta}/\omega_J) = \pi$.

intermediate regime ($J \sim \Delta$).

While this certainly wasn't an obstacle in the earlier days of singlet NMR, recent developments in the field of parahydrogen and field cycling NMR led to the need of sequence in the intermediate regime [111, 112]. Parahydrogen represents a particular realisation of a nuclear singlet-state connecting the fields of nuclear long-lived states and parahydrogen NMR [16, 17]. In practical applications parahydrogen is initially reacted with a precursor molecule resulting in a magnetically inequivalent spin system [16–19, 43, 113]. The overpopulated singlet-state originating from the parahydrogen pair may then be converted into magnetisation using one of the available singlet NMR sequences. In many cases this results in substantial signal enhancements. There is however no guarantee that the resulting spin system can be classified as either a strongly or weakly coupled spin system. The utilisation of intermediate spin systems is therefore very limited in the context of parahydrogen NMR.

Recently, the group of Jerschow extended the M2S to the intermediate regime by making use of a chemical shift scaling (CSS) element [110, 114]. The CSS element consists of a spin echo train that modulates the chemical shift difference in an average Hamiltonian sense [115]. The CSS element may then replace the free evolution periods of the M2S. If the scaled chemical shift term falls within the validity range of the M2S magnetisation to singlet-order transformation becomes possible.

As noted in the original publication introduction of CSS elements increases the number (π)-pulses of the M2S sequence considerably. To further compensate for error accumulation it is common practice to replace a (π)-pulse by its composite counterpart [116]. In general, this has been known to cause extensive heating of the sample [110].

The goal of this section is to extend the validity range of the M2S sequence from nearly equivalent systems to intermediate systems. In similar fashion to the M2S, the *generalised*-M2S is a consequence of simple geometric arguments. This avoids the necessity of introducing an increasing amount refocusing pulses to scale spin interactions in an average Hamiltonian sense [115].

3.2.1 Transfer scheme

Similar to the M2S, the generalised-magnetisation-to-singlet (gM2S) sequence utilises evolution blocks of the following type:

$$U_{\text{SE}}(\tau, y) = U_0(\tau) - R_y(\pi) - U_0(\tau), \quad (3.10)$$

which are generally known as spin-echo (SE) blocks. As a favourable side effect spin-echo blocks may also compensate for relaxation effects.

The spin-echo block is conveniently analysed within the single transition operator formalism. The Hamiltonian of equation 3.3 may be expressed as follows in terms of single transition operators

$$\begin{aligned} H_0 &= H_0^{12} + H_0^3 + H_0^4 \\ &= \{\omega_\Delta I_x^{12} - \omega_J I_z^{12} - \frac{1}{4}\omega_J \mathbb{1}^{12}\} + \{\frac{1}{4}\omega_J \mathbb{1}^3\} + \{\frac{1}{4}\omega_J \mathbb{1}^4\}. \end{aligned} \quad (3.11)$$

The rotation operator $R_y(\pi)$ may also be decomposed into orthogonal rotations with respect to the subspaces $\{1, 2\}$ and $\{3, 4\}$

$$R_y(\pi) = iR_z^{12}(\pi)R_z^{34}(\pi). \quad (3.12)$$

The echo propagator $U_{\text{SE}}(\tau, y)$ then decouples into two orthogonal transformations

$$U_{\text{SE}}(\tau, y) = U_{\text{SE}}^{12}(\tau, y)U_{\text{SE}}^{34}(\tau, y), \quad (3.13)$$

with individual echo propagators given below

$$\begin{aligned} U_{\text{SE}}^{12}(\tau, y) &= \Phi^{12}\left(-\frac{1}{2}\tau\omega_J\right) \exp\{-i\tau \boldsymbol{\omega} \cdot \mathbf{I}^{12}\} R_z^{12}(\pi) \exp\{-i\tau \boldsymbol{\omega} \cdot \mathbf{I}^{12}\} \\ U_{\text{SE}}^{34}(\tau, y) &= i\Phi^{34}\left(\frac{1}{2}\tau\omega_J\right) R_z^{34}(\pi) \end{aligned} \quad (3.14)$$

$$\boldsymbol{\omega}^T = \begin{bmatrix} \omega_\Delta & 0 & -\omega_J \end{bmatrix}.$$

The propagators $U_{\text{SE}}^{12}(\tau, y)$ and $U_{\text{SE}}^{34}(\tau, y)$ may be understood as elements of the group $\text{SU}(2)$. For fixed τ one may therefore represent an echo propagator as some effective rotation within the respective subspace. Focusing on the $\{1, 2\}$ subspace for the moment

one may represent $U_{\text{SE}}^{12}(\tau, y)$ as indicated below [117]:

$$U_{\text{SE}}^{12}(\tau, y) = \Phi^{12}\left(-\frac{1}{2}\tau\omega_J\right)R_{\mathbf{n}}^{12}(\theta). \quad (3.15)$$

The rotation axis \mathbf{n} and the rotation angle θ are defined as follows:

$$\mathbf{n} = \begin{bmatrix} \frac{\omega_x \omega_z (\cos(\tau\omega_e) - 1)}{\omega_e \sqrt{\omega_e^2 - \omega_z^2} \sin^2(\tau\omega_e)} \\ 0 \\ \frac{\omega_x^2 + \omega_z^2 \cos(\tau\omega_e)}{\omega_e \sqrt{\omega_e^2 - \omega_z^2} \sin^2(\tau\omega_e)} \end{bmatrix}, \quad (3.16)$$

$$\theta = 2 \cos^{-1} \left(-\frac{\omega_z}{\omega_e} \sin(\tau\omega_e) \right),$$

$$\omega_e = \sqrt{\boldsymbol{\omega} \cdot \boldsymbol{\omega}} = 2\pi \sqrt{J^2 + \Delta^2}.$$

To keep things compact the parametric dependence of \mathbf{n} and θ on $(\tau, \boldsymbol{\omega})$ is being suppressed.

By virtue of the rotation formula for SU(2) an equivalent representation of the rotation operator $R_{\mathbf{n}}^{12}(\theta)$ is given by the following expression [117]

$$R_{\mathbf{n}}^{12}(\theta) = \cos(\theta/2)\mathbb{1}^{12} - 2i \sin(\theta/2)\mathbf{n} \cdot \mathbf{I}^{12}. \quad (3.17)$$

In the case of the M2S the echo delay τ is chosen in such a way as to ensure the following relations

$$\mathbf{n}_x = 1 \quad \text{and} \quad \mathbf{n}_z = 0. \quad (3.18)$$

The appropriate delay and the resulting rotation angle are given by the expressions below:

$$\tau_{\text{M2S}} = \omega_e^{-1} \cos^{-1} \left(-\left(\frac{\omega_x}{\omega_z}\right)^2 \right) = (2\pi \sqrt{J^2 + \Delta^2})^{-1} \cos^{-1} \left(-\left(\frac{\Delta}{J}\right)^2 \right),$$

$$\theta_{\text{M2S}} = 2 \cos^{-1} \left(-\frac{\omega_z}{\omega_e} \sqrt{1 - \left(\frac{\omega_x}{\omega_z}\right)^4} \right) = 2 \sec^{-1} \left(\frac{J}{\sqrt{J^2 - \Delta^2}} \right). \quad (3.19)$$

In the limit of small near equivalence ($|\Delta| \ll |J|$) the evolution delay reduces to $\tau_{\text{M2S}} = 1/(4J)$ and the resulting echo block is often known as J-Synchronised-Echo (JSE)[118].

A single JSE of the M2S sequence therefore produces an effective rotation around the x -axis in the $\{1, 2\}$ subspace. The n -fold application of the M2S-JSE leads to an overall rotation through an angle $(n \times \theta_{\text{M2S}})$. For the M2S the echo number n is chosen as to generate effective $(\pi/2)_x^{12}$ - and $(\pi)_x^{12}$ -rotations. It can be shown that these two rotations are sufficient to perform full conversion from magnetisation to singlet-order [107, 119].

The relations of equation 3.18 may only be satisfied for strongly coupled systems $|\Delta| < |J|$. For systems outside the nearly equivalent regime $(\Delta/J) > 1$ one may only solve for the inverse-cosine function by allowing τ_{M2S} to take on imaginary values. This of course does not make much physical sense.

Physically speaking, in these cases a JSE is no longer able to generate pure effective rotations around the x -axis in the $\{1, 2\}$ subspace (see figure 3.2).

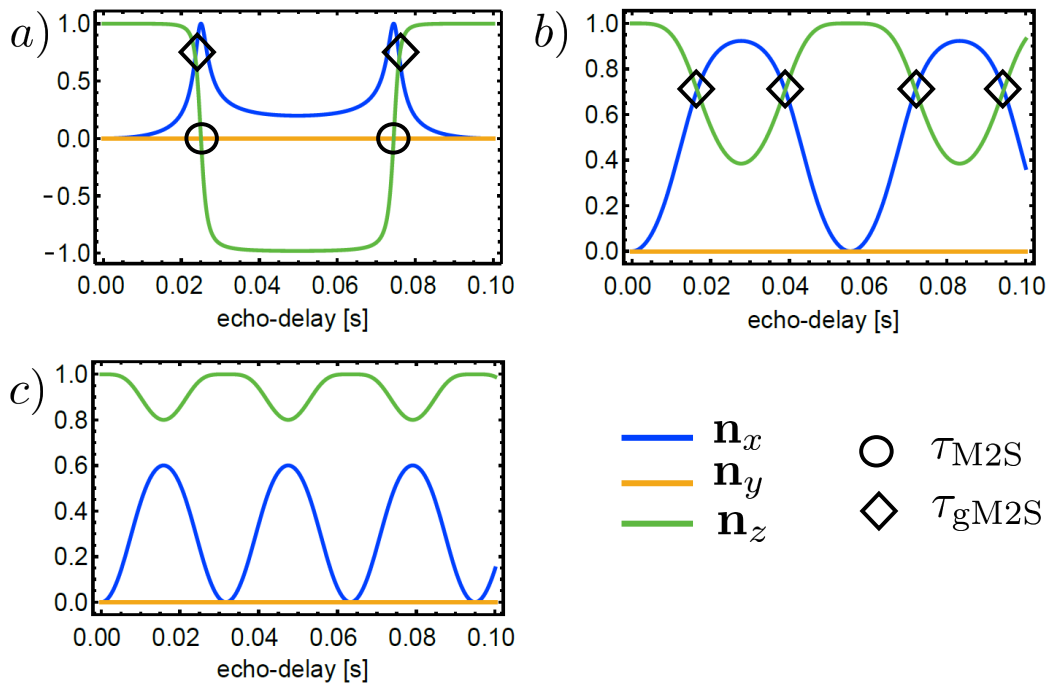


FIGURE 3.2: Graphical representation of the rotation axis components defined via equation 3.16 as a function of the echo delay. The M2S echo delay is indicated by black circles, whereas the gM2S echo delay is indicated by diamonds.

a) Rotation axis components for a nearly equivalent spin system ($J = 10$ Hz and $\Delta = 1$ Hz). In nearly equivalent spin systems it is always possible to choose an echo delay that generates a pure effective x -rotation ($\mathbf{n}_z = 0$). It is also possible to choose an echo delay that equalises the x and z -components (gM2S delay).

b) Rotation axis components for an intermediate spin system ($J = 10$ Hz and $\Delta = 15$ Hz). In the intermediate case it is no longer possible to choose echo delays that set the z component to zero. It is however still possible to find values of τ that fulfill the gM2S condition.

c) Rotation axis components for an inequivalent spin system ($J = 10$ Hz and $\Delta = 30$ Hz). Roughly speaking when $\Delta > 2J$ it is no longer possible to find an echo delay that fulfills the gM2S condition.

To overcome this issue the generalised-M2S (gM2S) modifies the conditions of equation 3.18 to the following:

$$\mathbf{n}_x = \mathbf{n}_z. \quad (3.20)$$

The geometric reasoning for this particular choice is illustrated in figure 3.3.

A (π)-rotation around an axis that is at an angle of $\pi/4$ with respect to the z -axis

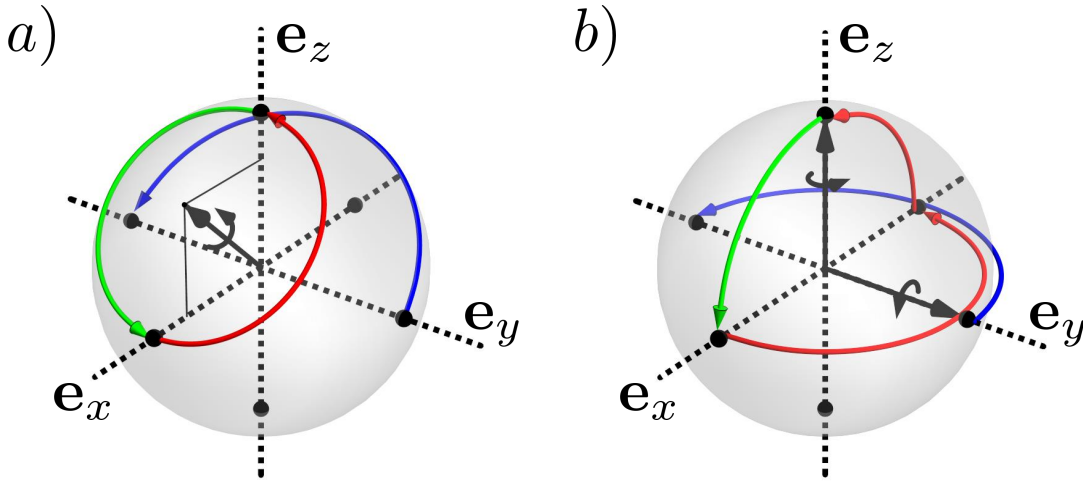


FIGURE 3.3: **a)** Graphical representation of the spatial rotation $R_{\mathbf{n}}(\pi)$ with \mathbf{n} being at an angle of $\pi/4$ with respect to the z -axis. The Cartesian basis vectors $\{e_x, e_y, e_z\}$ are being mapped to $\{e_z, -e_y, e_x\}$. **b)** Graphical representation of the sequence of rotations $R_y(\pi/2)R_z(\pi)$. This sequence of rotations performs the same mapping as rotation a) and illustrates the relation of equation 3.21.

is (almost) equivalent to a $(\pi/2)_y$ -rotation. The formal relation between these two operations is summarised below:

$$R_{\mathbf{n}}(\pi) = R_y(\pi/2)R_z(\pi), \quad \mathbf{n} = \begin{bmatrix} 1/\sqrt{2} & 0 & 1/\sqrt{2} \end{bmatrix}. \quad (3.21)$$

Instead of trying to generate a pure effective x -rotation the gM2S sequence generates an effective rotation around the $R_y(\pi/4)e_z$ -axis. This single operation is sufficient to perform conversion from magnetisation to singlet-order for systems classifying as nearly equivalent to intermediate.

In the case of the gM2S the echo delay is modified to the following relations

$$\tau_{\text{gM2S}} = \omega_e^{-1} \cos^{-1} \left(\frac{\omega_x(\omega_x + \omega_z)}{\omega_z(\omega_x - \omega_z)} \right) = (2\pi\sqrt{J^2 + \Delta^2})^{-1} \cos^{-1} \left(\frac{\Delta(J - \Delta)}{J(J + \Delta)} \right). \quad (3.22)$$

The resulting effective rotation angle θ_{gM2S} is indicated below:

$$\theta_{\text{gM2S}} = 2 \cos^{-1} \left(-\frac{\omega_z}{\omega_e} \sqrt{1 - \frac{\omega_x^2(\omega_x + \omega_z)^2}{\omega_z^2(\omega_x - \omega_z)^2}} \right) = 2 \cos^{-1} \left(J \sqrt{\frac{J^2 + 2J\Delta - \Delta^2}{J^2(J + \Delta)^2}} \right). \quad (3.23)$$

The delay for the gM2S is well defined as long as $(J + (1 - \sqrt{2})\Delta) \geq 0$. If this condition is met the gM2S is guaranteed to provide a valid effective rotation around the tilted $R_y(\pi/4)e_z$ -axis.

The gM2S proceeds in similar fashion to the M2S. The first step is to find an echo

number $n = n^*$ satisfying:

$$n^* \times \theta_{\text{gM2S}} \approx \pi \quad \text{mod } 2\pi, \quad (3.24)$$

to utilize equation 3.21. The effective propagator for the n^* -fold application of the gM2S echo is then approximately given by the following expression

$$U_{\text{SE}}^{n^*}(\tau_{\text{gM2S}}, y) \approx i^{n^*} \Phi^{12}(-n^* \tau_{\text{gM2S}} \omega_J / 2) \Phi^{34}(n^* \tau_{\text{gM2S}} \omega_J / 2) R_y^{12}(\pi/2) R_z^{12}(\pi) R_z^{34}(n^* \pi). \quad (3.25)$$

The effective propagator for an n^* -fold gM2S echo is therefore identical (up to some phase) to an n^* -fold M2S echo. The concatenation of elementary gM2S events is however slightly different to the M2S sequence. An idealised sequence of events for the gM2S is illustrated in figure 3.4.

The gM2S sequence starts by exchanging the states $|1\rangle$ and $|2\rangle$. The pulse element block that achieves this transformation is indicated in figure 3.4 a). The exact transformation of block a) is given by the following expression

$$\begin{aligned} U_{\text{gM2S}}^a &= U_{\text{SE}}^{n^*}(\tau_{\text{gM2S}}, y) - R_y(\pi) - U_{\text{SE}}^{n^*}(\tau_{\text{gM2S}}, y) \\ &= U_{\text{SE}}^{n^*}(\tau_{\text{gM2S}}, y) - i R_z^{12}(\pi) R_z^{34}(\pi) - U_{\text{SE}}^{n^*}(\tau_{\text{gM2S}}, y). \end{aligned} \quad (3.26)$$

Making use of equation 3.25 the propagator for block a) may be expressed as follows:

$$\begin{aligned} U_{\text{gM2S}}^a &= \\ & i^{n^*} \Phi^{12}(-n^* \tau_{\text{gM2S}} \omega_J / 2) \Phi^{34}(n^* \tau_{\text{gM2S}} \omega_J / 2) R_y^{12}(\pi/2) R_z^{12}(\pi) R_z^{34}(n^* \pi) \\ & i R_z^{12}(\pi) R_z^{34}(\pi) \\ & i^{n^*} \Phi^{12}(-n^* \tau_{\text{gM2S}} \omega_J / 2) \Phi^{34}(n^* \tau_{\text{gM2S}} \omega_J / 2) R_y^{12}(\pi/2) R_z^{12}(\pi) R_z^{34}(n^* \pi). \end{aligned} \quad (3.27)$$

After some manipulation one may express the propagator for block a) in a slightly more intuitive form as shown below

$$U_{\text{gM2S}}^a \approx \Phi^{12}(\pi) \Phi^{34}(-\pi/2) \Phi^{12}(-n^* \tau_{\text{gM2S}} \omega_J) \Phi^{34}(n^* \tau_{\text{gM2S}} \omega_J) \sigma_{12} R_z^{34}(\pi), \quad (3.28)$$

where the symbol σ has been used to indicate a state permutation to avoid confusion with spin permutation operators (usually denoted by P).

Block a) finishes by a suitable phase evolution step. It is difficult to see the immediate necessity for this step, but for now the following idealised phase evolution operation will be inserted

$$U_{\text{gM2S}}^\phi = \Phi^{12}(\alpha) \Phi^{34}(\beta). \quad (3.29)$$

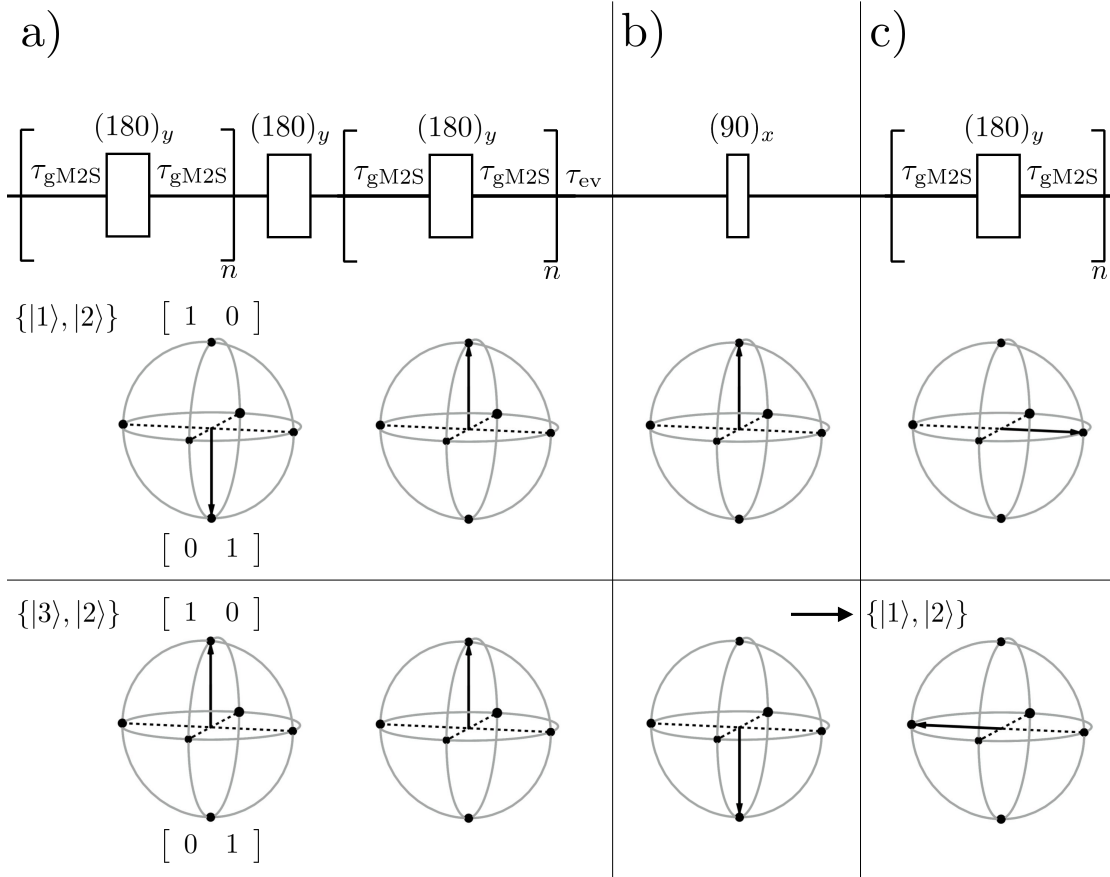


FIGURE 3.4: Illustration of the gM2S pulse sequence with corresponding action onto the Bloch sphere starting from $I_x = I_x^{23}$. The gM2S sequence may be analysed by following the dynamics of the $\{1, 2\}$ and $\{3, 2\}$ Bloch spheres simultaneously. **a)** The first part of the gM2S sequence performs an exchange of the states $|1\rangle$ and $|2\rangle$. The orientation of the top Bloch vector is flipped, whereas the orientation of the bottom Bloch vector remains unchanged. The exchange is not pure and adds a phase factor to both states. The phase factor is compensated for by an additional evolution period τ_{ev} . **b)** A $(\pi/2)_x$ exchanges the states $|2\rangle$ and $|3\rangle$. **c)** An additional gM2S echo-block rotates the Bloch vector in the $\{1, 2\}$ subspace. This transformation takes the bottom Bloch sphere $\{3, 2\}$ to a $\{1, 2\}$ Bloch sphere copy. Assuming a perfect phase compensation in the free evolution part of a) the two Bloch vectors end up in the transverse plane with opposite orientation. The resulting density operator in combination with its adjoint are easily shown to correspond to pure I_z^{12} or singlet-order.

Phase evolution is followed up by a single $(\pi/2)_x$ -pulse. For the current choice of basis the propagator for block b) takes a particular simple form

$$U_{\text{gM2S}}^b = \Phi^{23}(\pi/2)\sigma_{23}, \quad (3.30)$$

resulting in the exchange of states $|2\rangle$ and $|3\rangle$ with an additional $(\pi/2)$ phase shift. The last block of the gM2S sequence consists of an n^* -fold gM2S echo

$$U_{\text{gM2S}}^c = i^{n^*} \Phi^{12}(-n^* \tau_{\text{gM2S}} \omega_J / 2) \Phi^{34}(n^* \tau_{\text{gM2S}} \omega_J / 2) R_y^{12}(\pi/2) R_z^{12}(\pi) R_z^{34}(n^* \pi). \quad (3.31)$$

The idealised propagator for the gM2S sequence is therefore given by the following expression

$$U_{\text{gM2S}}^{\text{ideal}} = U_{\text{gM2S}}^{\text{c}} U_{\text{gM2S}}^{\text{b}} U_{\text{gM2S}}^{\phi} U_{\text{gM2S}}^{\text{a}}. \quad (3.32)$$

The action of the total gM2S propagator onto the initial density operator $\rho(0) = \frac{1}{2}I_x$ reduces to a simple expression

$$\begin{aligned} \rho_{\text{gM2S}} &= \frac{1}{2}(U_{\text{gM2S}}^{\text{ideal}})I_x(U_{\text{gM2S}}^{\text{ideal}})^\dagger = \frac{1}{2}(U_{\text{gM2S}}^{\text{ideal}})I_x^{23}(U_{\text{gM2S}}^{\text{ideal}})^\dagger \\ &= -\sin(\alpha - \beta - 2n^*\omega_J\tau_{\text{gM2S}})I_z^{12} - \cos(\alpha - \beta - 2n^*\omega_J\tau_{\text{gM2S}})I_y^{12}. \end{aligned} \quad (3.33)$$

An appropriate operator to measure the amount of singlet-order in a two-spin-1/2 system is given by the following expression

$$Q_{\text{SO}} = -\mathbf{I}_1 \cdot \mathbf{I}_2 = I_z^{12} + \frac{1}{4}(\mathbb{1}^{12} - \mathbb{1}^{34}). \quad (3.34)$$

The amount of singlet-order contained within the density operator ρ_{gM2S} is then calculated as follows:

$$q_{\text{SO}} = \frac{(Q_{\text{SO}}|\rho_{\text{gM2S}})}{(Q_{\text{SO}}|Q_{\text{SO}})} = -\frac{2}{3}\sin(\alpha - \beta - 2n^*\omega_J\tau_{\text{gM2S}}). \quad (3.35)$$

The necessity for the phase evolution step is now apparent. Without phase compensation the singlet-order amplitude q_{SO} would be limited by the product $(4\pi Jn^* \times \tau_{\text{gM2S}})$. There is however no guarantee that this product would maximise/minimise the sine function.

Assuming perfect phase compensation for the moment the maximum achievable singlet-amplitude for the gM2S sequence equals the theoretical maximum of $q_{\text{SO}}^{\text{max}} = \pm\frac{2}{3}$ [120]. In an actual experiment however the ideal phase propagator is replaced by a free-evolution period

$$U_{\text{gM2S}}^{\phi} \mapsto U_0(\tau_{\text{ev}}) \quad (3.36)$$

and a suitable evolution delay τ_{ev} . Determination of the correct evolution delay is not trivial, but may be done under the assumption that the product of the echo number n^* and the gM2S angle θ_{gM2S} are exactly equal to π :

$$n^* \times \theta_{\text{gM2S}} = \pi. \quad (3.37)$$

The singlet amplitude q_{SO} under the experimental propagator

$$U_{\text{gM2S}}^{\text{exp}} = U_{\text{gM2S}}^{\text{c}} U_{\text{gM2S}}^{\text{b}} U_0(\tau_{\text{ev}}) U_{\text{gM2S}}^{\text{a}} \quad (3.38)$$

is then given by

$$q_{\text{SO}} = \frac{2}{3} \left(\frac{\sin(4\pi Jn^*\tau_{\text{gM2S}})(\Delta^2 + J^2 \cos(\omega_e\tau_{\text{ev}}))}{(\omega_e/2\pi)^2} + \frac{J \cos(4\pi Jn^*\tau_{\text{gM2S}}) \sin(\omega_e\tau_{\text{ev}})}{\omega_e/(2\pi)} \right). \quad (3.39)$$

and the optimal evolution delay τ_{ev}^* may be shown to equal

$$\tau_{\text{ev}}^* = \begin{cases} \omega_e^{-1} \tan^{-1}(+J\omega_e/(2\pi) \sin(4\pi Jn^*\tau_{\text{gM2S}}), +(\omega_e/2\pi)^2 \cos(4\pi Jn^*\tau_{\text{gM2S}})) + 2\pi m \\ \omega_e^{-1} \tan^{-1}(-J\omega_e/(2\pi) \sin(4\pi Jn^*\tau_{\text{gM2S}}), -(\omega_e/2\pi)^2 \cos(4\pi Jn^*\tau_{\text{gM2S}})) + 2\pi m. \end{cases} \quad (3.40)$$

In practice however, the evolution delay τ_{ev}^* should always be subjected to experimental optimisation since the condition $n^* \times \theta_{\text{gM2S}} = \pi$ is rarely fulfilled.

To illustrate the optimality of the gM2S sequence figure 3.5 shows numerical optimisations of the transformation efficiency from transverse magnetisation to singlet order and back to transverse magnetisation ($\langle I_x \rightarrow \text{SO} \rightarrow I_x \rangle$) as a function of the mixing angle θ_{mix} . Similar to the maximum singlet amplitude $q_{\text{SO}}^{\text{max}}$ the transformation amplitude $\langle I_x \rightarrow \text{SO} \rightarrow I_x \rangle_{\text{max}}$ is bounded by $\pm \frac{2}{3}$.

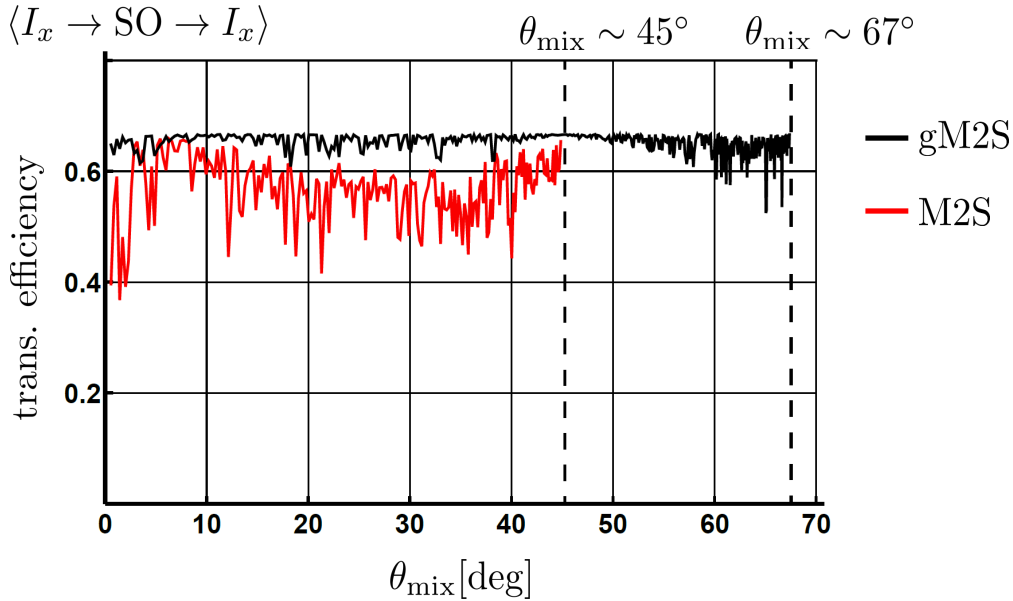


FIGURE 3.5: Numerical optimisation of the M2S (red) and gM2S (black) pulse sequence for transformation of transverse magnetisation to singlet order back to transverse magnetisation. The scalar coupling constant of the system was chosen to equal $J = 100$ Hz and the mixing angle θ_{mix} was discretised in steps of 0.5 degrees. For the M2S sequence the optimal echo delay was determined with the range $\tau_1 \in [0.8 \times \tau_{\text{M2S}}, 1.2 \times \tau_{\text{M2S}}]$. The optimal echo number was determined by equation 3.19. For the gM2S sequence optimal delays were determined within the range $\tau_1 \in [0.8 \times \tau_{\text{gM2S}}, 1.2 \times \tau_{\text{gM2S}}]$, $\tau_2 \in [0, \frac{2\pi}{\omega_e}]$. The echo number n was calculated according to equation 3.24. The dashed lines indicate the validity range of the M2S ($\theta_{\text{mix}} \sim 47^\circ$) and of the gM2S sequence ($\theta_{\text{mix}} \sim 67^\circ$).

Within the validity range of the gM2S, which is roughly given by $\theta_{\text{mix}} \in (0^\circ, 67^\circ]$, the transformation efficiency $\langle I_x \rightarrow \text{SO} \rightarrow I_x \rangle$ remains reasonably close to the theoretical maximum. Slight fluctuations are expected due to the constraint of n^* being an integer. For mixing angles exceeding $\sim 67^\circ$ the optimal evolution delay τ_{gM2S} becomes imaginary and the strategy of the gM2S sequence invalid. Systems with such large mixing angles

classify as inequivalent spin systems. Singlet excitation in this regime is well covered by other techniques [100, 105].

3.2.2 A simple example

The efficiency of the M2S sequence drops off with increasing Δ and reaches the "worst" case scenario when the scalar coupling constant equals the chemical shift difference ($J = \Delta$). In this regime the M2S parameters are as follows:

$$\tau_{\text{M2S}} = \frac{1}{2\sqrt{2}J} \quad \text{and} \quad \theta_{\text{M2S}}|_{J=\Delta} = \pi. \quad (3.41)$$

It is thus impossible to choose an echo-number n that generates an effective $(\pi/2)_x^{12}$ -rotation in the $\{1, 2\}$ subspace.

For the gM2S sequence the case of ($J = \Delta$) represents in some way the "best" case scenario. The effective rotation angle θ_{gM2S} is given by the expression below:

$$\tau_{\text{gM2S}} = \frac{1}{4\sqrt{2}J} \quad \text{and} \quad \theta_{\text{gM2S}}|_{J=\Delta} = \pi/2. \quad (3.42)$$

It follows that only two gM2S echoes ($n^* = 2$) are necessary to generate an effective $(\pi/2)_y^{12}$ -rotation in the $\{1, 2\}$ subspace and the optimal evolution delay τ_{ev}^* takes the form

$$\tau_{\text{ev}}^* = \frac{\tan^{-1}(\sqrt{2} \cot(\sqrt{2}\pi))}{2\sqrt{2}J\pi} \quad (3.43)$$

Substitution of the expressions above into equation 3.39 shows that efficiency of the gM2S sequence in the intermediate case is sufficiently close to the theoretical maximum

$$q_{\text{SO}} \approx 2/3. \quad (3.44)$$

A graphical representation of the gM2S pulse sequence for $J = \Delta$ is illustrated in figure 3.6. In contrast to the conventional M2S sequence the gM2S does have a simple geometric representation [107].

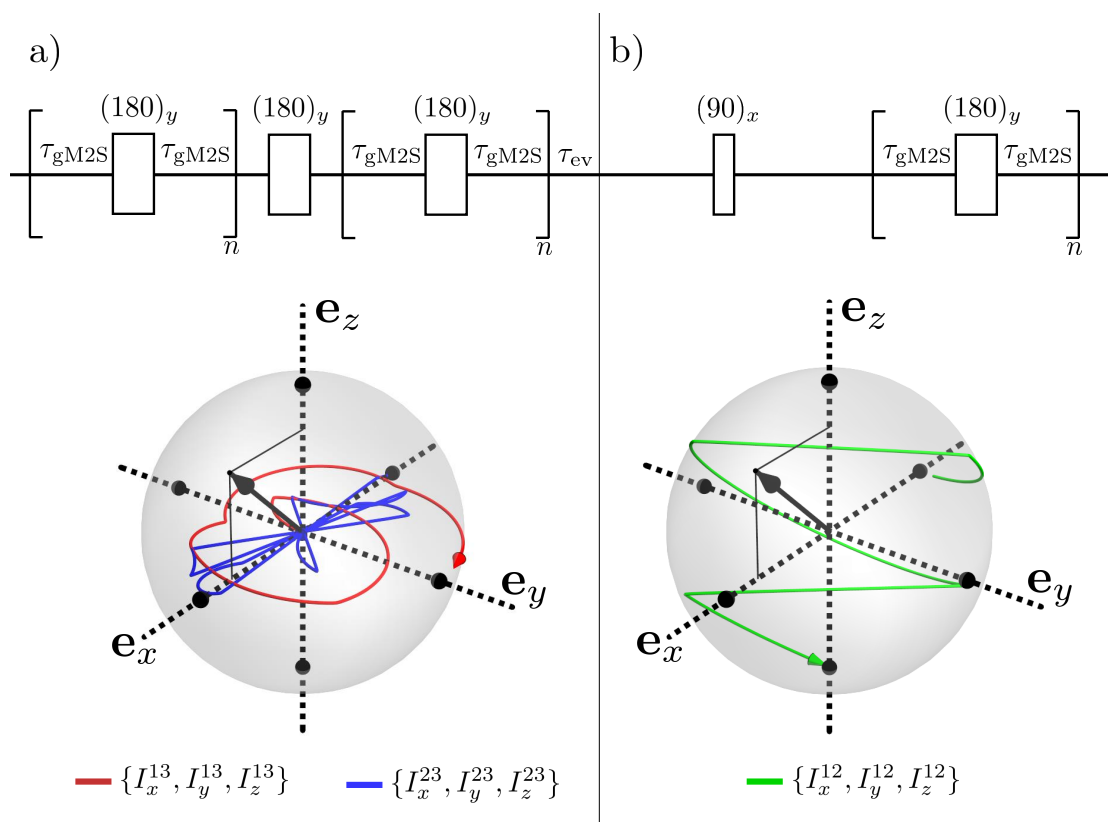


FIGURE 3.6: Geometric representation of the gM2S pulse sequence on a unit-sphere. The scalar coupling and chemical shift difference of the two spins were chosen to be equal ($J = \Delta = 10$ Hz). The initial density operator consisted of pure x -magnetisation: $\rho(0) = \frac{1}{2}I_x = I_x^{23}$. **a)** As explained in the main text, the first part of the gM2S sequence exchanges states $|1\rangle$ and $|2\rangle$. On the Cartesian unit sphere this is noticeable by the decrease (blue) and increase (red) of the vector norm in the $\{2, 3\}$ and $\{1, 3\}$ subspace, respectively. The system eventually arrives at I_y^{23} rather than I_x^{23} due to the additional phase evolution step. **b)** The $(\pi/2)_x$ -rotation exchanges states $|2\rangle$ and $|3\rangle$ and adds an additional phase factor. This takes the operator I_y^{23} to $-I_x^{12}$ into a different subspace. Here the gM2S echoes can be understood as follows. The free evolution period of the system is interrupted by a $(\pi)_z$ -rotation that reflects the projection in the xy -plane of the unit vector. In this way the unit vector traverses downwards towards $-I_z^{12}$.

3.2.3 Experimental demonstration

To compare the performance of the gM2S and M2S sequence singlet excitation has been performed for the ^{13}C pair in $^{13}\text{C}_2$ -labeled 1-methoxy-6-ethoxy-hex-3-yne (compound **I**) and for the central ^1H pair in tert-butyl propyl maleate diester (compound **II**). Chemical structures for **I** and **II** are shown in figure 3.7. Residual protons have been replaced by deuterons to reduce dipolar relaxation contributions from nearby protons.

Compound **I** has been thoroughly studied previously and represents the nearly equivalent case [121]. Its NMR parameters are summarised in table 3.1. Compound **II** displays a higher degree of asymmetry introducing a noticeable difference in the resonance frequency of the two protons. Table 3.1 indicates that **II** displays a mixing angle of $\sim 39^\circ$ at

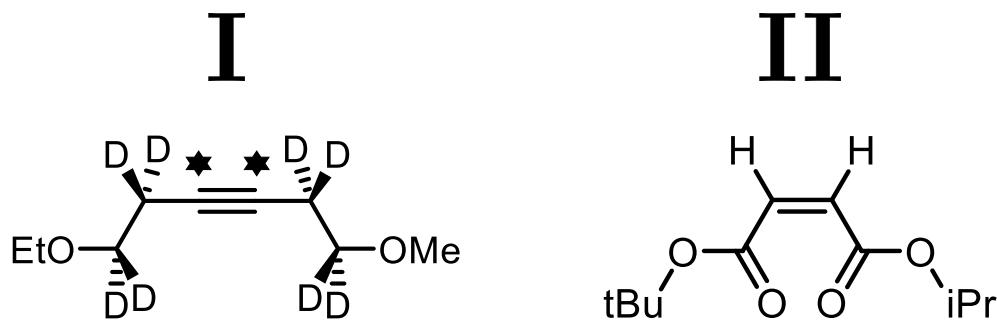


FIGURE 3.7: Chemical structures of 1-methoxy-6-ethoxy-hex-3-yne (**I**) and tert-butyl propyl maleate diester (**II**). Highlighted atoms for **I** indicate ^{13}C positions. Protons not shown have been replaced by deuterons.

a magnetic field strength of 9.4 T and therefore falls into the intermediate regime [110].

	compound I	compound II
nucleus	^{13}C	^1H
J_{12} [Hz]	171.0	12.0
Δ [ppm]	0.14	2.4×10^{-2}
θ_{mix} [deg]	~ 4.7	~ 38.7

TABLE 3.1: NMR parameters and relaxation time constants for compounds **I** and **II** at 9.4 T.

The general experimental strategy is indicated in figure 3.8 (top). Singlet order is excited in block **A** \rightarrow via either M2S or gM2S. The arrow indicates chronological application of the pulses from left to right. Excitation is followed up a singlet filtration step within Block **B**. The de-excitation of the singlet order is achieved via block **A** \leftarrow . Here the arrow indicates chronological application of the pulses from right to left. For the intermediate case an additional filtration block **C** is added to remove any multiple-quantum coherences generated during the de-excitation step. In contrast to the previous section the optimal evolution delays τ_{gM2S} and τ_{ev} are being replaced by the delays τ_1 and τ_2 . These are further subjected to experimental optimisation to compensate for finite pulse duration and uncertainty in the spin system parameters.

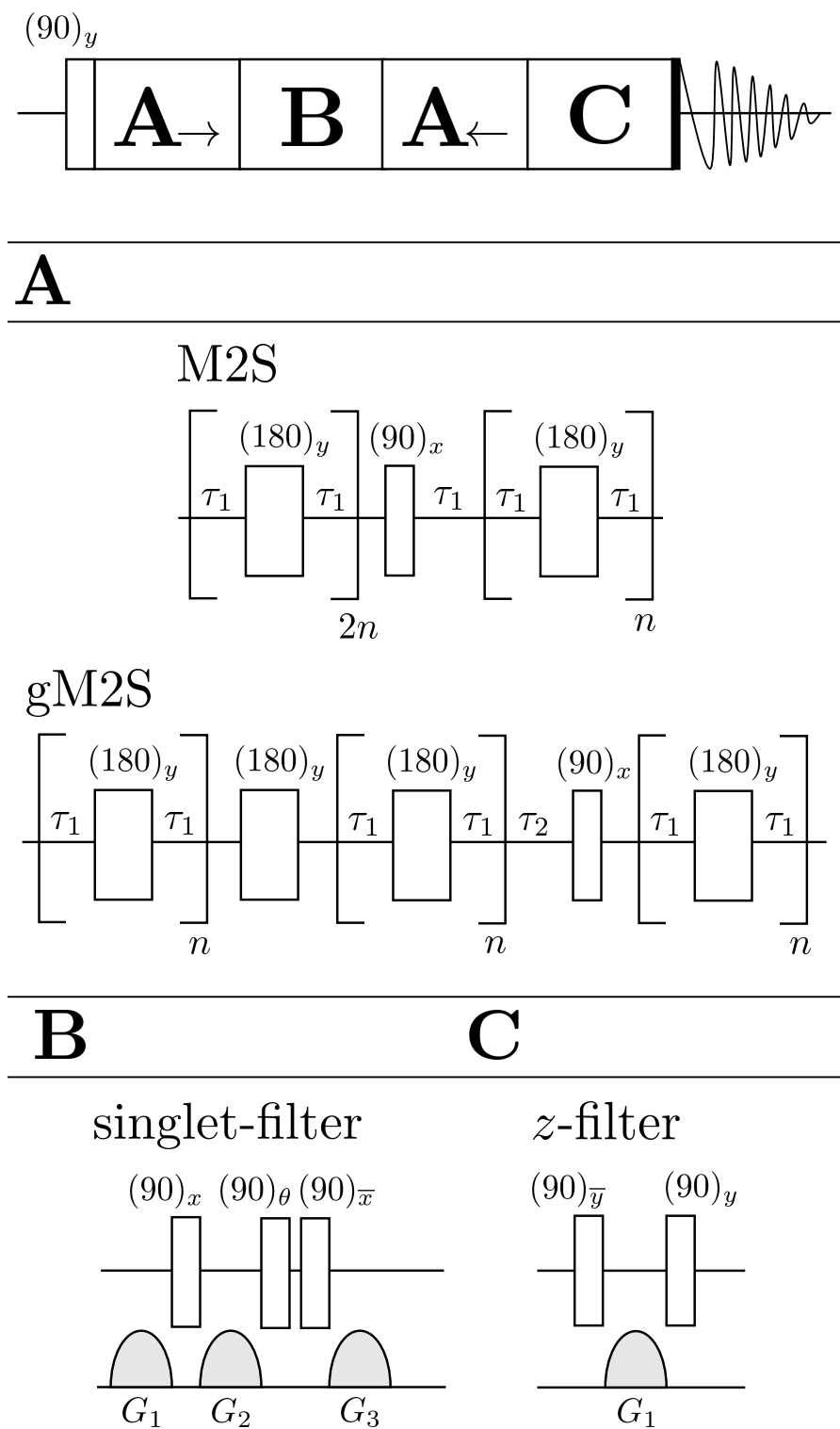


FIGURE 3.8: **top**) General pulse sequence scheme consisting of blocks \mathbf{A}_{\rightarrow} , \mathbf{B} , \mathbf{C} , \mathbf{A}_{\leftarrow} . Blocks \mathbf{A}_{\rightarrow} and \mathbf{A}_{\leftarrow} represent singlet excitation and de-excitation, respectively. Arrows indicate application of RF pulses from left to right or right to left. Singlet filtration occurs within \mathbf{B} . Block \mathbf{C} is reserved for additional signal editing if necessary. **A**) Singlet excitation schemes for the M2S and gM2S pulse sequence. **B**) Singlet filtration via a sequence of rf and gradient pulses. The angle θ is given by the magic angle $\sim 54.7^\circ$ [122]. **C**) Undesired artifacts after the de-excitation step may be filtered by application of gradient based z -filters [22].

The synthesis of compound **I** is described in reference 121. A total amount of 20 mg of compound **I** was dissolved in 0.5 mL deuterated methanol to reach a concentration of 200 mM. The resulting sample was subsequently degassed by several freeze-pump-cycles. Similarly the synthesis of compound **II** is described in reference 110. Experiments were performed on a degassed 5 mM solution in deuterated chloroform. The degassing procedure consisted again of several freeze-pump-cycles. The efficiency for singlet order excitation in compounds **I** and **II** employing experimentally optimised M2S and gM2S pulse sequences is shown in 3.9.

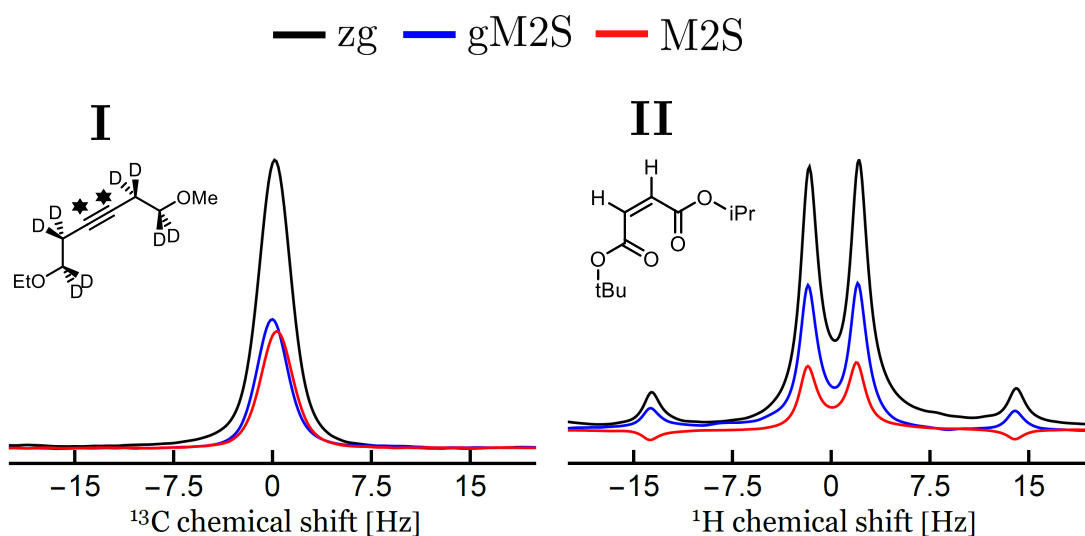


FIGURE 3.9: Performance comparison between M2S and gM2S for compounds **I** and **II**. The relevant spectral regions are highlighted, respectively. Pulse acquire spectra are given as references. Spectra were acquired using a basic two-step phase cycle and averaged over two transients. compound **I**) Experimental optimisation suggested the following evolution delays and echo numbers: $\tau_{\text{M2S}} = 1.38$ ms, $n_{\text{M2S}} = 12$, $\tau_{\text{gM2S}} = 1.33$ ms, $\tau_{\text{ev}} = 1.29$ ms and $n_{\text{gM2S}} = 19$. compound **II**) Experimental optimisation suggested the following evolution delays and echo numbers: $\tau_{\text{M2S}} = 15.4$ ms, $n_{\text{M2S}} = 10$, $\tau_{\text{gM2S}} = 14.6$ ms, $\tau_{\text{ev}} = 4.2$ ms and $n_{\text{gM2S}} = 2$.

Not too surprisingly M2S and gM2S display similar performance in the near-equivalence regime in which both transfer strategies are applicable. Integration of the resulting spectra and comparison with the pulse acquire reference indicates that both sequences preserve approximately $\zeta_{\text{M2S}}^{\text{I}} = \zeta_{\text{gM2S}}^{\text{I}} \approx 42\%$ of the initial magnetisation. This is less than the theoretical maximum for the passage of transverse magnetisation through singlet order and back to transverse magnetisation: $\langle I_x \rightarrow \text{SO} \rightarrow I_x \rangle_{\text{max}} = \frac{2}{3}$ [120]. A possible explanation are short coherence lifetimes caused by the nearby deuterons. In that case some of the magnetisation is lost before it may be converted to long-lived singlet order.

Differences in performance for the M2S and the gM2S should be expected as the system becomes less equivalent. As figure 3.9 shows for compound **II** the M2S sequence seems to

perform poorly and the outer peaks display a 180° phase shift with respect to the inner transitions. This is possibly due to excitation of unwanted single-quantum coherences in the reversion step. Such artifacts could possibly be removed using a conventional z -filter [22].

To ensure a fair efficiency comparison between M2S and gM2S, the absolute value of the relevant spectral region was integrated: In this case the M2S sequence preserves approximately $\zeta_{\text{M2S}}^{\text{II}} \approx 23\%$ of the transverse magnetisation whereas the gM2S preserves roughly $\zeta_{\text{gM2S}}^{\text{II}} \approx 52\%$. For this particular model system the gM2S therefore performs approximately twice as well as the M2S sequence and is reasonably close to the theoretical maximum.

3.3 Singlet mediated double quantum excitation

Double quantum (DQ) excitation has been an integral part of NMR for several decades [97, 123–125]. In general double quantum techniques are used to reduce spectral complexity. This is achieved by exploiting the rotational properties of multiple quantum coherences. These transform irreducibly under elements of the rotation group $\text{SO}(2)$. As a consequence signal components originating from DQ terms may be selectively filtered out by phase cycling techniques [117, 126–129].

In the 80s, Ad Bax et al. proposed the so-called INADEQUATE experiment (see figure 3.10). The INADEQUATE experiment is designed to suppress signals originating from single spin-species and to observe DQ terms originating from scalar coupled spin-pairs.

This makes the INADEQUATE experiment interesting for singlet NMR applications. Here one often faces a similar situation. Selective isotope labelling can be complicated and initial experiments are often performed on natural abundance material [130–132]. Interpretation of the results is simplified by filtration of signals originating from the singlet pair and other components. Existing methods to this problem are based on pulsed field gradients or phase cycling techniques [122, 130, 133, 134].

The idea of pulsed field gradient methods is to construct a physical realisation of the $\text{SO}(3)$ group average. The $\text{SO}(3)$ group average projects the system onto the fully symmetric representation, which for NMR purposes can be equated with the singlet-state [129]. This is done by insertion of suitable combinations of radio-frequency pulses and pulsed field gradients into the pulse sequence [122].

Isotropic filtering on the other hand refers to singlet-filtration via phase cycling techniques [133, 134]. Similar to pulsed field gradient methods isotropic filtering requires modification of the original sequence by insertion of new pulse elements. The phases are related to the positions of the polyhedra-vertices [134, 135].

In both cases, the original pulse sequence has to be modified by insertion of additional

pulse elements and the efficiency of the filtration step depends upon pulse performance. Additionally polyhedral phase cycles tend to take a long time. Even the simplest cycle requires at least 12 steps to be completed.

This chapter takes inspiration from the INADEQUATE experiment and extends its applicability to strongly coupled systems. In its original formulation the INADEQUATE experiment was aimed towards weakly coupled spin systems. In strongly coupled spin systems however, the DQ excitation time for INADEQUATE sequence becomes impractically long. To overcome this problem an alternative DQ excitation scheme is presented. The excitation time for the presented scheme will be shown to be shorter by a factor $\sim J/\Delta$.

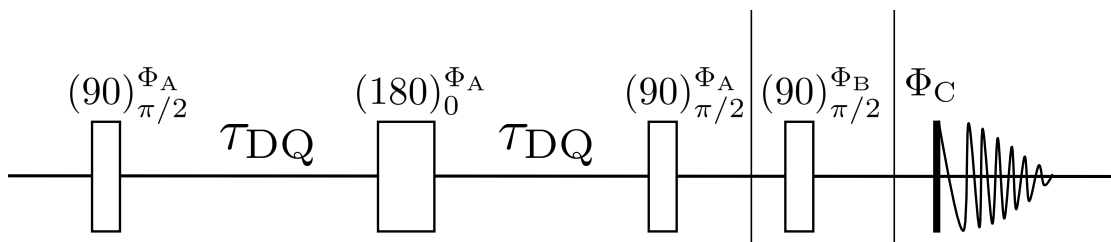


FIGURE 3.10: Schematic representation of the INADEQUATE pulse sequence. The INADEQUATE pulse sequence is subdivided into three parts (vertical lines). These blocks constitute the phase cycle. Pulse elements are abbreviated by $(\theta)_{\phi}^{\Phi}$, where θ represents the flip angle, ϕ the base phase and Φ the additional phase shift due to the phase cycle. The receiver with its phase is indicated by a bold vertical line. A standard phase cycle for a DQ-filtered INADEQUATE experiment is given by the following set of phases: $\Phi_A = \{0, 0, 0, 0\}$, $\Phi_B = \{0, \frac{1}{2}\pi, \pi, \frac{3}{2}\pi\}$, $\Phi_C = \{0, \frac{3}{2}\pi, \pi, \frac{1}{2}\pi\}$.

3.3.1 Double quantum excitation in equivalent spin systems

Extension of the INADEQUATE experiment to strongly coupled spin systems has received little attention within the NMR community [136]. Reference [136] demonstrated that the INADEQUATE experiment may be used to fully excite DQ coherences in strongly coupled spin systems, but they did not provide an optimal evolution delay τ_{DQ}^* that maximises the DQ amplitude.

To discuss limitations of the INADEQUATE experiment it is however useful to derive τ_{DQ}^* . The problem may be stated by considering transformations from the following initial to target state:

$$\rho_a = \frac{1}{2}I_x = I_x^{23}, \quad \rho_b = -I_y^{23} = \frac{i}{2}R_y(\pi/2)(I_{1+}I_{2+} - I_{1-}I_{2-}). \quad (3.45)$$

For the INADEQUATE this transformation is realised by a suitable spin echo. The spin echo may be analysed by considering the propagator at time points $T = \frac{2\pi}{\omega_e}$:

$$U_0\left(\frac{2\pi}{\omega_e}\right) = \Phi^{12}\left(\pi - \frac{\pi\omega_J}{2\omega_e}\right)\Phi^{34}\left(\frac{\pi\omega_J}{2\omega_e}\right) = \Phi^{12}(\pi)R_z^{14}\left(-\pi\frac{\omega_J}{\omega_e}\right)R_z^{23}\left(-\pi\frac{\omega_J}{\omega_e}\right), \quad (3.46)$$

which indicates the necessary z -rotation in the $\{2, 3\}$ subspace to transform I_x^{23} into I_y^{23} . The INADEQUATE propagator at multiple integers of the period is then given by the following expression

$$\begin{aligned} U_{\text{DQ}} &= U_0\left(m\frac{2\pi}{\omega_e}\right)R_x(\pi)U_0\left(m\frac{2\pi}{\omega_e}\right) \\ &= \Phi^{12}(2m\pi)\Phi^{23}(\pi)R_z^{14}\left(-2m\pi\frac{\omega_J}{\omega_e}\right)R_z^{23}\left(-2m\pi\frac{\omega_J}{\omega_e}\right). \end{aligned} \quad (3.47)$$

A straightforward calculation then shows that the DQ amplitude picks up a sinusoidal time-dependence

$$q_{\text{DQ}}(m) = \left(\rho_b \left| U_{\text{DQ}} \rho_a U_{\text{DQ}}^\dagger \right.\right) = \sin\left(2\pi m\left(1 - \frac{\omega_J}{\omega_e}\right)\right). \quad (3.48)$$

For strongly coupled spin systems it is permissible to replace m by $\omega_e t/2\pi$. The optimal evolution delay for a DQ excitation is then approximately given by the expression below

$$\tau_{\text{DQ}}^* \approx \frac{J + \sqrt{J^2 + \Delta^2}}{4\Delta^2}. \quad (3.49)$$

The excitation delay τ_{DQ}^* indicates that experimental realisation of the INADEQUATE experiment becomes increasingly difficult for strongly coupled spin systems. As the difference in chemical shift becomes smaller (or the J -coupling becomes larger) the optimal delay becomes impractically long ($\tau_{\text{DQ}}^* \sim \frac{J}{\Delta^2}$).

This result can be rationalised as follows. In the limit of negligible chemical shift difference the free evolution propagator may be expressed as follows

$$U_0|_{\Delta=0} = \phi^1\left(-\frac{3}{2}J\pi\tau\right)\phi^{234}\left(\frac{1}{2}J\pi\tau\right). \quad (3.50)$$

States $|2\rangle$ and $|3\rangle$ always remain in-phase and DQ excitation is impossible. For non-vanishing $\Delta \ll J$ any accumulated phase difference originates from second order effects due to the coupling of states $|1\rangle$ and $|2\rangle$.

Notice however that even in the case of vanishing chemical shift difference states $|1\rangle$ and $|3\rangle$ run out of phase, where the phase difference builds up on the order of J .

This suggests the following idealised sequence of events for DQ excitation in strongly coupled systems

$$U_{\text{DQ}} = \sigma_{12}\phi^1\left(-\frac{3}{2}J\pi\tau\right)\phi^{234}\left(\frac{1}{2}J\pi\tau\right)\sigma_{12}. \quad (3.51)$$

The physical realisation of these operations is easily implemented by borrowing results from singlet NMR. The swap operation σ_{12} is given by the first block of the gM2S sequence (see figure 3.4) and the phase propagator may be generated by a suitable free evolution period. The phase accumulation step relies on the different eigenvalues of the singlet and triplet states. For the remainder of this chapter we will therefore refer to

this scheme as singlet-mediated-double-quantum (smDQ) excitation

$$U_{\text{smDQ}} = U_{\text{gM2S}}^a U_0(\tau_{\text{ev}}) U_{\text{gM2S}}^a. \quad (3.52)$$

In the strongly coupled limit the smDQ propagator may be expressed as shown below

$$\begin{aligned} U_{\text{smDQ}} &\approx U_{\text{gM2S}}^a \phi^1\left(-\frac{3}{2}J\pi\tau_{\text{ev}}\right) \phi^{234}\left(\frac{1}{2}J\pi\tau_{\text{ev}}\right) U_{\text{gM2S}}^a \\ &= \Phi^{12}(\pi) \Phi^{34}(-\pi/2) \Phi^{12}(-n^* \tau_{\text{gM2S}} \omega_J) \Phi^{34}(n^* \tau_{\text{gM2S}} \omega_J) \sigma_{12} R_z^{34}(\pi) \\ &\quad - \phi^1\left(-\frac{3}{2}J\pi\tau_{\text{ev}}\right) \phi^{234}\left(\frac{1}{2}J\pi\tau_{\text{ev}}\right) - \\ &\quad \Phi^{12}(\pi) \Phi^{34}(-\pi/2) \Phi^{12}(-n^* \tau_{\text{gM2S}} \omega_J) \Phi^{34}(n^* \tau_{\text{gM2S}} \omega_J) \sigma_{12} R_z^{34}(\pi). \end{aligned} \quad (3.53)$$

Making use of the commutation rules for single transition operators the above expression may be put into a more concise form:

$$\begin{aligned} U_{\text{smDQ}} &\approx \Phi^{12}(2\pi) \Phi^{12}(-2n^* \tau_{\text{gM2S}} \omega_J) \Phi^{34}(2n^* \tau_{\text{gM2S}} \omega_J) \Phi^{1234}(\omega_J \tau_{\text{ev}}/4) \sigma_{12} \Phi^1(-\omega_J \tau_{\text{ev}}) \sigma_{12} \\ &= \Phi^{12}(2\pi) \Phi^{12}(-2n^* \tau_{\text{gM2S}} \omega_J) \Phi^{34}(2n^* \tau_{\text{gM2S}} \omega_J) \Phi^{1234}(\omega_J \tau_{\text{ev}}/4) \Phi^2(-\omega_J \tau_{\text{ev}}). \end{aligned} \quad (3.54)$$

Since the total propagator has been reduced to a product of phase operations the smDQ amplitude may be calculated by collecting the accumulated phase of states $|2\rangle$ and $|3\rangle$

$$\begin{aligned} q_{\text{smDQ}}(\tau_{\text{ev}}) &= \left(\rho_b \left| U_{\text{smDQ}} \rho_a U_{\text{smDQ}}^\dagger \right. \right) \\ &= -\frac{i}{2} (\exp(-i(2\pi - 2n^* \tau_{\text{gM2S}} \omega_J - \frac{3}{4}\omega_J \tau_{\text{ev}})) \exp(i(2n^* \tau_{\text{gM2S}} \omega_J + \frac{1}{4}\omega_J \tau_{\text{ev}})) - \text{c.c.}) \\ &= \sin((4n^* \tau_{\text{gM2S}} + \tau_{\text{ev}}) \omega_J). \end{aligned} \quad (3.55)$$

The extrema of the smDQ amplitude occur at $\tau_{\text{ev}}^* = \frac{2k+1}{4J} - 4n^* \tau_{\text{gM2S}}$, where the integer k is chosen to ensure a positive evolution delay.

A qualitative comparison between the duration of the INADEQUATE sequence and the smDQ sequence may be performed in the limit of nearly equivalent systems. The evolution delays τ_{DQ} , τ_{gM2S} and the echo number n^* are then approximated by the expressions below:

$$\tau_{\text{DQ}}^* \approx \frac{1}{2} \frac{J}{\Delta^2}, \quad \tau_{\text{gM2S}} \approx \frac{1}{4J}, \quad n^* \approx \frac{\pi J^2}{2\sqrt{2}(J - \Delta)\Delta} \implies \tau_{\text{ev}}^* \approx \frac{2k + 1 - 4n^*}{4J}. \quad (3.56)$$

The smallest value that ensures positive values for τ_{ev}^* is given by $k = 2n^*$ and the phase evolution delay τ_{ev}^* then reduces to $1/(4J)$. It follows that the ratio of the INADEQUATE duration and the smDQ duration is on the order of $\frac{J}{\Delta}$

$$\frac{T_{\text{DQ}}}{T_{\text{smDQ}}} = \frac{2\tau_{\text{DQ}}^*}{4n^* \times 2\tau_{\text{gM2S}} + \tau_{\text{ev}}^*} \approx \frac{\sqrt{2} J}{\pi \Delta} \sim \frac{J}{\Delta}. \quad (3.57)$$

For nearly equivalent spin systems the smDQ sequence should thus displays a much shorter double quantum excitation time than the standard INADEQUATE sequence.

3.3.2 Experimental demonstration

A full implementation of the smDQ and INADEQUATE pulse sequences are indicated in figure 3.11.

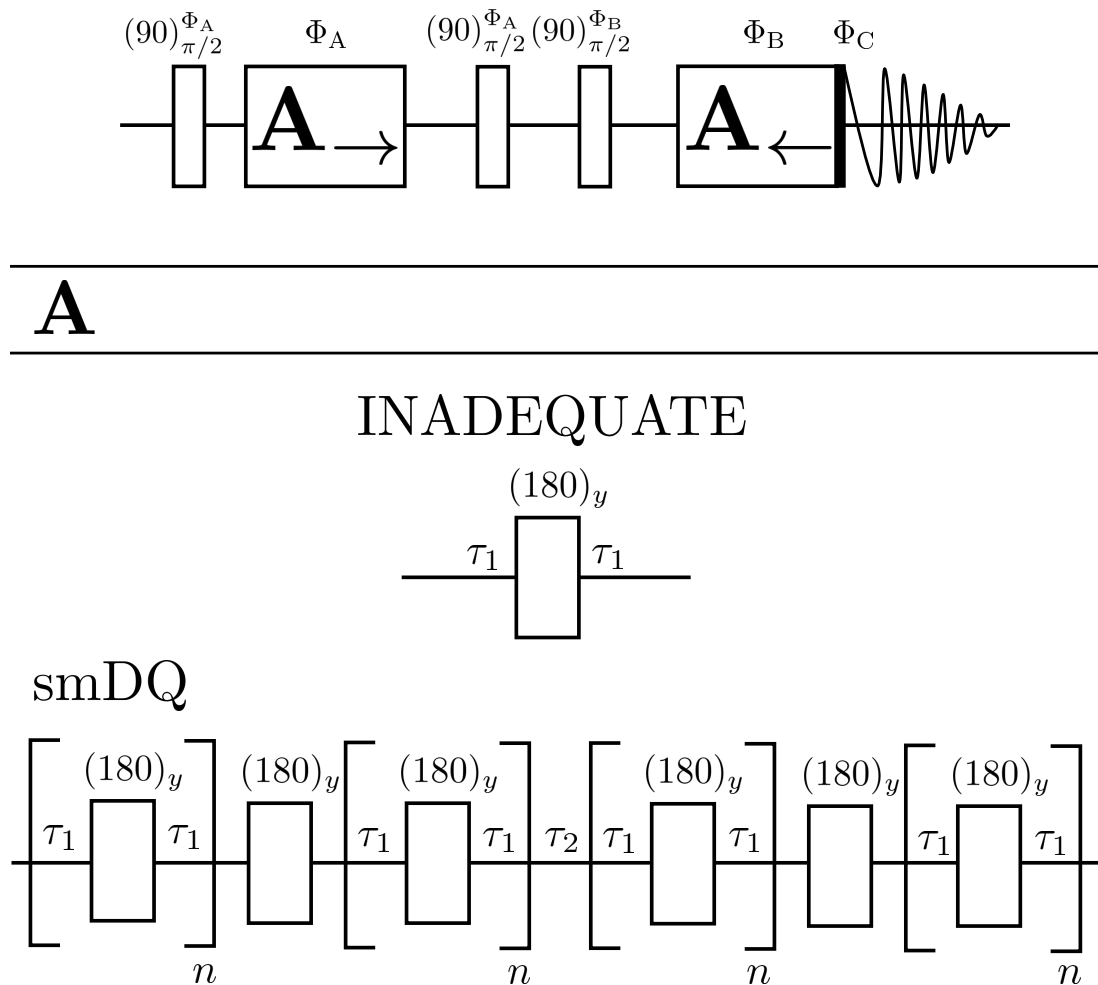


FIGURE 3.11: **top**) General refocused DQ excitation scheme. Arrows indicate application of RF pulses from left to right or right to left. **A**) INADEQUATE and smDQ pulse sequences. For nearly equivalent systems the optimal echo delay for the INADEQUATE scheme is given by equation 3.49. For the smDQ scheme the optimal values for τ_1 and n may be determined from equation 3.22 and 3.24, respectively. The delay τ_2 is approximately given by $1/(4J)$ in the nearly equivalent case. A sufficient DQ phase cycle is given by: $\Phi_A = \{0, 0, 0, 0\}$, $\Phi_B = \{0, \frac{1}{2}\pi, \pi, \frac{3}{2}\pi\}$, $\Phi_C = \{0, \frac{3}{2}\pi, \pi, \frac{1}{2}\pi\}$.

In the previous section the smDQ sequence has been derived in the context of nearly equivalent spin systems. As a consequence the identical sample of compound **I** that has been used to perform the gM2S experiments has been used to experimentally demonstrate the smDQ sequence. Experiments were performed at a magnetic field strength of

16.44 T and a temperature of 300 K. The NMR parameters for compound **I** at 16.44 T are summarised in table 3.2.

compound I	J_{12} [Hz]	Δ [ppm]	θ_{mix} [deg]	T_1 [s]	T_2 [s]
	171	0.14	~ 8.2	6.43	293.6×10^{-3}

TABLE 3.2: NMR parameters for compounds **I** at a magnetic field strength of 16.44 T.

The relevant spectral region of the double quantum filtered INADEQUATE and smDQ experiments are shown in figure 3.12. A pulse acquire spectrum averaged over four transients is given as reference.

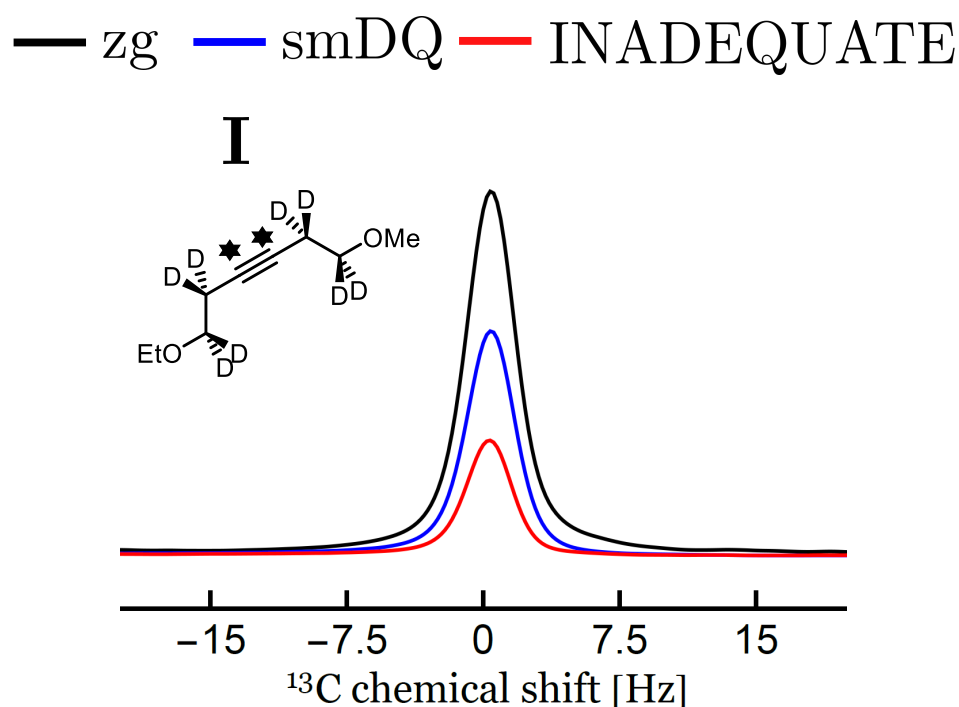


FIGURE 3.12: Double quantum filtered carbon spectra for compound **I**. Double quantum excitation has been performed using the smDQ sequence (blue) and the INADEQUATE sequence (red). A pulse acquire spectrum (black) is given as reference. Double quantum filtered spectra were acquired using the schemes indicated in figure 3.11. The pulse acquire spectrum was simply averaged over four transients. The optimal DQ excitation time for the INADEQUATE was $\tau_{\text{DQ}} = 140$ ms. The smDQ sequence used evolution delays of $\tau_1 = 1.35$, $\tau_2 = 1.35$ and an echo number of $n = 11$.

Experimental optimisation indicated an optimal evolution delay of $\tau_{\text{DQ}} = 140$ ms for the INADEQUATE experiment. The smDQ experiment utilised evolution delays $\tau_1 = \tau_2 = 1.35$ ms and an echo number of $n = 11$, which agrees with the gm2S experiments (see figure 3.9). The total duration for the DQ excitation blocks are then given by $T_{\text{DQ}} \sim 280$ ms and $T_{\text{smDQ}} \sim (8 \times n + 1)\tau_1 \sim 120$ ms. As argued previously the smDQ

sequence is expected to be faster than the INADEQUATE sequence for nearly equivalent spin systems. For compound **I** the smDQ sequence is approximately 2 times faster. Additionally the smDQ sequence displays a much higher transformation efficiency than the INADEQUATE sequence. An integral comparison with the pulse acquire spectrum shows that the smDQ sequence preserve 60 % of the total magnetisation, whereas the INADEQUATE sequence preserves only 30 %. For nearly equivalent spin systems the INADEQUATE is much more susceptible to relaxation effects due to relatively long DQ evolution delays. Table 3.2 indicates that the transverse relaxation time constant T_2 for compound **I** equals approximately 300 ms. A substantial loss of magnetisation during the DQ excitation period of 280 ms should be expected. The smDQ sequence on the other hand achieves DQ excitation via a train refocusing pulses. These compensate throughout the whole sequence for relaxation effects making the smDQ excitation more reliable for spin systems with short relaxation time constants.

Chapter 4

Conclusions

This thesis studied particular aspects of dissipative and coherent dynamics of nuclear spin ensembles.

In chapter 2 we have revisited the description of a spin ensemble in thermal contact with its environment, which represents one of the oldest problems of magnetic resonance theory. Early considerations on this matter by Bloch, Wangsness, Redfield and Abragam led to what is nowadays known as semi-classical relaxation theory [28–30]. The main result of their combined efforts was the so-called inhomogeneous master equation (IME) suitable for the description of thermal experiments at the time. A closer look, however, shows that the semi-classical approach is only valid for systems remaining close to thermal equilibrium (weak-order approximation) and therefore fails to describe thermal equilibration of nuclear spin systems deviating strongly from their thermal equilibrium position. A restriction which the early founders were fully aware of.

It is remarkable that it took almost 80 years of technical advancement to routinely generate spin configurations ranging outside the weak-order approximation [8–11, 16, 19, 43]. For the description of such systems chapter 2 described the reformulation of semi-classical NMR relaxation theory within the Lindbladian formalism [26, 59]. The Lindblad formalism may be understood within a simple state transition picture and thus provides a straightforward algorithm to correctly thermalise the relaxation superoperator. A detailed comparison between the Lindblad formalism and existing thermalisation methods revealed, that only the Lindblad formalism is capable of correctly taking the environmental temperature dependence of the relaxation rate constants into account.

The necessity of the Lindblad formulation has been demonstrated experimentally by studying the spin-isomer conversion process of fullerene-encapsulated water molecules [39, 81, 87, 88]. A technique known as bullet dynamic nuclear polarisation (DNP) has been used to generate a highly non-equilibrium para fraction at ordinary temperatures [11, 39].

The spin isomer conversion process involves the reorganisation of the non-magnetic singlet populations and the magnetic triplet populations. This leads to an observable increase in the samples magnetisation over time. It was shown that the IME is incapable of describing the recovery dynamics appropriately. A reliable description of the relaxation dynamics was only possible within the presented Lindblad formalism. And while we have demonstrated the necessity of the Lindblad formalism for fullerene-encapsulated water molecules, its applicability is by no means restricted to such model systems. Continuous developments in the field of hyperpolarised NMR have started to generate highly ordered spin systems leading to significant signal enhancements [8–19].

The generation of hyperpolarised material, in form of parahydrogen for example, would be rather useless without the necessary tools to transform it into observable magnetisation. In particular efficient conversion methods for singlet order are of great practical interest. Singlet order displays remarkable relaxation properties and is often used to "preserve" highly ordered states. A variety of such techniques has been developed in the context of nuclear long-lived states [99, 100, 103, 105, 119]. Recently, singlet order excitation in the intermediate regime has experienced increasing attention due to continuous developments of field NMR cycling techniques [110–112].

Existing techniques however do not perform very well in the intermediate regime. Chapter 3 has addressed this issue by providing a generalisation of the magnetisation-to-singlet (M2S) pulse sequence which was originally developed for nearly equivalent spin systems. The generalised-magnetisation-to-singlet (gM2S) provides a simple method for optimal singlet order excitation in spin-1/2 pairs displaying a mixing angle up to approximately 66° . The gM2S sequence should therefore prove to be useful for the study of singlet order in intermediate systems.

The elementary building blocks of the gM2S sequence can in some way be understood as logical gates that exchange particular angular momentum spin states. As such they are easily visualised and readily incorporated into other pulse sequence schemes. Based on the gM2S building blocks an efficient method for double quantum excitation in nearly equivalent spin systems has been discussed in chapter 3. For nearly equivalent systems the proposed singlet-mediated-double-quantum (smDQ) excitation scheme provides a much more time efficient solution than conventional methods such as the INADEQUATE sequence [123, 136]. The performance of the smDQ sequence has been demonstrated experimentally in combination with a basic double quantum phase cycle. These types of experiments may prove useful for the study of long-lived nuclear spin order which often involve isotopic labeling. The smDQ sequence may be used to study natural abundance material and offers an alternative to gradient based or polyhedral based filtration schemes [122, 133, 134].

Appendix A

Appendix

A.1 Lindblad form

First consider the Fourier transformation of the unit-step function

$$\int_{-\infty}^{\infty} h(t) \exp(i\omega t) dt = \int_0^{\infty} \exp(i\omega t) dt = \pi\delta(\omega) - i \text{PV} \left(\frac{1}{\omega} \right), \quad (\text{A.1})$$

where $h(t)$ denotes the unit-step function and PV the Cauchy principal value.

The bath correlation functions are related to the spectral densities as follows:

$$\langle B_{\alpha'}^{\Lambda'\dagger}(\tau) B_{\alpha}^{\Lambda}(0) \rangle = \frac{1}{2\pi} \int_{-\infty}^{\infty} K_{\alpha\alpha'}^{\Lambda\Lambda'}(\omega) \exp(-i\omega\tau) d\omega. \quad (\text{A.2})$$

The one-sided Fourier transformation of the bath correlation functions in equation 2.119 may then be expressed as shown below:

$$\begin{aligned} \int_0^{\infty} \langle B_{\alpha'}^{\Lambda'\dagger}(\tau) B_{\alpha}^{\Lambda}(0) \rangle \exp(i\omega\tau) d\tau &= \frac{1}{2\pi} \int_0^{\infty} \int_{-\infty}^{\infty} K_{\alpha\alpha'}^{\Lambda\Lambda'}(\omega') \exp(i(\omega - \omega')\tau) d\omega' d\tau \\ &= \frac{1}{2\pi} \int_{-\infty}^{\infty} K_{\alpha\alpha'}^{\Lambda\Lambda'}(\omega') \int_0^{\infty} \exp(i(\omega - \omega')\tau) d\tau d\omega' \\ &= \frac{1}{2\pi} \int_{-\infty}^{\infty} K_{\alpha\alpha'}^{\Lambda\Lambda'}(\omega') \left\{ \pi\delta(\omega - \omega') - i \text{PV} \left(\frac{1}{\omega - \omega'} \right) \right\} d\omega' \\ &= \frac{1}{2} K_{\alpha\alpha'}^{\Lambda\Lambda'}(\omega) - \frac{i}{2\pi} \int_{-\infty}^{\infty} K_{\alpha\alpha'}^{\Lambda\Lambda'}(\omega') \text{PV} \left(\frac{1}{\omega - \omega'} \right) d\omega'. \end{aligned} \quad (\text{A.3})$$

In a similar manner one can show the following:

$$\int_{-\infty}^0 \langle B_{\alpha'}^{\Lambda'\dagger}(\tau) B_{\alpha}^{\Lambda}(0) \rangle \exp(i\omega\tau) d\tau = \frac{1}{2} K_{\alpha\alpha'}^{\Lambda\Lambda'}(\omega) + \frac{i}{2\pi} \int_{-\infty}^{\infty} K_{\alpha\alpha'}^{\Lambda\Lambda'}(\omega') \text{PV} \left(\frac{1}{\omega - \omega'} \right) d\omega'. \quad (\text{A.4})$$

The above representations of the one-sided Fourier transformation may then be substituted into equation 2.119.

The combination of the principal value leads to a commutator that is known as dynamic frequency shift.

The decaying part is proportional to the spectral density $K_{\alpha\alpha'}(\omega)$. The minus sign preceding the sum of equation 2.119 and the factor of 1/2 are usually absorbed into the definition of the Lindbladian resulting in the presented Lindblad equation.

A.2 Eigenoperators

The dipolar eigenoperators in the case of a homonuclear Zeeman interaction are summarised in Table A.1. A generic eigenoperator is denoted by $T_{km}^{(ij)}$. Where the superscript (ij) indicates angular momentum coupling of spins I_i and I_j resulting in a spherical tensor operator of total angular momentum k and z -angular momentum m .

$m \setminus k$	2	1
± 2	$\frac{1}{2} I_1^\pm I_2^\pm$	-
± 1	$\mp \frac{1}{2} (I_1^\pm I_{2z} + I_{1z} I_2^\pm)$	$\mp \frac{1}{\sqrt{2}} I_j^\pm$
0	$-\frac{1}{2\sqrt{6}} (I_1^+ I_2^- + I_1^- I_2^+ - 4I_{1z} I_{2z})$	I_{jz}

TABLE A.1: Eigenoperators of \hat{H}_A for a homonuclear coupled spin-1/2 pair.

The dipolar eigenoperators in the case of a heteronuclear Zeeman interaction are summarised in Table A.2. The eigenoperators are denoted by $T_{k_1 k_2 m_1 m_2}^{(ij)}$. For the heteronuclear case the superscript (ij) indicates the direct product of spherical tensor operators of spins I_i and I_j with total angular momentum k_1 and k_2 and z -angular momentum m_1 and m_2 , respectively.

$(m_1, m_2) \setminus (k_1, k_2)$	(1,1)	(1,0)	(0,1)	(0,0)
$(\pm 1, \pm 1)$	$\frac{1}{2} I_1^\pm I_2^\pm$	-	-	
$(\mp 1, \pm 1)$	$-\frac{1}{2\sqrt{6}} I_1^\mp I_2^\pm$	-	-	
$(\pm 1, 0)$	$\mp \frac{1}{2} I_1^\pm I_{2z}$	$\mp \frac{1}{\sqrt{2}} I_1^\pm$	-	-
$(0, \pm 1)$	$\mp \frac{1}{2} I_{1z} I_2^\pm$	-	$\mp \frac{1}{\sqrt{2}} I_2^\pm$	-
$(0, 0)$	$\sqrt{\frac{2}{3}} I_{1z} I_{2z}$	I_{1z}	I_{2z}	-

TABLE A.2: Eigenoperators of \hat{H}_A for a heteronuclear coupled spin-1/2 pair.

Similarly one may define quadrupolar eigenoperators for the case that the dominant

interaction is given by Zeeman contributions. The corresponding eigenoperators are summarised in Table A.3. The generic eigenoperator takes the form $T_{2m}^{(i)}$.

$m \setminus k$	2
± 2	$\frac{1}{2} I_i^\pm I_i^\pm$
± 1	$\mp \frac{1}{2} (I_1^\pm I_{1z} + I_{1z} I_1^\pm)$
0	$\frac{1}{\sqrt{6}} (3I_{1z} I_{2z} - 2\mathbb{1})$

TABLE A.3: Eigenoperators of $\hat{H}_A = \omega^0 \hat{I}_z$ for quadrupolar interactions.

A.3 Longitudinal recovery for singlet-triplet-conversion

We briefly outline the derivation of equation 2.161. First we project out the population block of the relaxation superoperator.

$$\begin{aligned}
 \left[\hat{\Gamma}_{\text{LB}}^\theta \right]_{4 \times 4} = & \\
 & \left[\begin{array}{c|c|c|c}
 |S_0\rangle \langle S_0| & |T_+\rangle \langle T_+| & |T_0\rangle \langle T_0| & |T_-\rangle \langle T_-| \\
 \hline
 -\Sigma_1 & \frac{1}{2}(1-\kappa)R_1^{\text{ran}}\theta(-\omega^0) & \frac{1}{2}(1-\kappa)R_1^{\text{ran}} & \frac{1}{2}(1-\kappa)R_1^{\text{ran}}\theta(\omega^0) \\
 \hline
 \frac{1}{2}(1-\kappa)R_1^{\text{ran}}\theta(\omega^0) & -\Sigma_2 & \frac{1}{10}\theta(\omega^0)(2R_1^{\text{DD}} + 5(1+\kappa)R_1^{\text{ran}}) & \frac{2}{5}R_1^{\text{DD}}\theta(2\omega^0) \\
 \hline
 \frac{1}{2}(1-\kappa)R_1^{\text{ran}} & \frac{1}{10}\theta(-\omega^0)(2R_1^{\text{DD}} + 5(1+\kappa)R_1^{\text{ran}}) & -\Sigma_3 & \frac{1}{10}\theta(\omega^0)(2R_1^{\text{DD}} + 5(1+\kappa)R_1^{\text{ran}}) \\
 \hline
 \frac{1}{2}(1-\kappa)R_1^{\text{ran}}\theta(-\omega^0) & \frac{2}{5}R_1^{\text{DD}}\theta(-2\omega^0) & \frac{1}{10}\theta(-\omega^0)(2R_1^{\text{DD}} + 5(1+\kappa)R_1^{\text{ran}}) & -\Sigma_4
 \end{array} \right], \\
 & \theta(\omega) = \exp\left(-\frac{1}{2}\omega^0\beta\theta\right),
 \end{aligned} \tag{A.5}$$

where Σ_j indicates the sum over all the other elements in one column.

To proceed it is advantageous to perform a change of basis. The transformation matrix is given by the expression below

$$X = \begin{bmatrix} \frac{1}{2} & \frac{\sqrt{3}}{2} & 0 & 0 \\ \frac{1}{2} & -\frac{1}{2\sqrt{3}} & -\frac{1}{\sqrt{6}} & -\frac{1}{\sqrt{2}} \\ \frac{1}{2} & -\frac{1}{2\sqrt{3}} & \sqrt{\frac{2}{3}} & 0 \\ \frac{1}{2} & -\frac{1}{2\sqrt{3}} & -\frac{1}{\sqrt{6}} & \frac{1}{\sqrt{2}} \end{bmatrix}. \tag{A.6}$$

To simplify notation we denote the transformed population block as follows

$$X^{-1} \left\{ \left[\hat{\Gamma}_{\text{LB}}^\theta \right]_{4 \times 4} \right\} X = \begin{bmatrix} 0 & 0 & 0 & 0 \\ 0 & \sigma_{22} & 0 & \sigma_{24} \\ 0 & 0 & \sigma_{33} & \sigma_{34} \\ \sigma_{41} & \sigma_{42} & \sigma_{43} & \sigma_{44} \end{bmatrix} \quad (\text{A.7})$$

and enumerate the transformed populations:

$$\begin{bmatrix} P_1 \\ P_2 \\ P_3 \\ P_4 \end{bmatrix} = X^{-1} \begin{bmatrix} |S_0\rangle \langle S_0| \\ |T_+\rangle \langle T_+| \\ |T_0\rangle \langle T_0| \\ |T_-\rangle \langle T_-| \end{bmatrix}. \quad (\text{A.8})$$

To a good approximation the dynamics of P_2 are decoupled from the dynamics of P_4

$$\begin{bmatrix} 0 & 0 & 0 & 0 \\ 0 & \sigma_{22} & 0 & \sigma_{24} \\ 0 & 0 & \sigma_{33} & \sigma_{34} \\ \sigma_{41} & \sigma_{42} & \sigma_{43} & \sigma_{44} \end{bmatrix} \approx \begin{bmatrix} 0 & 0 & 0 & 0 \\ 0 & \sigma_{22} & 0 & 0 \\ 0 & 0 & \sigma_{33} & \sigma_{34} \\ \sigma_{41} & \sigma_{42} & \sigma_{43} & \sigma_{44} \end{bmatrix}, \quad (\text{A.9})$$

leading to the following set of equations

$$\frac{d}{dt} \begin{bmatrix} P_1(t) \\ P_2(t) \\ P_3(t) \\ P_4(t) \end{bmatrix} = \begin{bmatrix} 0 & 0 & 0 & 0 \\ 0 & \sigma_{22} & 0 & 0 \\ 0 & 0 & \sigma_{33} & \sigma_{34} \\ \sigma_{41} & \sigma_{42} & \sigma_{43} & \sigma_{44} \end{bmatrix} \begin{bmatrix} P_1(t) \\ P_2(t) \\ P_3(t) \\ P_4(t) \end{bmatrix}. \quad (\text{A.10})$$

The solutions for $P_1(t)$ and $P_2(t)$ are easily found

$$P_1(t) = P_1(0), \quad P_2(t) = \exp(\sigma_{22}t)P_2(0). \quad (\text{A.11})$$

The solution for $P_3(t)$ is formally given by

$$P_3(t) = \exp(\sigma_{33}t)P_3(0) + \sigma_{34} \int_0^t \exp(\sigma_{33}(t-s))P_4(s)ds. \quad (\text{A.12})$$

We interpret the variable $(t-s)$ as a "memory time" and perform a 0-th order Markov approximation [137]

$$P_3(t) \approx \exp(\sigma_{33}t)P_3(0) + \frac{\sigma_{34}}{\sigma_{33}}P_4(t). \quad (\text{A.13})$$

The dynamics for $P_4(t)$ then reduce to the following

$$\begin{aligned} \frac{d}{dt}P_4(t) = & \sigma_{41}P_1(0) + \sigma_{42} \exp(\sigma_{22}t)P_2(0) \\ & + \sigma_{43} \left\{ \exp(\sigma_{33}t)P_3(0) + \frac{\sigma_{34}}{\sigma_{33}}P_4(t) \right\} + \sigma_{44}P_4(t), \end{aligned} \quad (\text{A.14})$$

which is easily solved.

The solution may then be transformed back into the original representation. Using the appropriate initial conditions: $P_1(0) = \frac{1}{2}$, $P_2(0) = \frac{\sqrt{3}}{2}$, $P_3(0) = 0$ and $P_4(0) = 0$ in combination with the high-temperature and fast-motion approximation results in equation 2.161.

Bibliography

- [1] I. I. Rabi, *Physical Review*, 1936, **49**, 324–328.
- [2] E. M. Purcell, H. C. Torrey and R. V. Pound, *Physical Review*, 1946, **69**, 37–38.
- [3] F. Bloch, W. W. Hansen and M. Packard, *Physical Review*, 1946, **70**, 474–485.
- [4] P. C. Lauterbur, *Nature*, 1973, **242**, 190–191.
- [5] P. Mansfield and A. A. Maudsley, *The British Journal of Radiology*, 1977, **50**, 188–194.
- [6] A. Kumar, R. R. Ernst and K. Wthrich, *Biochemical and Biophysical Research Communications*, 1980, **95**, 1–6.
- [7] K. Wthrich, G. Wider, G. Wagner and W. Braun, *Journal of Molecular Biology*, 1982, **155**, 311–319.
- [8] A. Abragam, *Une nouvelle methode de polarisation dynamique des noyaux atomiques dans les solides*, Centre d'études nucléaires de Saclay, Gif-sur-Yvette (S.-et-O.), 1958.
- [9] L. R. Becerra, G. J. Gerfen, R. J. Temkin, D. J. Singel and R. G. Griffin, *Physical Review Letters*, 1993, **71**, 3561–3564.
- [10] J. H. Ardenkjaer-Larsen, B. Fridlund, A. Gram, G. Hansson, L. Hansson, M. H. Lerche, R. Servin, M. Thaning and K. Golman, *Proceedings of the National Academy of Sciences of the United States of America*, 2003, **100**, 10158–10163.
- [11] K. Kouil, H. Kouilov, S. Bartram, M. H. Levitt and B. Meier, *Nature Communications*, 2019, **10**, 1–6.
- [12] A. Kastler, *J. Phys. Radium*, 1950, **11**, 255–265.
- [13] B. Driehuys, G. D. Cates, E. Miron, K. Sauer, D. K. Walter and W. Happer, *Applied Physics Letters*, 1996, **69**, 1668–1670.
- [14] C. R. Bowers, H. W. Long, T. Pietrass, H. C. Gaede and A. Pines, *Chemical Physics Letters*, 1993, **205**, 168–170.

- [15] G. Navon, Y.-Q. Song, T. Rm, S. Appelt, R. E. Taylor and A. Pines, *Science*, 1996, **271**, 1848–1851.
- [16] C. R. Bowers and D. P. Weitekamp, *Journal of the American Chemical Society*, 1987, **109**, 5541–5542.
- [17] J. Natterer and J. Bargon, *Progress in Nuclear Magnetic Resonance Spectroscopy*, 1997, **31**, 293–315.
- [18] K. Golman, O. Axelsson, H. Jhannesson, S. Mnsson, C. Olofsson and J. S. Petersson, *Magnetic Resonance in Medicine*, 2001, **46**, 1–5.
- [19] R. W. Adams, J. A. Aguilar, K. D. Atkinson, M. J. Cowley, P. I. P. Elliott, S. B. Duckett, G. G. R. Green, I. G. Khazal, J. Lpez-Serrano and D. C. Williamson, *Science*, 2009, **323**, 1708–1711.
- [20] F. Bloch, *Physical Review*, 1946, **70**, 460–474.
- [21] D. Fleisch, *A Student's Guide to Maxwell's Equations by Daniel Fleisch*, 2008.
- [22] M. H. Levitt, *Spin dynamics: basics of nuclear magnetic resonance*, Wiley, 2001.
- [23] W. Gerlach and O. Stern, *Zeitschrift fr Physik*, 1922, **9**, 349–352.
- [24] G. E. Uhlenbeck and S. Goudsmit, *Die Naturwissenschaften*, 1925, **13**, 953–954.
- [25] J. J. Sakurai and J. Napolitano, *Modern Quantum Mechanics by J. J. Sakurai*, 2017.
- [26] H.-P. Breuer and F. Petruccione, *The Theory of Open Quantum Systems*, Oxford University Press, 2007.
- [27] C. Bengs and M. H. Levitt, *Journal of Magnetic Resonance*, 2019, 106645.
- [28] R. K. Wangsness and F. Bloch, *Physical Review*, 1953, **89**, 728–739.
- [29] A. G. Redfield, *IBM J. Res. Dev.*, 1957, **1**, 19–31.
- [30] A. Abragam, *Principles of Nuclear Magnetism*, Clarendon Press, Oxford, 1983.
- [31] P. S. Hubbard, *Reviews of Modern Physics*, 1961, **33**, 249–264.
- [32] R. R. Ernst, G. Bodenhausen and A. Wokaun, *Principles of Nuclear Magnetic Resonance in One and Two Dimensions*, Clarendon Press, 1990, vol. 1.
- [33] M. Mehring, *Principles of High Resolution NMR in Solids*, Springer-Verlag, Berlin Heidelberg, 2nd edn., 1983.
- [34] C. P. Slichter, *Principles of Magnetic Resonance*, Springer-Verlag, Berlin Heidelberg, 3rd edn., 1990.

- [35] M. Goldman, *Quantum Description of High-Resolution NMR in Liquids*, Clarendon Press, Oxford : New York, Reprint edition edn., 1991.
- [36] J. Kowalewski and L. Maler, *Nuclear Spin Relaxation in Liquids: Theory, Experiments, and Applications, Second Edition*, CRC Press, Boca Raton, 2nd edn., 2017.
- [37] J. Cavanagh, W. J. Fairbrother, A. G. Palmer III Professor, N. J. Skelton and M. Rance, *Protein NMR Spectroscopy: Principles and Practice*, Academic Press, Amsterdam ; Boston, 2nd edn., 2006.
- [38] A. Schweiger and G. Jeschke, *Principles of Pulse Electron Paramagnetic Resonance*, Oxford University Press, Oxford, New York, 2001.
- [39] B. Meier, K. Kouil, C. Bengs, H. Kouilov, T. C. Barker, S. J. Elliott, S. Alom, R. J. Whitby and M. H. Levitt, *Physical Review Letters*, 2018, **120**, 266001.
- [40] J. Haupt, *Physics Letters A*, 1972, **38**, 389–390.
- [41] M. Icker and S. Berger, *Journal of Magnetic Resonance*, 2012, **219**, 1–3.
- [42] J.-N. Dumez, B. Vuichoud, D. Mammoli, A. Bornet, A. C. Pinon, G. Stevanato, B. Meier, G. Bodenhausen, S. Jannin and M. H. Levitt, *The Journal of Physical Chemistry Letters*, 2017, **8**, 3549–3555.
- [43] M. G. Pravica and D. P. Weitekamp, *Chemical Physics Letters*, 1988, **145**, 255–258.
- [44] J. Jeener, in *Advances in Magnetic and Optical Resonance*, ed. J. S. Waugh, Academic Press, 1982, vol. 10, pp. 1–51.
- [45] M. H. Levitt and L. Di Bari, *Physical Review Letters*, 1992, **69**, 3124–3127.
- [46] M. H. Levitt and L. Di Bari, *Bulletin of Magnetic Resonance*, 1994, **16**, 94–114.
- [47] T. O. Levante and R. R. Ernst, *Chemical Physics Letters*, 1995, **241**, 73–78.
- [48] C. N. Banwell and H. Primas, *Molecular Physics*, 1963, **6**, 225–256.
- [49] F. Bloch and A. Siegert, *Physical Review*, 1940, **57**, 522–527.
- [50] P. S. Hubbard, *Physical Review A*, 1972, **6**, 2421–2433.
- [51] N. G. Van Kampen, *Physica*, 1974, **74**, 239–247.
- [52] R. Kubo, *Journal of the Physical Society of Japan*, 1962, **17**, 1100–1120.
- [53] J. H. Freed, in *Electron Spin Relaxation in Liquids: Based on lectures given at the NATO Advanced Study Institute held at Sptind, Norway, in August 1971*, ed. L. T. Muus and P. W. Atkins, Springer US, Boston, MA, 1972, pp. 387–410.

- [54] A. A. Nevzorov, *Journal of Magnetic Resonance*, 2014, **249**, 9–15.
- [55] I. Kuprov, *Journal of Magnetic Resonance*, 2016, **270**, 124–135.
- [56] K. Mlmer and Y. Castin, *Quantum and Semiclassical Optics: Journal of the European Optical Society Part B*, 1996, **8**, 49–72.
- [57] H.-P. Breuer and J. Piilo, *EPL (Europhysics Letters)*, 2009, **85**, 50004.
- [58] J. Piilo, K. Hrknen, S. Maniscalco and K.-A. Suominen, *Physical Review A*, 2009, **79**, 062112.
- [59] G. Schaller, *Open Quantum Systems Far from Equilibrium*, Springer International Publishing, 2014.
- [60] P. S. Hubbard, *Physical Review*, 1969, **180**, 319–326.
- [61] J.-N. Dumez, P. Hkansson, S. Mamone, B. Meier, G. Stevanato, J. T. Hill-Cousins, S. S. Roy, R. C. D. Brown, G. Pileio and M. H. Levitt, *The Journal of Chemical Physics*, 2015, **142**, 044506.
- [62] N. Privault, *Understanding Markov Chains: Examples and Applications*, Springer Singapore, 2nd edn., 2018.
- [63] C. Bengs and M. H. Levitt, *Magnetic Resonance in Chemistry*, 2018, **56**, 374–414.
- [64] A. Kossakowski, *Reports on Mathematical Physics*, 1972, **3**, 247–274.
- [65] G. Lindblad, *Communications in Mathematical Physics*, 1976, **48**, 119–130.
- [66] V. Gorini, A. Kossakowski and E. C. G. Sudarshan, *Journal of Mathematical Physics*, 1976, **17**, 821–825.
- [67] M. M. Wolf and J. I. Cirac, *Communications in Mathematical Physics*, 2008, **279**, 147–168.
- [68] D. Chruciski and A. Kossakowski, *Journal of Physics B: Atomic, Molecular and Optical Physics*, 2012, **45**, 154002.
- [69] A. Karabanov, G. Kwiatkowski and W. Kckenberger, *Molecular Physics*, 2014, **112**, 1838–1854.
- [70] R. Annabestani and D. G. Cory, *Quantum Information Processing*, 2017, **17**, 15.
- [71] S. A. Egorov and J. L. Skinner, *Chemical Physics Letters*, 1998, **293**, 469–476.
- [72] P. Schofield, *Physical Review Letters*, 1960, **4**, 239–240.
- [73] S. A. Egorov, K. F. Everitt and J. L. Skinner, *The Journal of Physical Chemistry A*, 1999, **103**, 9494–9499.

- [74] M. Carravetta and M. H. Levitt, *The Journal of Chemical Physics*, 2005, **122**, 214505.
- [75] G. Pileio and M. H. Levitt, *Journal of Magnetic Resonance*, 2007, **187**, 141–145.
- [76] E. Vinogradov and A. K. Grant, *Journal of Magnetic Resonance*, 2007, **188**, 176–182.
- [77] A. K. Grant and E. Vinogradov, *Journal of Magnetic Resonance*, 2008, **193**, 177–190.
- [78] G. Pileio and M. H. Levitt, *The Journal of Chemical Physics*, 2009, **130**, 214501.
- [79] K. Gopalakrishnan and G. Bodenhausen, *Journal of Magnetic Resonance*, 2006, **182**, 254–259.
- [80] R. Sarkar, P. Ahuja, P. R. Vasos and G. Bodenhausen, *Physical Review Letters*, 2010, **104**, 053001.
- [81] S. J. Elliott, C. Bengs, K. Kouril, B. Meier, S. Alom, R. J. Whitby and M. H. Levitt, *ChemPhysChem*, 2018, **19**, 251–255.
- [82] P. Jensen and P. R. Bunker, *Molecular Symmetry and Spectroscopy*, Nrc Pubns, Ottawa, 2nd edn., 1998.
- [83] K. Dill and S. Bromberg, *Molecular Driving Forces: Statistical Thermodynamics in Chemistry, Physics, Biology, and Nanoscience*, Garland Science, London ; New York, 2nd edn., 2010.
- [84] W. Greiner and B. Mller, *Quantum Mechanics: Symmetries*, Springer-Verlag, Berlin Heidelberg, 1989.
- [85] S. Mamone, M. Concistr, E. Carignani, B. Meier, A. Krachmalnicoff, O. G. Johannessen, X. Lei, Y. Li, M. Denning, M. Carravetta, K. Goh, A. J. Horsewill, R. J. Whitby and M. H. Levitt, *The Journal of Chemical Physics*, 2014, **140**, 194306.
- [86] B. Meier, S. Mamone, M. Concistr, J. Alonso-Valdesueiro, A. Krachmalnicoff, R. J. Whitby and M. H. Levitt, *Nature Communications*, 2015, **6**, 1–4.
- [87] K. Komatsu, M. Murata and Y. Murata, *Science*, 2005, **307**, 238–240.
- [88] K. Kurotobi and Y. Murata, *Science*, 2011, **333**, 613–616.
- [89] A. Krachmalnicoff, R. Bounds, S. Mamone, S. Alom, M. Concistr, B. Meier, K. Kouil, M. E. Light, M. R. Johnson, S. Rols, A. J. Horsewill, A. Shugai, U. Nagel, T. Rm, M. Carravetta, M. H. Levitt and R. J. Whitby, *Nature Chemistry*, 2016, **8**, 953–957.

- [90] L. Olsen, O. Christiansen, L. Hemmingsen, S. P. A. Sauer and K. V. Mikkelsen, *The Journal of Chemical Physics*, 2002, **116**, 1424–1434.
- [91] W. Research, 2019.
- [92] B. Meier, J.-N. Dumez, G. Stevanato, J. T. Hill-Cousins, S. S. Roy, P. Hkansson, S. Mamone, R. C. D. Brown, G. Pileio and M. H. Levitt, *Journal of the American Chemical Society*, 2013, **135**, 18746–18749.
- [93] S. S. Roy, P. J. Rayner, P. Norcott, G. G. R. Green and S. B. Duckett, *Physical Chemistry Chemical Physics*, 2016, **18**, 24905–24911.
- [94] A. J. Horsewill, *Progress in Nuclear Magnetic Resonance Spectroscopy*, 1999, **35**, 359–389.
- [95] A. BaratiFarimani, Y. Wu and N. R. Aluru, *Physical Chemistry Chemical Physics*, 2013, **15**, 17993–18000.
- [96] S. Vega and A. Pines, *The Journal of Chemical Physics*, 1977, **66**, 5624–5644.
- [97] A. Wokaun and R. R. Ernst, *The Journal of Chemical Physics*, 1977, **67**, 1752–1758.
- [98] S. Vega, *The Journal of Chemical Physics*, 1978, **68**, 5518–5527.
- [99] M. Carravetta, O. G. Johannessen and M. H. Levitt, *Physical Review Letters*, 2004, **92**, 153003.
- [100] M. Carravetta and M. H. Levitt, *Journal of the American Chemical Society*, 2004, **126**, 6228–6229.
- [101] A. S. Kiryutin, K. L. Ivanov, A. V. Yurkovskaya, H.-M. Vieth and N. N. Lukzen, *Physical Chemistry Chemical Physics*, 2013, **15**, 14248–14255.
- [102] A. S. Kiryutin, A. V. Yurkovskaya, N. N. Lukzen, H.-M. Vieth and K. L. Ivanov, *The Journal of Chemical Physics*, 2015, **143**, 234203.
- [103] S. J. DeVience, R. L. Walsworth and M. S. Rosen, *Physical Review Letters*, 2013, **111**, 173002.
- [104] T. Theis, Y. Feng, T. Wu and W. S. Warren, *The Journal of Chemical Physics*, 2014, **140**, 014201.
- [105] R. Sarkar, P. Ahuja, D. Moskau, P. R. Vasos and G. Bodenhausen, *ChemPhysChem*, 2007, **8**, 2652–2656.
- [106] S. Kadlecěk, K. Emami, M. Ishii and R. Rizi, *Journal of Magnetic Resonance*, 2010, **205**, 9–13.

- [107] M. C. D. Tayler and M. H. Levitt, *Physical Chemistry Chemical Physics*, 2011, **13**, 5556–5560.
- [108] S. J. Elliott and G. Stevanato, *Journal of Magnetic Resonance*, 2019, **301**, 49–55.
- [109] J. Eills, G. Stevanato, C. Bengs, S. Giggler, S. J. Elliott, J. Alonso-Valdesueiro, G. Pileio and M. H. Levitt, *Journal of Magnetic Resonance*, 2017, **274**, 163–172.
- [110] B. Kharkov, X. Duan, E. S. Tovar, J. W. Canary and A. Jerschow, *Physical Chemistry Chemical Physics*, 2019, **21**, 2595–2600.
- [111] A. S. Kiryutin, A. N. Pravdivtsev, K. L. Ivanov, Y. A. Grishin, H.-M. Vieth and A. V. Yurkovskaya, *Journal of Magnetic Resonance*, 2016, **263**, 79–91.
- [112] I. V. Zhukov, A. S. Kiryutin, A. V. Yurkovskaya, Y. A. Grishin, H.-M. Vieth and K. L. Ivanov, *Physical Chemistry Chemical Physics*, 2018, **20**, 12396–12405.
- [113] M. Goldman and H. Jhannesson, *Comptes Rendus Physique*, 2005, **6**, 575–581.
- [114] G. A. Morris, N. P. Jerome and L.-Y. Lian, *Angewandte Chemie International Edition*, 2003, **42**, 823–825.
- [115] U. Haeberlen and J. S. Waugh, *Physical Review*, 1968, **175**, 453–467.
- [116] M. H. Levitt and R. Freeman, *Journal of Magnetic Resonance (1969)*, 1979, **33**, 473–476.
- [117] S. Scherer, *Symmetrien und Gruppen in der Teilchenphysik*, Springer Spektrum, 2016.
- [118] G. Pileio, *Progress in Nuclear Magnetic Resonance Spectroscopy*, 2017, **98-99**, 1–19.
- [119] G. Pileio, M. Carravetta and M. H. Levitt, *Proceedings of the National Academy of Sciences*, 2010, **107**, 17135–17139.
- [120] M. H. Levitt, *Journal of Magnetic Resonance*, 2016, **262**, 91–99.
- [121] G. Pileio, J. T. Hill-Cousins, S. Mitchell, I. Kuprov, L. J. Brown, R. C. D. Brown and M. H. Levitt, *Journal of the American Chemical Society*, 2012, **134**, 17494–17497.
- [122] M. C. D. Tayler and M. H. Levitt, *Journal of the American Chemical Society*, 2013, **135**, 2120–2123.
- [123] A. Bax, R. Freeman and S. P. Kempell, *Journal of Magnetic Resonance (1969)*, 1980, **41**, 349–353.

- [124] M. Rance, O. W. Srensen, G. Bodenhausen, G. Wagner, R. R. Ernst and K. Wthrich, *Biochemical and Biophysical Research Communications*, 1983, **117**, 479–485.
- [125] A. J. Shaka and R. Freeman, *Journal of Magnetic Resonance (1969)*, 1983, **51**, 169–173.
- [126] A. D. Bain, *Journal of Magnetic Resonance (1969)*, 1984, **56**, 418–427.
- [127] G. Bodenhausen, H. Kogler and R. R. Ernst, *Journal of Magnetic Resonance (1969)*, 1984, **58**, 370–388.
- [128] M. H. Levitt, P. K. Madhu and C. E. Hughes, *Journal of Magnetic Resonance*, 2002, **155**, 300–306.
- [129] J.-Q. Chen, J. Ping and F. Wang, *Group Representation Theory for Physicists*, World Scientific, 2nd edn., 2002.
- [130] K. Claytor, T. Theis, Y. Feng and W. Warren, *Journal of Magnetic Resonance*, 2014, **239**, 81–86.
- [131] J. T. Hill-Cousins, I.-A. Pop, G. Pileio, G. Stevanato, P. Hkansson, S. S. Roy, M. H. Levitt, L. J. Brown and R. C. D. Brown, *Organic Letters*, 2015, **17**, 2150–2153.
- [132] L. J. Brown, G. Pileio, M. H. Levitt and R. C. D. Brown, *Journal of Labelled Compounds and Radiopharmaceuticals*, 2017, **60**, 135–139.
- [133] G. Pileio and M. H. Levitt, *Journal of Magnetic Resonance*, 2008, **191**, 148–155.
- [134] S. Mamone, G. Pileio and M. H. Levitt, *Symmetry*, 2010, **2**, 1423–1449.
- [135] *Pulsed Magnetic Resonance: NMR, ESR, and Optics: A Recognition of E. L. Hahn*, ed. D. M. S. Bagguley, Oxford University Press, Oxford, New York, 1992.
- [136] T. Nakai and C. A. Mcdowell, *Molecular Physics*, 1993, **79**, 965–983.
- [137] N. G. Van Kampen, *Physics Reports*, 1985, **124**, 69–160.